POLITECNICO DI TORINO

Laurea Magistrale in Ingegneria Elettronica

"Progettazione analogica e di Potenza"

Tesi di Laurea Magistrale

Proposal of a new algorithm for efficient design of LLC resonant converter, based on time domain analysis

Relatore: Claudio Sansoè

Correlatori: Wilmar Martinez
Sergio Perez

Candidato: Simone Forno

Dicembre 2023

Prefazione

Ho svolto questa tesi durante la mia esperienza Erasmus, lontano da casa, dalla famiglia e dai miei amici piú stretti; questo ha reso il lavoro piú difficile ma anche piú eccitante date tutte le sfide che si sono presentate.
Mi sento innanzitutto in dovere di ringraziare la mia famiglia, che mi ha dato l'opportunitá di vivere questa fantastica esperienza e che ha sempre creduto in me, anche nei momenti piú difficili; uno speciale ringraziamento va a mio padre che grazie alla sua saggezza ed esperienza mi ha aiutato in alcuni punti fondamentali.
Un grande grazie anche ai coinquilini ed amici belga e agli amici che ho conosciuto qui in Belgio, specialmente quelli con cui ho condiviso l'intera esperienza di studio.
Un grazie di cuore va ai miei amici di sempre che mi hanno fatto sentire con loro per tutto l'anno nonostante la distanza, a quelli che sono venuti a visitare questo fantastico posto e quelli che pur volendo non son riusciti.
Un grande e grosso grazie anche a Zuo che mi ha dato un grande aiuto durante la settimana passata in EnergyVille per fare le attivitá in laboratorio, nonostante avesse molte altre cose da fare.
Un sentito grazie anche al relatore Claudio che nonostante molti altri impegni lavorativi é riuscito a darmi saggi consigli. Ultimo ma non per importanza, vorrei ringraziare il mio relatore della KU Leuven Wilmar ed il mio supervisore Sergio per avermi dato l'opportunitá di lavorare su questa tesi con loro e il loro gruppo di ricerca.

Simone Forno

Preface

I made this thesis while being an Erasmus student, away from my hometown, family and close friends; this made this work more difficult but more exciting thanks to all challenges that it gave to me.
I have to thank my whole family first, that gave me the opportunity to live this fantastic experience and that always believed in me, even in the most difficult moments; a special thanks goes to my father because with his wisdom and knowledge, he helped me solving some key challenges.
A big thank you goes also to my Belgian kotmates and friends and to the friends I met here in Belgium, especially those with whom I shared the whole study experience.
A heartfelt thanks goes to my lifelong friends that made me feel with them all year round, to the ones that came and visit this beautiful country and to the ones that have wanted but have not been able to.
An important thanks goes also to my italian supervisor Claudio that even a lot of other task to do, he managed to help me with some wise advice.
A very big thank you also to Zuo that gave me a very big help during the week that I passed in EnergyVille to make the laboratory activity despite having many other things to do.
Last but not the least I'd like to thank also my promoter Wilmar and my supervisor Sergio for the opportunity to work on this interesting thesis with them and their research group.

Simone Forno

Contents

Prefazione i

Preface iii

Abstract vii

List of Figures and Tables ix

List of Abbreviations and Symbols xiii

1 Introduction 1

1.1 Context . . . 1
1.2 Research goals . . . 2
1.3 Thesis structure . . . 3

2 Literature review 5

2.1 FHA "First harmonic Approximation" . . . 5
2.2 Complete model . . . 11
2.3 TDA "Time Domain analysis" . . . 12
2.4 Loss Model . . . 18

3 Mode solvers 23

3.1 PN MODE . . . 24
3.2 NP MODE . . . 27
3.3 PO MODE . . . 30
3.4 PON MODE . . . 34
3.5 NOP MODE . . . 38
3.6 Conclusion . . . 41

4 Main solver and simulation environment 43

4.1 Elements needed for the general algorithm of the solver . . . 44
4.2 Time consumption . . . 50
4.3 General algorithm of the solver . . . 51
4.4 Simulation environment . . . 52
4.5 Conclusion . . . 54

5 Proposed algorithm and example of use 55

5.1 Proposed algorithm . . . 55
5.2 Example . . . 56
5.3 Chosen design . . . 59

5.4 Simulation of the chosen design . . . 59
5.5 Conclusion . . . 61

6 Laboratory implementation **63**
6.1 Magnetic design . . . 63
6.2 Measuring the transformer . . . 68
6.3 Measuring the inductor . . . 68
6.4 Test setup . . . 69
6.5 Implementation A . . . 70
6.6 Implementation B . . . 71
6.7 Implementation C . . . 76
6.8 Implementation D . . . 79
6.9 Testing of the final configuration . . . 82

7 Conclusion **85**
7.1 Evaluation of research question . . . 85
7.2 Further research . . . 85

A Interesting values **89**
A.1 Interesting values for PN mode . . . 89
A.2 Interesting values for NP mode . . . 92
A.3 Interesting values for PO mode . . . 95
A.4 Interesting values for PON mode . . . 97
A.5 Interesting values for NOP mode . . . 101

B Mathematical Analysis **105**
B.1 Integral of general form, 1 . . . 105
B.2 Integral of general form, 2 . . . 105
B.3 Integral of general form, 3 . . . 106
B.4 Integral of general form, 4 . . . 106
B.5 Peak of general form, 1 . . . 107

Bibliography **109**

Abstract

The design of a DC-DC, LLC resonant converter, is difficult because FHA methods give result that may be inaccurate and TDA methods use design algorithms that can be difficult and not that straightforward; the idea of this work is to develop design method based on TDA that is the more straightforward possible. To do that, a numerical solver has been developed, it is based on the standard TDA modeling and it can analyze in a short time a big amount of possible configuration; it gives as output the most suitable configuration in term of the chosen figure of merit (that can be efficiency, volume, ...); in this case the chosen figure of merit is efficiency.
The following contents are present in this thesis: mathematical description of the solver, description of the design method and its algorithm, detailed example run of the algorithm and laboratory implementation of the output values from the algorithm in a specific case of interest.

List of Figures and Tables

List of Figures

1.1 Considered topology. . . . 3

2.1 Half bridge inverter. . . . 5
2.2 FHA waveforms of the inverter. . . . 6
2.3 FHA approximation of the inverter. . . . 7
2.4 Schematic of the rectifier. . . . 7
2.5 FHA waveforms of the rectifier. . . . 7
2.6 Linearized model of the rectifier. . . . 8
2.7 Schematic of the simplified LLC tank. . . . 9
2.8 Sketch of the transfer function of the simplified LLC tank. . . . 10
2.9 Schematic of the linearized LLC tank. . . . 10
2.10 Possible bode plot of linearized LLC tank depending on the relative position of $f_{p1,2}$ and f_{p3}. . . . 11
2.11 a) low frequency approximation, b) high frequency approximation. . . . 11
2.12 Linearized model of an LLC converter using the FHA. . . . 12
2.13 Example of an LLC converter. Source [12]. . . . 13
2.14 Simplified representations of an LLC converter. Source [12]. . . . 13
2.15 P, O, N states of an LLC converter. Source [12]. . . . 14
2.16 Waveforms of the canonical modes of an LLC converter. Source [6]. . . . 16
2.17 Example of boundaries between modes. Source [6]. . . . 17
2.18 Simulation of a "low frequency mode", in the left picture output and resonant current, in the right picture voltage on the capacitor and on the magnetizing inductance. . . . 17
2.19 Voltage, current and power during a turn on-off cycle of an ideal switch. Source [16]. . . . 19
2.20 Gate and channel voltages, currents in the channel during a turn-on cycle. Source [10]. . . . 20

3.1 General waveforms of PN mode. Source [6]. . . . 24
3.2 Passage from P to O state. Source [12]. . . . 26
3.3 Sketch of unwanted waveforms. . . . 26
3.4 General waveforms of NP mode. Source [6]. . . . 27

3.5 Passage from N to O state. Source [12]. 29
3.6 Sketch of unwanted waveforms. 29
3.7 General waveforms of PO mode. Source [6]. 30
3.8 Passage from two O state with different input voltage. Source [12]. . . . 32
3.9 General waveforms of PON mode. Source [6]. 34
3.10 Sketch of O-interval duration problem. 36
3.11 General waveforms of NOP mode. Source [6]. 38
3.12 Sketch of O-interval duration problem. 40

4.1 Flowchart of a generic solver. 48
4.2 Flowchart of the main solver. 51
4.3 Complete model implemented in Simulink. 53
4.4 Complete model implemented in LTSPICE. 54

5.1 Half period of: 1) Resonant current from the analytical model, 2) Magnetizing current from the analytical model, 3) Secondary current from the analytical model, 4) Resonant current from the SIMULINK simulation, 5) Secondary current from the SIMULINK simulation. . . . 60
5.2 Half period of: 1) Voltage on resonant capacitor from the analytical model, 2) Voltage on primary side from the analytical model, 3) Voltage on resonant capacitor from the SIMULINK simulation, 4) Voltage on primary side from the SIMULINK simulation. 60
5.3 Some periods of: RED) Resonant current from the SPICE simulation, GREEN) Magnetizing current from the SPICE simulation, LIGHT BLUE) Secondary current from the SPICE simulation. 61
5.4 Some periods of: BLUE) Voltage on resonant capacitor from the SPICE simulation, RED) Voltage on primary side from the SPICE simulation. . 61

6.1 Indicative iterative flowchart of the work done in laboratory. 64
6.2 Three tests performed to characterize the transformer. 68
6.3 Test setup used in the laboratory. 69
6.4 In BLUE the primary side and in the two different GREENs the secondary sides of transformer A. 70
6.5 Photo of transformer A. 70
6.6 In BLUE the primary side and in the two different GREENs the secondary sides of transformer B. 71
6.7 Photo of transformer B. 71
6.9 WITH INDUCTOR: 1) Gate of high-side MOSFET, 2) Voltage on the primary side of the trasformer, 3) Voltage on upper secondary side, 4) Current of the upper diode. 72
6.8 WITH INDUCTOR: 1) Gate of high-side MOSFET, 2) Voltage on the resonant capacitor, 3) Voltage on the primary side of the trasformer, 4) Resonant current. 73

6.10 WITH INDUCTOR: 1) Gate of high-side MOSFET, 2) Voltage on the primary side of the trasformer, 3) Voltage on lower secondary side, 4) Current of the lower diode. 73
6.11 NO INDUCTOR: 1) Gate of high-side MOSFET, 2) Voltage on the resonant capacitor, 3) Voltage on the primary side of the trasformer, 4) Resonant current. 74
6.12 NO INDUCTOR: 1) Gate of high-side MOSFET, 2) Voltage on the primary side of the trasformer, 3) Voltage on upper secondary side, 4) Current of the upper diode. 74
6.13 NO INDUCTOR: 1) Gate of high-side MOSFET, 2) Voltage on the primary side of the trasformer, 3) Voltage on lower secondary side, 4) Current of the lower diode. 75
6.14 Photo of transformer C. 77
6.17 NO INDUCTOR: 1) Gate of high-side MOSFET, 2) Lower secondary side, 3) Upper secondary side, 4) Current of the upper diode. 77
6.15 WITH INDUCTOR: 1) Gate of high-side MOSFET, 2) Lower secondary side, 3) Upper secondary side, 4) Current of the upper diode. 78
6.18 1) Gate of high-side MOSFET, 2) Lower secondary side, 3) Upper secondary side, 4) Current of the lower diode. 78
6.16 WITH INDUCTOR: 1) Gate of high-side MOSFET, 2) Lower secondary side, 3) Upper secondary side, 4) Current of the lower diode. 79
6.19 Photo of the front of the improved secondary side. 80
6.20 Photo of the back side of the improved secondary side. 80
6.21 WITH INDUCTOR: 1) Gate of high-side MOSFET, 2) Upper diode voltage, 3) Lower diode voltage, 4) Resonant current. 81
6.22 NO INDUCTOR: 1) Gate of high-side MOSFET, 2) Upper diode voltage, 3) Lower diode voltage, 4) Resonant current. 82
6.23 Display of the power supply and active load in the nominal conditions. . 83
6.24 Impedance of the positive cable for the connection to the active load. . 84
6.25 Impedance of the negative cable for the connection to the active load. . 84

B.1 Flowchart of the algorithm to compute the minimum, the maximum and the peak 108

List of Tables

3.1 Coefficient for minimum voltage on magnetizing inductance in PO mode. 33

4.1 Value needed as input for the solver. 47
4.2 Specification used for the test of the solver. 50
4.3 Results of number of evaluated sets and time consumed. 51

5.1 Specification of the converter. 56
5.2 Report of the run of the main solver. 58

5.3 Passives of the implemented converter. 59
5.4 Interesting values from the waveforms. 59
5.5 Loss model applied on the chosen design. 59

6.1 Interesting values from ETD54 datasheet. 64
6.2 Interesting values from Litz wires datasheets. 65
6.3 Interesting values from 0077076A7 datasheet. 67
6.4 Coefficients for core losses calculation for the chosen core of the inductor. 67
6.5 Characteristics of transformer B. 71
6.6 Characterization of transformer B. 72
6.7 Test condition of the circuit with transformer B. 72
6.8 Analysis of the seen inductance in experiment B. 75
6.9 Characteristics of transformer C. 76
6.10 Characterization of transformer C. 77
6.11 Testing condition of transformer C. 77
6.12 Analysis of the seen inductance in experiment C. 79
6.13 Testing condition of transformer C. 81
6.14 Analysis of the seen inductance in experiment D. 82
6.15 Values to calculate efficiencies. 83

A.1 Coefficient for RMS resonant current in PN mode. 90
A.2 Coefficient for peak resonant current in PN mode. 90
A.3 Coefficient for RMS and average output current in PN mode. 91
A.4 Coefficient for peak resonant voltage in PN mode. 92
A.5 Coefficient for RMS resonant current in NP mode. 92
A.6 Coefficient for peak resonant current in NP mode. 93
A.7 Coefficient for RMS and average output current in NP mode. 94
A.8 Coefficient for peak resonant voltage in NP mode. 95
A.9 Coefficient for RMS resonant current in PO mode. 95
A.10 Coefficient for peak resonant current in PO mode. 96
A.11 Coefficient for RMS and average output current in PO mode. 97
A.12 Coefficient for peak resonant voltage in PO mode. 98
A.13 Coefficient for RMS resonant current in PON mode. 98
A.14 Coefficient for peak resonant current in PON mode. 99
A.15 Coefficient for RMS and average output current in PON mode. 100
A.16 Coefficient for peak resonant voltage in PON mode. 101
A.17 Coefficient for RMS resonant current in NOP mode. 102
A.18 Coefficient for peak resonant current in NOP mode. 102
A.19 Coefficient for RMS and average output current in NOP mode. 103
A.20 Coefficient for peak resonant voltage in NOP mode. 104

List of Abbreviations and Symbols

Abbreviations

AC	Alternate Current
DC	Direct Current
ESR	Equivalent Series Resistance
EV	Electric Vehicles
FHA	First Harmonic Approximation
LED	Light Emitting Diodes
MOSFET	Metal Oxide Semiconductor Field Effect Transistor
PV	Photovoltaic
RMS	Root Mean Square
TDA	Time Domain Analysis
ZCS	Zero-Current switching
ZVS	Zero-Voltage switching

Symbols

A_e	Effective magnetic area
A_L	Inductance factor of a winding
A_{Cu}	Copper cross section of a wire
C_{ds}	MOSFET's capacitance seen between drain and source
C_r	Resonant capacitor
D_w	Outer diameter of a wire
$ESR_{C_{out}}$	ESR of output capacitor
ESR_{C_r}	ESR of resonant capacitor
f_r	Series resonant frequency of the tank
f_m	Lower resonant frequency of the tank
f_{sw}	Switching frequency of the inverter
H_w	Height of the available space for the winding in the transformer
i_L	Current in the resonant inductance
i_M	Current in the magnetizing inductance
l_N	Average length of a turn on the core
$L_{l,P}$	Primary side leakage inductance of a transformer
$L_{l,S}$	Secondary side leakage inductance of a transformer
$L_{m,P}$	Primary side magnetizing inductance of a transformer
$L_{m,S}$	Secondary side magnetizing inductance of a transformer
L_r	Resonant inductance
N	Turn-ratio of the transformer
N_{L_m}	Number of values of magnetizing inductance tested
N_{L_r}	Number of values of resonant inductance tested
N_{C_r}	Number of values of resonant capacitance tested
N_N	Number of values of transformer turn ratio tested
N_p	Numbers of turns on primary side of a transformer
N_s	Numbers of turns on secondary side of a transformer
N_t	Numbers of turns on the core for the inductor
R_{ch}	MOSFET's channel resistance
R_{diode}	Diode's on-resistance
R_L	Load resistance
R_{L_r}	Resistance of resonant inductor
R_p	Transformer's primary side resistance
R_s	Transformer's secondary side resistance
$tan(\delta)_{C_r}$	Dissipation factor or the resonant capacitor
t_1	Boundary between first and second interval
t_2	Boundary between second and third interval

t_{rise}	Rising time of the current in the MOSFET's channel @ turn-ON
t_{fall}	Falling time of the current in the MOSFET's channel @ turn-OFF
t_N	Time duration of an N-interval
t_O	Time duration of an O-interval
t_P	Time duration of an P-interval
T_s	Switching period
v_C	Voltage across the resonant capacitor
v_M	Voltage across the magnetizing inductance
V_1	Input DC voltage of the equivalent circuit
V_2	Output DC voltage of the equivalent circuit
V_e	Effective magnetic volume
V_i	Input DC voltage of the converter
V_o	Output DC voltage of the converter
V_γ	Forward voltage drop of a diode
$V_{\gamma,body}$	Forward voltage drop of MOSFET's body diode
W_w	Width of the available space for the winding in the transformer
ω_r	Series resonant pulsation of the tank
ω_m	Lower resonant pulsation of the tank

Chapter 1

Introduction

1.1 Context

We are living in a period of changes toward a more sustainable world and one of the main challenge is the electrification because if we want to be less dependant from fossiles resources we need that. Voltage converters are widely used in all the chain needed for the electrification, from production to usage of electrical energy, so the increase of their efficiency, the reduction of their cost and the simplification of their realization are key points.

During 1970's switching converters were introduced and the nowadays well known topologies like buck, boost and buck-boost DC-DC converters were established; they have high efficiency but not the best in class since they cannot achieve soft switching in easy way, this brings also to higher EMI than devices that can achieve that [1].

This work studies LLC resonant converters because they seems to be a good choice thanks to their high efficiency and small volume, in fact they are widely used in applications like PV converter, EV charging stations, LED driving systems and consumer power supply, as said in [22].

The main advantages of LLC converters are:

- It is easy to achieve ZVS at turn-on and ZCS at turn-off, this leads to higher efficiencies;
- They can be made with a limited number of passives, the resonant inductor can be embedded as leakage of the transformer, this helps to have higher power density than other converters [3].

And the main disadvantages are:

- Design methods based on FHA are not so straightforward [10], but they needs iterations and they are not so accurate if the switching frequency is far from

the series resonant one [23], while the ones made with TDA are more accurate but there are no direct formulas for the design [8];

- The dynamic behaviour is not that good with standard modulation techniques.

1.2 Research goals

The idea behind this thesis is to make some research to mitigate the first disadvantage written in the previous paragraph. The idea is to develop a tool that helps the designer during a design of an LLC converter, making the design the most straightforward possible.
The core of the work is the generation of a MATLAB tool that can analyze in short time an high number of passives configurations, that are automatically generated.
With that core program it is then possible to study the configurations in order to maximize the wanted figure, that can be one of the following, taken as examples:

- Efficiency;
- Occupied volume;
- Dynamic response;
- Cost;
- ...

In this work, the studied figure of merit is the efficiency.

The research question is the following:
Is it possible to generate a straightforward design method for an LLC converter using TDA theory and loss calculation?

1.2.1 Key points

Here there is a short explanation of some important choices made for this work.

Time Domain Analysis

The TDA is used instead of FHA because it has a better accuracy in describing the converter's waveforms also far away from the series resonant frequency respect to FHA and because a wide literature is present.

Chosen topology

Only one specific topology has been chosen to be studied in this work, this to make things simpler even if it can be expanded to others.
All this thesis refers to an LLC converter with half bridge at the primary side, that

uses a transformer with center-tapped secondary side with a passive rectification on the output side, it is shown in figure 1.1.

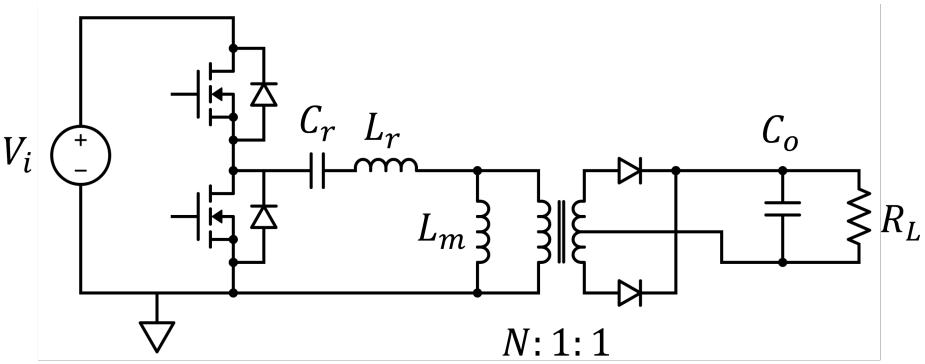

FIGURE 1.1: Considered topology.

1.3 Thesis structure

After this introductory chapter, in the second chapter there is a literature review that describes the basic knowledge used to develop the further chapters and in the third one, the math used for the core of the program is explained in details.
The fourth chapter describes the main solver, it implements the math described in the previous chapter; simulation environments used for this thesis are briefly shown also. Chapter five describes the proposed algorithm to design LLC converters, along with an example run of it with a step-by-step explanation. The values resulting from the output of the algorithm are simulated at the end of this part to verify their correctness.
In the last chapter, there is an explanation of the laboratory activities that brought to the realization of the converter with the specification found with the algorithm.

Chapter 2

Literature review

This unit explains some knowledge already present in literature, that is useful for the understanding of the dissertion.

2.1 FHA "First harmonic Approximation"

Differently to standard DC-DC converter for which the state-space averaging is mainly used because it can generate a good linear model, with resonant converters it is not possible to use this technique, because the main part of the information is not carried in DC but with the switching frequency that excite the system, that normally it is also near the resonant frequency of the tank. One possible technique is the First Harmonic Approximation, that consist in considering for all signal only their first harmonic, so that the inner part of the system can be analyzed with traditional theory of phasors. In the following sections, each block of the converter is analyzed with such approximation: inverter, rectifier, resonant tank.

2.1.1 The inverter

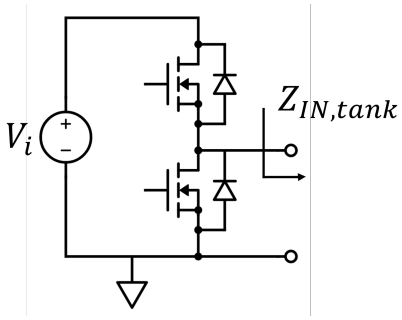

FIGURE 2.1: Half bridge inverter.

The inverter (figure 2.1) generates a square wave from the input voltage, that is approximated with the only first harmonic of the Fourier series as it is visible in

figure 2.2.

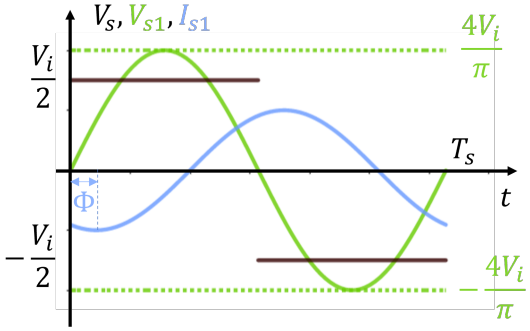

Figure 2.2: FHA waveforms of the inverter.

The fourier series of a square wave with null DC value and amplitude from h to -h can be expressed as:

$$\sum_{n=1,3,5,\ldots}^{\inf} \frac{4h}{n\pi} sin(n\omega t) \tag{2.1}$$

Only the first harmonic is taken, neglecting the DC part so voltage at the tank input is approximated as:

$$V_{S1}(t) = \frac{2V_i}{\pi} sin(\omega t) \tag{2.2}$$

This because it is an half bridge so $h = \frac{V_{IN}}{2}$ but in the case we want to study a full bridge, $h = V_{IN}$ and so:

$$V_{S1}(t) = \frac{4V_i}{\pi} sin(\omega t) \tag{2.3}$$

The output current depends on the load impedance of the stage:

$$V_{S1}(t) = I_{S1,max} sin(\omega t + \phi) \tag{2.4}$$

The last thing needed to characterize the inverter is the amount of current drawn from the source, it can be approximated as a DC current with the value that correspond to the average current that pass via the upper MOSFET, so only half period:

$$I_{IN} = \langle I_{S1} \rangle_{\frac{T_s}{2}} = \frac{2}{T_s} \int_0^{\frac{T_s}{2}} I_{S1,max} sin(\omega t + \phi) dt = \cdots = \frac{2}{\pi} I_{S1,max} cos(\phi) \tag{2.5}$$

So the final FHA approximation of the inverter is the following (figure 2.3):

If it is used a full bridge, the output become $V_s = \frac{4V_i}{\pi}$.

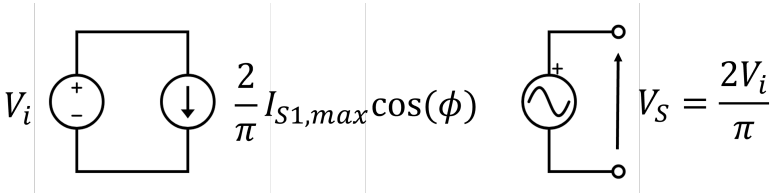

FIGURE 2.3: FHA approximation of the inverter.

2.1.2 The rectifier

As it is said in the introduction the analyzed rectifier is the one represented in figure 2.4, the idea is to represent the element as it is seen from the side of the tank, in order to understand how it affect the transfer function of the resonant tank itself.

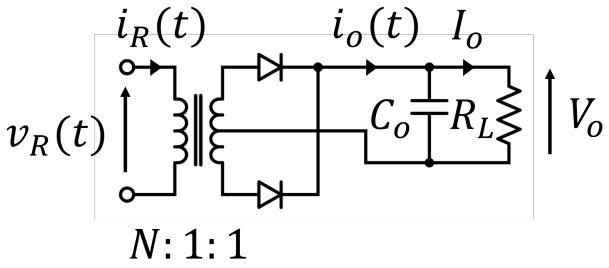

FIGURE 2.4: Schematic of the rectifier.

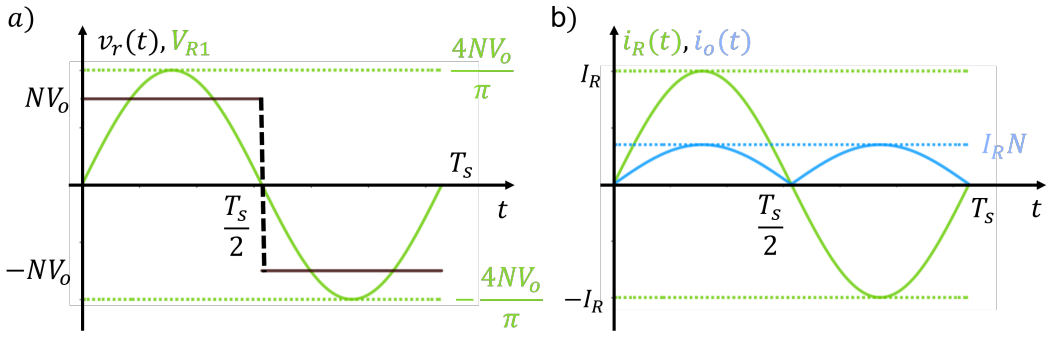

FIGURE 2.5: FHA waveforms of the rectifier.

The studied rectifier is a current driven rectifier, but similar analysis can be done with voltage driven rectifier that has constant current output.

Thanks to the constant output voltage, the secondary voltage is or $+V_o$ or $-V_o$, depending on which diode is conducting. Consequently the primary side voltage is NV_o or $-NV_o$, using the FHA it's possible to approximate this with a sinusoid (2.5 a)):

$$v_R(t) \approx V_{R1}(t) = \frac{4NV_o}{\pi} sin(\omega t) \tag{2.6}$$

If we consider a purely resistive load, the absorbed power from the secondary is purely real, so currents and voltages on the primary are aligned and on the secondary they are modified by the factor N and rectified, as in figure 2.5 b). And the current at primary can expressed as:

$$i_R(t) = I_R sin(\omega t) \tag{2.7}$$

As said before, the output current is constant and its value can be obtained integrating the secondary current for half period:

$$I_o = \frac{2}{T_s} \int_0^{\frac{T_s}{2}} \frac{I_R}{n} sin(\omega t) dt = \cdots = \frac{2NI_R}{\pi} \tag{2.8}$$

So:

$$I_R = \frac{NI_o\pi}{2} \tag{2.9}$$

Now that current and voltages on the primary side are approximated, we can divide formula 2.6 and 2.7 substituted with 2.9 to obtain the input equivalent resistance:

$$R_{eq} = \frac{v_R(t)}{i_R(t)} = \frac{\frac{4NV_o}{\pi} sin(\omega t)}{I_R sin(\omega t)} = \frac{\frac{4NV_o}{\pi}}{\frac{I_o\pi}{2N}} = \frac{8N^2}{\pi^2}\frac{V_o}{I_o} = \frac{8N^2}{\pi^2} R_L \tag{2.10}$$

The linearized equivalent of the rectifier is therefore the one in figure 2.6.

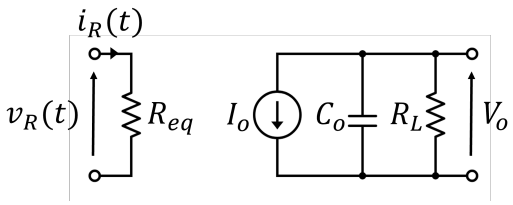

Figure 2.6: Linearized model of the rectifier.

In which:

$$R_{eq} = \frac{8N^2}{\pi^2} R_L, \qquad I_o = \frac{2NI_R}{\pi} \tag{2.11}$$

2.1.3 The tank

This part focuses on the transfer function of an LLC tank in the s-domain.

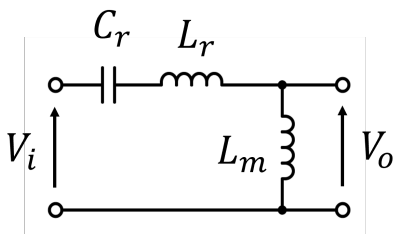

FIGURE 2.7: Schematic of the simplified LLC tank.

Simplified transfer function

First we study the transfer function without load, as in figure 2.7.

Using voltage partitioning:

$$V_o = \frac{sL_m}{sL_m + sL_r + \frac{1}{sC_r}} V_i \tag{2.12}$$

It's possible to obtain the transfer function:

$$H(s) = \frac{V_o}{V_i} = \frac{s^2 L_m C_r}{1 + s^2 C_r (L_m + L_r)} \tag{2.13}$$

That has two zeros in the origin:

$$f_{Z1} = f_{Z2} = 0 \tag{2.14}$$

And two complex conjugate poles:

$$1 + s_p^2 C_r (L_m + L_r) = 0 \tag{2.15}$$

$$s_{p1,2} = \pm\sqrt{-\frac{1}{C_r(L_m + L_r)}} = j\omega_{p1,2} \tag{2.16}$$

$$f_{p1,2} = \pm\frac{1}{2\pi}\sqrt{\frac{1}{C_r(L_m + L_r)}} \tag{2.17}$$

Since there is no term with s at denominator, in this case $Q = \infty$, so the sketch of the transfer function is the one in figure 2.8.

Transfer function

The more complete model includes also the equivalent resistance from the rectifier, as in figure 2.9, from which it is possible to derive the transfer function:

$$V_o = \frac{sL_m // R_L}{sL_m // R_L + sL_r + \frac{1}{sC_r}} V_i = \frac{\frac{sL_m L_r}{sL_m + L_r}}{\frac{sL_m L_r}{sL_m + L_r} + sL_r + \frac{1}{sC_r}} V_i \tag{2.18}$$

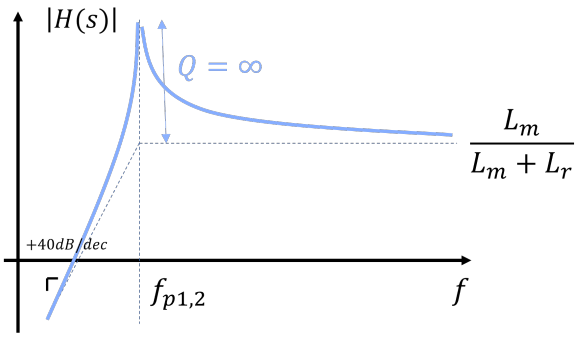

Figure 2.8: Sketch of the transfer function of the simplified LLC tank.

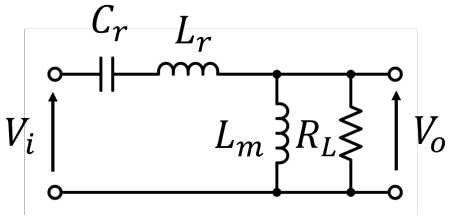

Figure 2.9: Schematic of the linearized LLC tank.

$$H(s) = \frac{V_o}{V_i} = \frac{s^2 L_m R_L C_r}{s^2 L_m R_L C_r + s^2 C_r L_r (s L_m + R_L) + s L_m + R_L} = \tag{2.19}$$

$$= \frac{s^2 L_m R_L C_r}{s^3 C_r L_r L_m + s^2 R_L C_r (L_R + L_m) + s L_m + R_L} \tag{2.20}$$

The two zeros are in the same position:

$$f_{Z1} = f_{Z2} = 0 \tag{2.21}$$

The positions of the two poles are not so easy to determine, but there are two complex conjugate poles ($f_{p1,2}$) and a simple pole (f_{p3}), in order to sketch the bode plot, we still need to determine their relative position, so to understand if the bode plot is more similar to 2.10 a) or b).

To do that it is possible to simplify the parallel between L_m and R_L looking at it equivalent at low (figure 2.11 a)) and high (figure 2.11 b)) frequency:

- Low frequency: $sL_m << R_L$ so $sL_m // R_L \approx sL_m$;
- High frequency: $sL_m >> R_L$ so $sL_m // R_L \approx R_L$;

Since at lower frequency the circuit is the same studied before it is possible to say that the bode plot of the transfer function of the tank will be similar to 2.10 a). Complex conjugate poles at lower frequency are approximated as follows:

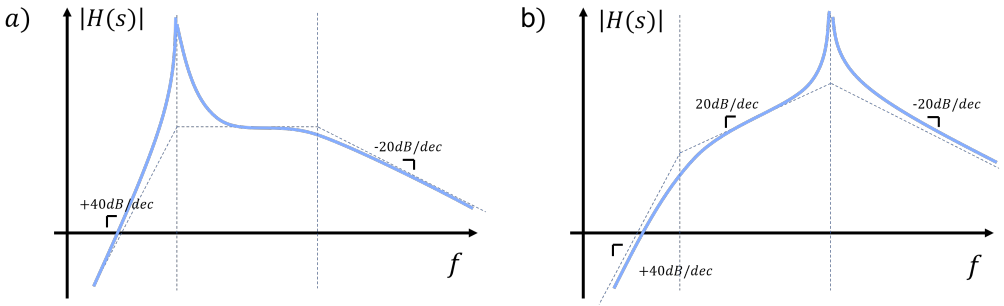

FIGURE 2.10: Possible bode plot of linearized LLC tank depending on the relative position of $f_{p1,2}$ and f_{p3}.

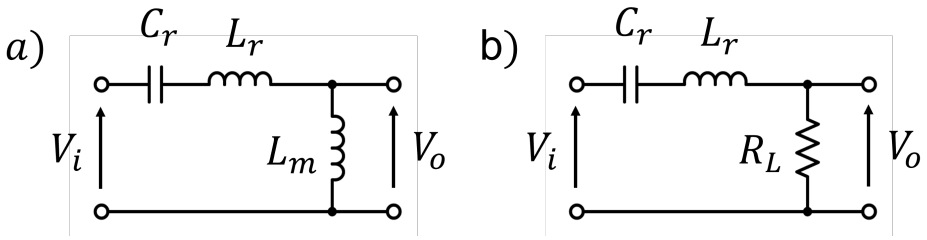

FIGURE 2.11: a) low frequency approximation, b) high frequency approximation.

$$f_{p1,2} \approx \pm \frac{1}{2\pi} \sqrt{\frac{1}{C_r(L_m + L_r)}} \tag{2.22}$$

For high frequency (figure 2.11, b) we study the transfer function of the tank neglecting the contribution of the magnetizing inductor, so it is the transfer function of an series RLC circuit:

$$H(s) = \frac{R_L}{R_L + sL_r + \frac{1}{sC_r}} \tag{2.23}$$

This is also called series resonant frequency of the converter and is:

$$f_{p3} \approx \frac{1}{2\pi} \sqrt{\frac{1}{C_r L_r}} \tag{2.24}$$

2.2 Complete model

After this part the linearized model of the converter can be written.

In figure 2.12 there is the linearized model in which:

- V_i is the DC voltage at the input;
- I_i is the DC current drawn from the input source;

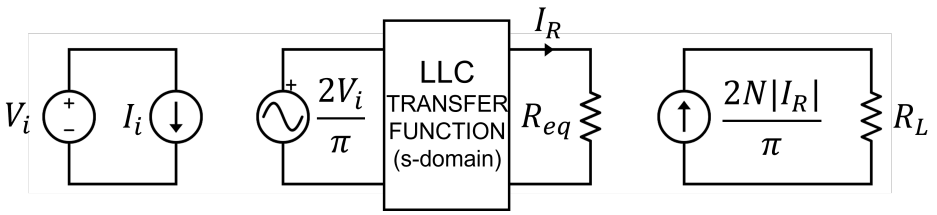

Figure 2.12: Linearized model of an LLC converter using the FHA.

- $\frac{2V_i}{\pi}$ is the phasor representing the input voltage of the tank;
- I_R is the phasor of the current at the output of the tank;
- R_{eq} is the equivalent load generated from the rectifier on the tank;
- $\frac{2N|I_R|}{\pi}$ is the DC current delivered to the load.

2.3 TDA "Time Domain analysis"

The analysis in the time domain consist in studying the converter in the time variable, studying, for each interval in which the switches are in different configurations, the simplified representation of it with differential equations. One of the first paper describing this is [12] and the assumption in this study are:

- Constant 50% dutycycle;
- Null deadtime;
- Constant input voltage;
- Constant output voltage;
- Null voltage drop on rectifiers;
- No leakage inductance at secondary side of the trasformer.

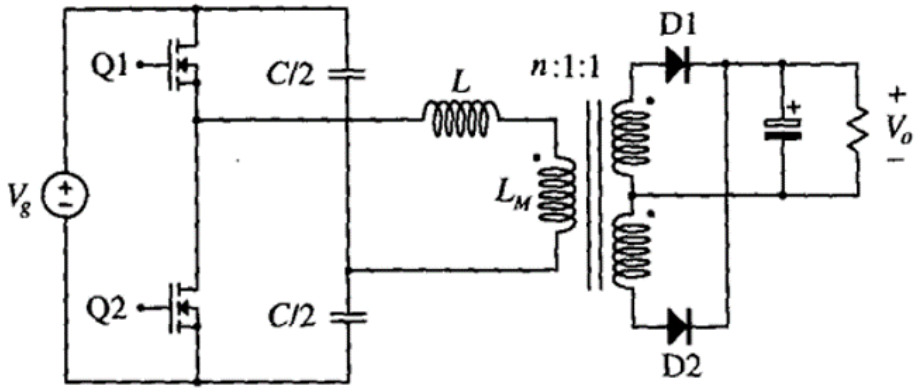

FIGURE 2.13: Example of an LLC converter. Source [12].

2.3.1 States

If the considered topology is the one present in figure 2.13 and according to the state's combinations of the switches, six possible simplified representations (states) are possible (figure 2.14) where:

- V_1 depends on input voltage and type of bridge ($V_1 = V_g$ if full-bridge and $V_1 = V_g/2$ if half bridge;
- V_2 depends on output voltage and transformer turn ratio ($V_2 = NV_0$).

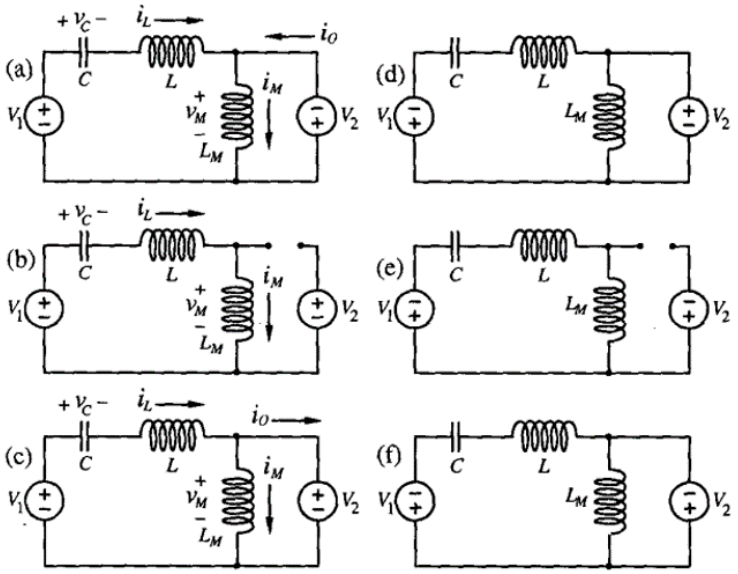

FIGURE 2.14: Simplified representations of an LLC converter. Source [12].

According to [12] and others, since the duty cycle is 50%, each half period has same waveform of the other, but symmetric with zero, so it is possible to successfully study only three of this representations, that from now on will be called "P", "O", "N". They are extracted in figure 2.15, and they can be recognized looking at the waveform in this way:

- P state if the voltage on magnetizing inductance is above zero and fixed to $+NV_o$;
- N state if the voltage on magnetizing inductance is negative and fixed to $-NV_o$;
- O state if the voltage on magnetizing inductance oscillates.

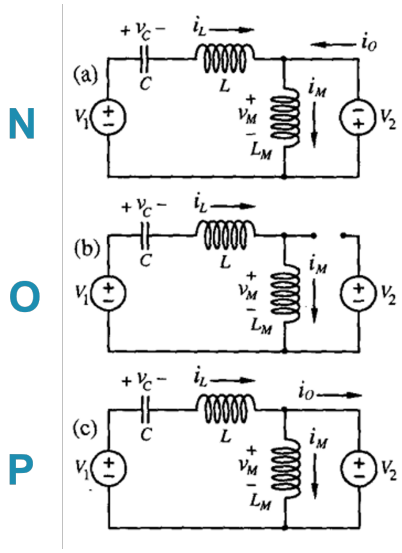

Figure 2.15: P, O, N states of an LLC converter. Source [12].

Notation

According with the previous section the resonant frequencies of the converter are calculated like:

$$\begin{cases} \omega_r = \frac{1}{\sqrt{C_r L_r}} \\ \omega_m = \frac{1}{\sqrt{C_r (L_m + L_r)}} \end{cases} \tag{2.25}$$

P state

In this state, as stated by [20] the general solution of the simplified circuit is:

$$L_r C_r \frac{d^2}{dt^2} v_{C_r} + v_{C_r} = V_i - NV_o \tag{2.26}$$

Solving the differential equation, the following equations describe the state (can be found in [12] in a different normalization):

$$\begin{cases} v_C(t) = K_a cos(\omega_r t) + K_b sin(\omega_r t) + V_i - NV_o \\ i_L(t) = C_r \omega_r (-K_a sin(\omega_r t) + K_b cos(\omega_r t)) \\ v_M(t) = NV_o \\ i_M(t) = \frac{NV_o}{L_m} t + i_M(0) \\ i_O(t) = i_L(t) - i_M(t) \end{cases} \tag{2.27}$$

N state

Similarly in the N state, the general solution of the simplified circuit is:

$$L_r C_r \frac{d^2}{dt^2} v_{C_r} + v_{C_r} = V_i + NV_o \tag{2.28}$$

And the following they are the equations that describe this state (can be found in [12] in a different normalization):

$$\begin{cases} v_C(t) = K_a cos(\omega_r t) + K_b sin(\omega_r t) + V_i + NV_o \\ i_L(t) = C_r \omega_r (-K_a sin(\omega_r t) + K_b cos(\omega_r t)) \\ v_M(t) = -NV_o \\ i_M(t) = -\frac{NV_o}{L_m} t + i_M(0) \\ i_O(t) = i_M(t) - i_L(t) \end{cases} \tag{2.29}$$

O state

In this state, the equivalent circuit is slightly different and the equation that describes it is [20]:

$$(L_r + L_m) C_r \frac{d^2}{dt^2} v_{C_r} + v_{C_r} = V_i \tag{2.30}$$

That if solved, give rise to the following formulas (can be found in [12] in a different normalization):

$$\begin{cases} v_C(t) = K_a cos(\omega_m t) + K_b sin(\omega_m t) + V_i \\ i_L(t) = C_r \omega_m (-K_a sin(\omega_m t) + K_b cos(\omega_m t)) \\ v_M(t) = \frac{L_m}{L_m + L_r} (-K_a cos(\omega_m t) - K_b sin(\omega_m t) \\ i_M(t) = i_L(t) \\ i_O(t) = i_M(t) - i_L(t) = 0 \end{cases} \tag{2.31}$$

2.3.2 Modes

In half period more than one state can be present, their order and number on each half period states the mode in which the converter is working, there are theoretically infinite possible modes, but only some of them are of interest in LLC theory.

Canonical modes

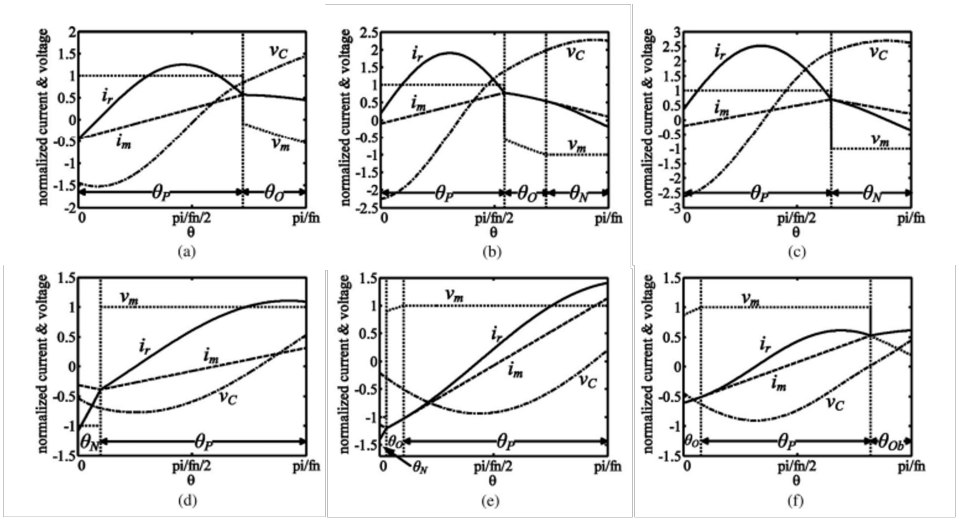

Figure 2.16: Waveforms of the canonical modes of an LLC converter. Source [6].

These are the canonically studied modes as described in articles like [6] and [12]:

- Figure 2.16 (a): PO mode;
- Figure 2.16 (b): PON mode;
- Figure 2.16 (c): PN mode;
- Figure 2.16 (d): NP mode;
- Figure 2.16 (e): NOP mode;
- Figure 2.16 (f): OPO mode.

Given a resonant tank, changing frequency and nominal load, it is possible to pass from one mode to the other, with the behaviour that is described by figures similar to figure 2.17.

Cut-off mode

In some configurations, it is possible to see that if the switching frequency is much higher than resonant frequency the converter goes in the so-called cut-off mode, in which the converter stays theoretically only in the O-state.

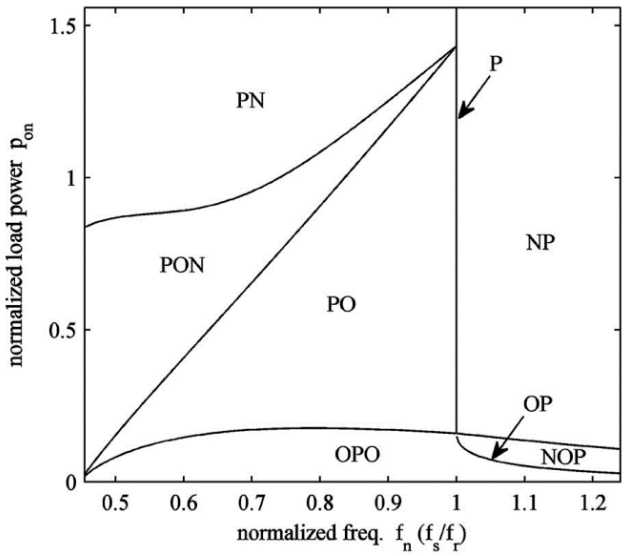

FIGURE 2.17: Example of boundaries between modes. Source [6].

Lower frequency modes

If instead the switching frequency is much lower than the series resonant frequency, there can be modes in which multiple N and P states are present in each semi-period as possible to see in the simulation presented in figure 2.18. These are not studied in this work.

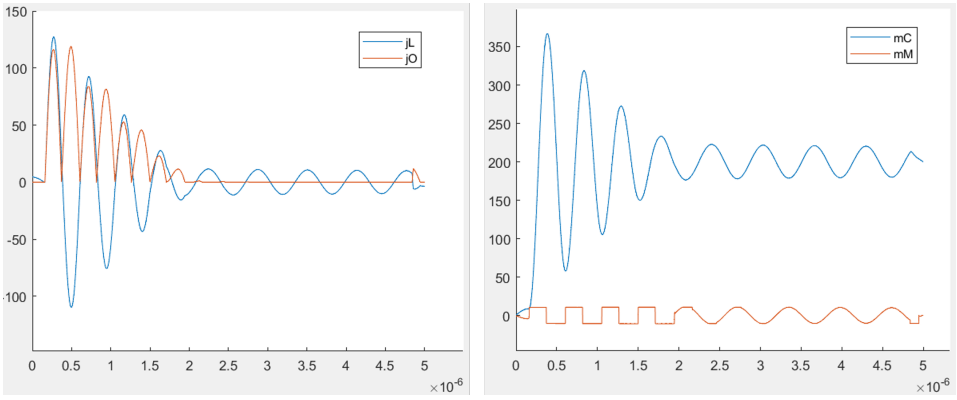

FIGURE 2.18: Simulation of a "low frequency mode", in the left picture output and resonant current, in the right picture voltage on the capacitor and on the magnetizing inductance.

2.4 Loss Model

This section briefly explains the losses that will be taken into account in later chapters.

2.4.1 MOSFET losses

The losses considered in the MOSFET are conduction and switching losses.

Conduction losses

Considering:

- the dead-time negligible respect to the period;
- converter secondary side to be symmetric so that resonant current in the two half periods is symmetric;
- the MOSFETs are identical.

The total conduction loss of the bridge can be calculated as follow:

$$P_{MOS,cond} = a \cdot R_{MOS} \cdot i_{L,RMS}^2 \tag{2.32}$$

Where $a = 1$ if there is an half-bridge and $a = 2$ if there is a full-bridge inverter.

Turn-on and turn-off losses

Power losses occur because during switching period both current and voltage on the switch are not zero, if their behaviour is approximated as linear, the instantaneous power loss has triangular waveform, similar to what is represented in figure 2.19. If ZVS is achieved during turn-on and considering linear behaviour of voltages and currents, turn-on and turn-off losses can be studied, for a single MOSFET, as:

$$P_{MOS,turn-ON} = \frac{f_{sw}}{2} V_{off} I_{on} \cdot t_{SWdelay} = \frac{f_{sw}}{2} V_{body\_diode} I_{L,turn-ON} \cdot t_{rise} \tag{2.33}$$

$$P_{MOS,turn-OFF} = \frac{f_{sw}}{2} V_{off} I_{on} \cdot t_{SWdelay} = \frac{f_{sw}}{2} V_{in} I_{L,turn-OFF} \cdot t_{fall} \tag{2.34}$$

Zero Voltage Switching at primary

To achieve ZVS during turn-on, a proper dead-time has to be inserted to make the parasitic capacitor to discharge before turning on the device, as sketched in figure 2.20, a general condition for this to be feasible is that the energy in the resonant tank is enough to discharge parasitic capacitors so, as also said by [10], to have ZVS a necessary condition is:

$$L_m i_{L,peak}^2 > C_{oss} V_{ds}^2 \tag{2.35}$$

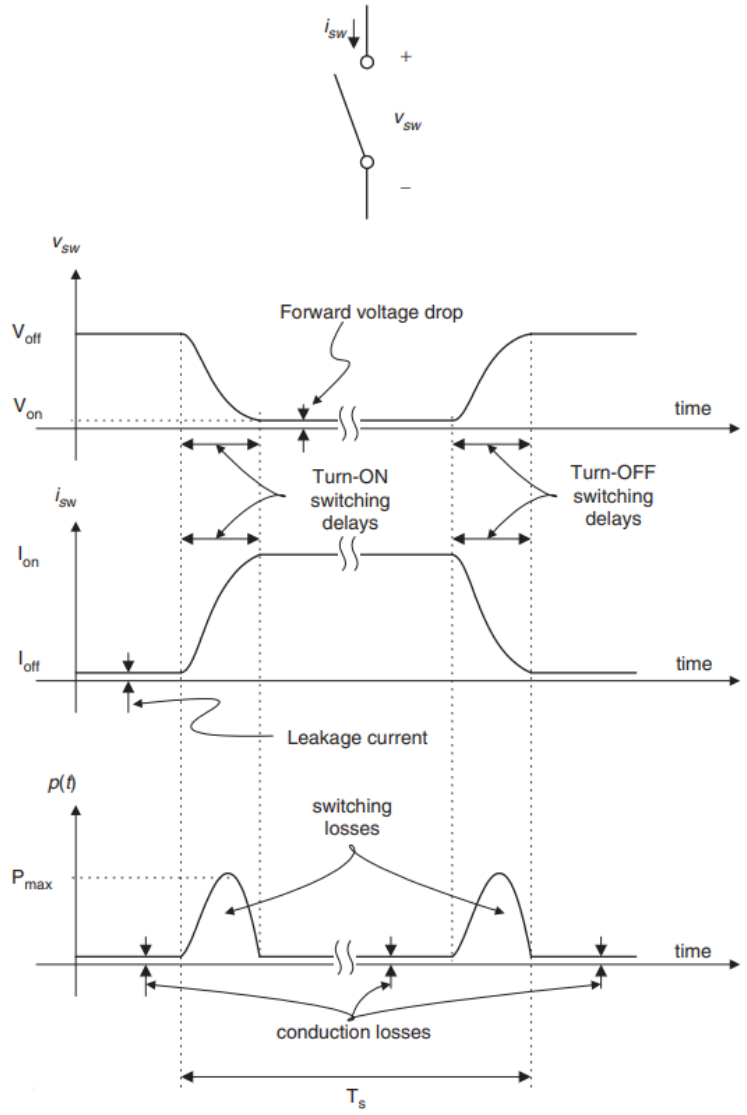

FIGURE 2.19: Voltage, current and power during a turn on-off cycle of an ideal switch. Source [16].

And if the current is constant during all the dead-time, the minimum dead-time can be found as:

$$t_{dead} > t_{dead,MIN}, \quad t_{dead,MIN} = \frac{2C_{oss}V_{ds}}{I_{ds}} \tag{2.36}$$

Where C_{oss} is the parasitic capacitance of each single MOSFET because they are seen in parallel from the point of view of the current that charge-discharge them.

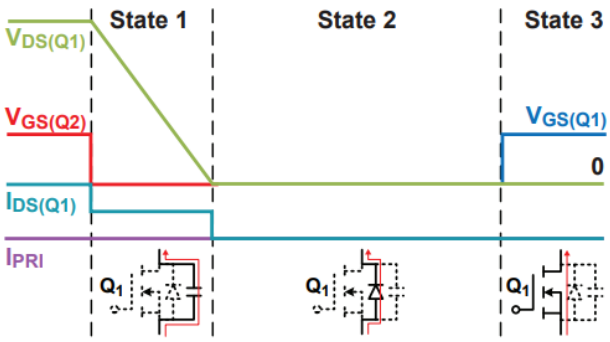

Figure 2.20: Gate and channel voltages, currents in the channel during a turn-on cycle. Source [10].

Body diode losses

Losses can happen in the body diode due to conduction and reverse recovery; conduction losses can be studied as:

$$P_{MOS,body\_conduction} = V_{body\_diode} I_{ds} (t_{dead} - t_{dead,MIN}) \tag{2.37}$$

Switching losses

Concluding this little part, it is possible to calculate switching losses as:

$$\begin{aligned} P_{MOS,switch} = & a \cdot (P_{MOS,turn-ON} + P_{MOS,turn-OFF} + \\ & + P_{MOS,body\_conduction} + P_{MOS,body\_recovery}) \end{aligned} \tag{2.38}$$

Where $a = 1$ if there is an half-bridge and $a = 2$ if there is a full-bridge inverter.

2.4.2 Magnetic elements losses

Inductors and transformer losses can be studied with same equations, considering the separate effects of conduction and core losses.

Conduction losses

In first approximation, as if the radius of the wire is less than skin depth, so that skin effect and proximity effects can be neglected:

$$r_{wire} < \delta(n) = \sqrt{\frac{2\rho_{cu}}{2\pi n f_{sw} \mu_0}} \tag{2.39}$$

Conduction losses can be calculated as:

$$P_{cond} = R_{DC} \cdot i^2_{L,RMS} \tag{2.40}$$

Core losses

Core losses can be instead computed using Steinmetz equation [21]:

$$P_{core} = k \cdot f_{sw}^{a} \cdot B^{b} \tag{2.41}$$

Were the coefficients k, a and b are given by the manufacturer of the used cores.

2.4.3 Rectifier losses

If the diode is studied using its simplified model, conduction losses can be studied as:

$$P_{diode} = b \cdot (V_{gamma} I_{o,medio} + R_{on} I_{o,RMS}^{2}) \tag{2.42}$$

Where $b = 2$ if there is a center-tap secondary, and $b = 4$ if a full-bridge rectifier is present.
If more precise calculations are needed, it is possible to add also recovery losses.

2.4.4 Capacitor losses

Losses in capacitor (resonant and output) can be studied using or the ESR or the loss angle, depending on the values present on the datasheet, as:

$$P_{capacitor} = ESR \cdot i_{C,RMS}^{2} = tan(\delta) X_c \cdot i_{C,RMS}^{2} = \frac{tan(\delta)}{2\pi f_{sw} C} \cdot i_{C,RMS}^{2} \tag{2.43}$$

Chapter 3

Mode solvers

This chapter presents in details the mathematical formulation used to study the modes and for each mode the following are included:

- Waveform calculation: they are computed solving the systems that describe each mode (presented in chapter 2) and the relative boundary conditions, this is done analytically for some modes and numerically for some others, generally speaking the boundary condition needed to solve the systems are:
  - Continuity of voltages on the resonant capacitor at the boundary of two states;
  - Continuity of current in resonant and magnetizing inductance at the boundary of two states;
  - Symmetry of all waveform due to the fact that it is assumed that waveform in the first and second half period are the same;
  - Zero output current at state changes.
- Boundaries evaluation; they are a set of equations useful to determine if the waveform obtained with previous points are consistent with the mode studied;
- Analytical calculation of important values that are useful for the loss calculation and/or for the design and choose of component for the converter (in appendix A):
  - RMS current in the tank (In MOSFETs, resonant capacitor, resonant inductor and in the primary of the transformer);
  - Current at turn-on and turn-off of the MOSFETs;
  - RMS current on the secondary side (diodes and secondary of the transformer);
  - Average current in the rectifying diodes;
  - RMS current on the output capacitor;
  - Peak voltage on the resonant capacitor;
  - Peak resonant current.

3.1 PN MODE

This section describes PN mode.

3.1.1 Waveforms calculation

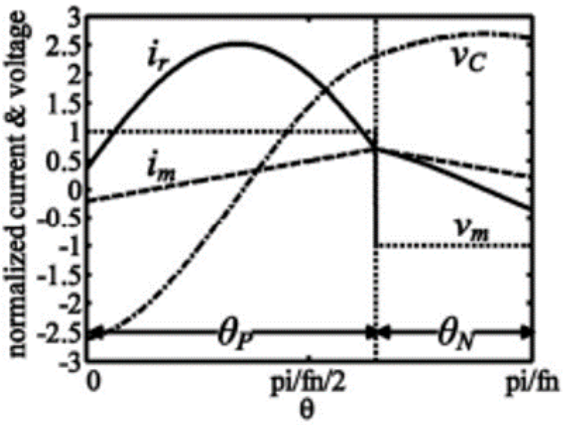

Figure 3.1: General waveforms of PN mode. Source [6].

The first part of the waveforms in figure 3.1 is a P-state, that can be described with equations 2.27, changing the name of the coefficients:

$$\begin{cases} v_{C_P}(t) = K_1 cos(\omega_r t) + K_2 sin(\omega_r t) + V_i - NV_o \\ i_{L_P}(t) = C_r \omega_r (-K_1 sin(\omega_r t) + K_2 cos(\omega_r t)) \\ v_{M_P}(t) = NV_o \\ i_{M_P}(t) = \frac{NV_o}{L_m} t + i_{M_P}(0) \\ i_{O_P}(t) = N[i_{L_P}(t) - i_{M_P}(t)] \end{cases} \tag{3.1}$$

While the second part is an N-state and can be described by equations 2.29 changing the coefficients and making a time translation, so that it begins when the other ends:

$$\begin{cases} v_{C_N}(t) = K_3 cos(\omega_r (t - t_1)) + K_4 sin(\omega_r (t - t_1)) + V_i + NV_o \\ i_{L_N}(t) = C_r \omega_r (-K_3 sin(\omega_r (t - t_1)) + K_4 cos(\omega_r (t - t_1))) \\ v_{M_N}(t) = -NV_o \\ i_{M_N}(t) = -\frac{NV_o}{L_m}(t - t_1) + i_{M_N}(t_1) \\ i_{O_N}(t) = N[i_{M_N}(t) - i_{L_N}(t)] \end{cases} \tag{3.2}$$

For this problem the unknowns are 7: $K_1, K_2, K_3, K_4, i_{M_P}(0), i_{M_N}(t_1), t_1$. This is possible to solve in close form (this means that given the values of the passives, of the input voltage and of the switching frequency, all parameters including output voltage

and all waveforms can be directly found), as stated in [12], where it is expressed in another notation; the result using the notation of this text are:

$$\begin{cases} K_1 = NV_o(m_C(0) - 1/M + 1) \\ K_2 = NV_o j_L(0) \\ K_3 = NV_o(m_C(\theta_3) - 1/M - 1) \\ K_4 = NV_o j_L(\theta_3) \\ i_{M_P}(0) = -I_{BASE} l\phi \\ i_{M_N}(t_1) = I_{BASE}\gamma l/2 \\ t_1 = (\gamma/2 - \phi)/\omega_0 \end{cases} \tag{3.3}$$

Where all the not known values are directly expressed in [12].

3.1.2 Boundaries with other modes

Looking at figure 2.17, it is possible to see that we have to distinguish PN-NP, PN-PO, PN-PON boundaries as well as the boundaries with lower frequency modes.

PN-NP boundary

This boundary is easy to study, because it is the unitary normalized frequency, so to be in PN mode:

$$f_{sw} < f_r = \frac{1}{2\pi\sqrt{L_r C_r}} \tag{3.4}$$

PN-PO, PN-PON boundary

These two boundaries are the same, the idea is that after P-state the converter doesn't have to go into O-state, but it must go into P-state. The voltage on the primary side, unequivocally determined the state in which the converter is:

- If $v_M > NV_o$ the converter is in P-state;
- If $v_M < -NV_o$ the converter is in N-state;
- If $-NV_o < v_M < NV_o$ the converter is in O-state.

It is possible to study what does it happen at the end of the P-state, studying as if there is a transition between P-state and O-state (illustrated in figure 3.2), but if in the hypothetical O-state, $v_M < -NV_o$ it means that the device went in N-state instead and the other diode started conducting:

$$\begin{gathered} v_M(t_1^+) < -NV_o \\ (V_i - v_C(t_1))\frac{L_m}{L_m + L_r} < -NV_o \end{gathered} \tag{3.5}$$

So we have to impose 3.5 to be sure to stay in PN mode.

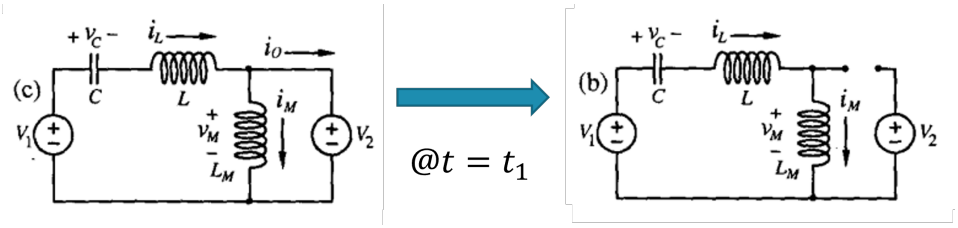

Figure 3.2: Passage from P to O state. Source [12].

Boundary with lower frequency modes

These modes happen if there are more than one P-state or N-state, in figure 3.3 a sketch of what it is intended to exclude with these conditions. To be in the good case we have to impose:

$$\begin{cases} i_M(0) < i_L(0) \\ i_M(\frac{T_s}{2}) > i_L(\frac{T_s}{2}) \\ \omega_r t_1 < \frac{3}{2}\pi \\ \omega_r(\frac{T_s}{2} - t_1) < \frac{3}{2}\pi \end{cases} \tag{3.6}$$

In which the two first conditions simply say that it starts in P-state and it ends in N-state, and the last two impose that for sure if the first two are true we are in the "first" P-state (checking if the system is in 3.3.a and not 3.3.c), since a complete P-state or N-state has a maximum angular duration of about π.

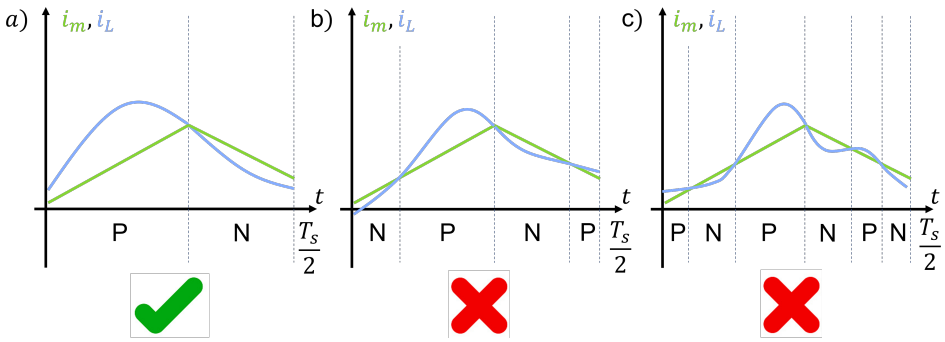

Figure 3.3: Sketch of unwanted waveforms.

3.1.3 Interesting values

The analytical calculation of the interesting values needed for the loss model is shown in appendix A.1.

3.2 NP MODE

This section studies the NP mode.

3.2.1 Waveforms calculation

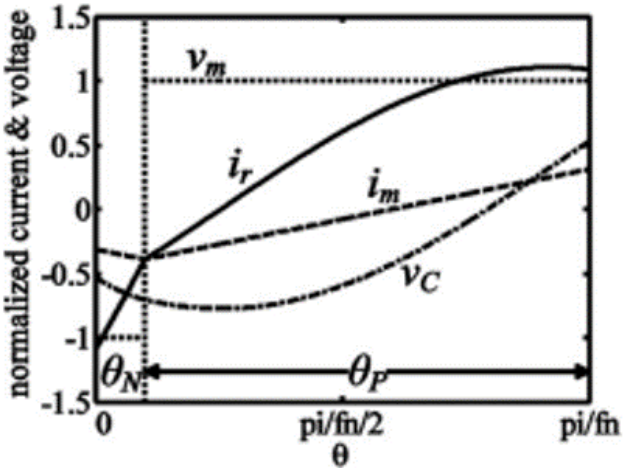

FIGURE 3.4: General waveforms of NP mode. Source [6].

The first part of the waveforms in figure 3.4 is a N-state, that can be described with equation 2.29, changing the name of the coefficients:

$$\begin{cases} v_{C_N}(t) = K_1 cos(\omega_r t) + K_2 sin(\omega_r t) + V_i + NV_o \\ i_{L_N}(t) = C_r \omega_r (-K_1 sin(\omega_r t) + K_2 cos(\omega_r t)) \\ v_{M_N}(t) = -NV_o \\ i_{M_N}(t) = -\frac{NV_o}{L_m} t + i_{M_N}(0) \\ i_{O_N}(t) = N[i_{M_N}(t) - i_{L_N}(t)] \end{cases} \tag{3.7}$$

While the second part is an P-state and can be described by equations 2.27 changing the coefficients and making a time translation, so that it begins when the other ends:

$$\begin{cases} v_{C_P}(t) = K_3 cos(\omega_r (t - t_1)) + K_4 sin(\omega_r (t - t_1)) + V_i - NV_o \\ i_{L_P}(t) = C_r \omega_r (-K_3 sin(\omega_r (t - t_1)) + K_4 cos(\omega_r (t - t_1))) \\ v_{M_P}(t) = +NV_o \\ i_{M_P}(t) = \frac{NV_o}{L_m}(t - t_1) + i_{M_P}(t_1) \\ i_{O_P}(t) = N[i_{L_P}(t) - i_{M_P}(t)] \end{cases} \tag{3.8}$$

Also for this problem the unknowns are 7: $K_1, K_2, K_3, K_4, i_{M_N}(0), i_{M_P}(t_1), t_1$. Similarly to PN mode, it is possible to solve in close form also this mode (this

means that given the values of the passives, of the input voltage and of the switching frequency, all parameters including output voltage and all waveforms can be directly found), as stated in [12], where it is expressed in another normalization; the result using the normalization of this text are:

$$\begin{cases} K_1 = NV_o(m_C(0) - 1/M - 1) \\ K_2 = NV_o j_L(0) \\ K_3 = NV_o(m_C(\theta_1) - 1/M + 1) \\ K_4 = NV_o j_L(\theta_3) \\ i_{M_N}(0) = -I_{BASE} l\phi \\ i_{M_P}(t_1) = -I_{BASE}\gamma l/2 \\ t_1 = (\gamma/2 - \phi)/\omega_0 \end{cases} \tag{3.9}$$

Where all the not known values are directly expressed in [12].

3.2.2 Boundaries with other modes

Looking at figure 2.17 it is possible to see that we have to distinguish NP-PO, NP-PON, NP-PN and NP-NOP boundaries as well as the boundaries with lower frequency modes.

NP-PO, NP-PON, NP-PN boundary

These boundaries are the same and are easy to study, because they are the unitary normalized frequency, so to be in NP mode:

$$f_{sw} > f_r = \frac{1}{2\pi\sqrt{L_r C_r}} \tag{3.10}$$

NP-NOP boundary

As stated in the previous section, it is possible to unequivocally determine the state of the converter looking at the primary side voltage:

- If $v_M > NV_o$ the converter is in P-state;
- If $v_M < -NV_o$ the converter is in N-state;
- If $-NV_o < v_M < NV_o$ the converter is in O-state.

It is possible to study what happens at the end of the N-state, studying as if there is a transition between N-state and O-state (presented in figure 3.5), but if in the hypothetical O-state, $v_M > NV_o$ it means that the device went in P-state instead, and the other diode started conducting:

$$v_M(t_1^+) > NV_o$$

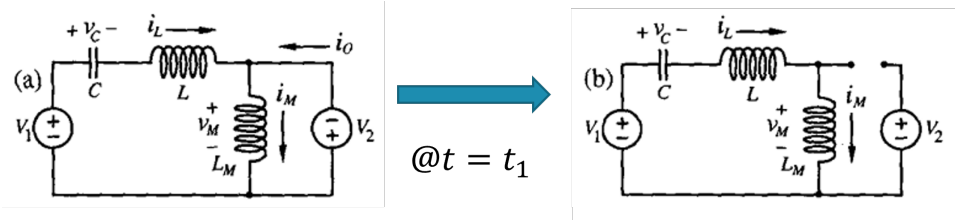

FIGURE 3.5: Passage from N to O state. Source [12].

$$(V_i - v_C(t_1))\frac{L_m}{L_m + L_r} > NV_o \tag{3.11}$$

So we have to impose 3.11 to be sure to stay in NP mode.

Boundary with lower frequency modes

The reasoning is the same made with PN mode, in figure 3.6 a sketch of what is intended to exclude with these conditions. To be in the good case we have to impose:

$$\begin{cases} i_M(0) > i_L(0) \\ i_M(\frac{T_s}{2}) < i_L(\frac{T_s}{2}) \\ \omega_r t_1 < \frac{3}{2}\pi \\ \omega_r(\frac{T_s}{2} - t_1) < \frac{3}{2}\pi \end{cases} \tag{3.12}$$

In which the two first conditions simply say that it starts in N-state and ends in P-state, and the last two impose that for sure if the first two are true we are in the "first" N-state (checking if the system is in 3.6.a and not 3.6.c), since a complete P-state or N-state has a maximum angular duration of about π.

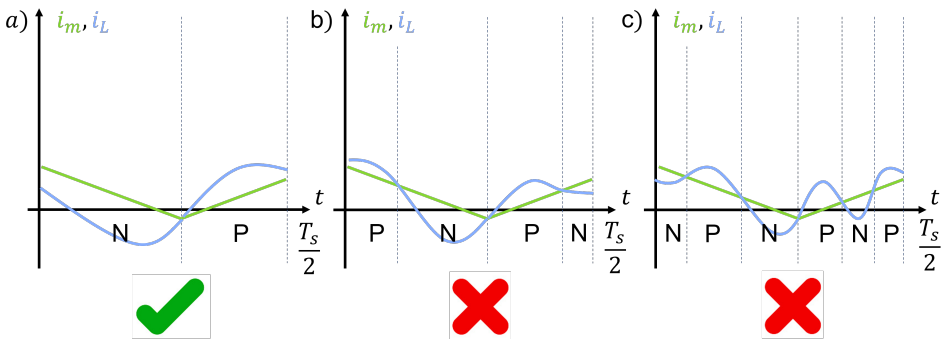

FIGURE 3.6: Sketch of unwanted waveforms.

3.2.3 Interesting values

The analytical calculation of the interesting values needed for the loss model is shown in appendix A.2.

3.3 PO MODE

This section studies PO mode.

3.3.1 Waveforms calculation

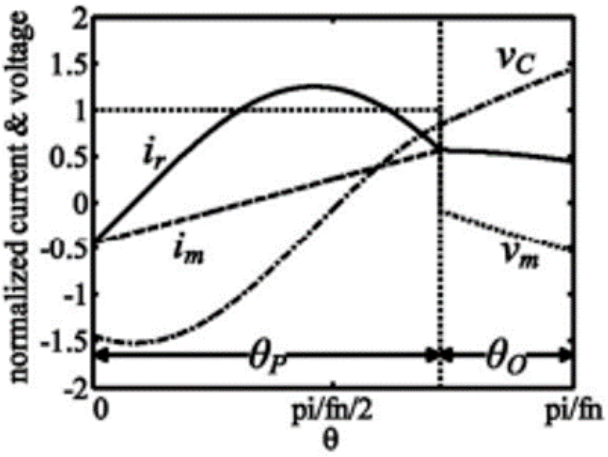

Figure 3.7: General waveforms of PO mode. Source [6].

The first part of the waveforms in figure 3.1 is a P-state, that can be described with equation 2.27, changing the name of the coefficients:

$$\begin{cases} v_{C_P}(t) = K_1 cos(\omega_r t) + K_2 sin(\omega_r t) + V_i - NV_o \\ i_{L_P}(t) = C_r \omega_r (-K_1 sin(\omega_r t) + K_2 cos(\omega_r t)) \\ v_{M_P}(t) = NV_o \\ i_{M_P}(t) = \frac{NV_o}{L_m} t + i_{M_P}(0) \\ i_{O_P}(t) = N[i_{L_P}(t) - i_{M_P}(t)] \end{cases} \tag{3.13}$$

While the second part is an O-state and it can be described by equations 2.31 changing the coefficients and making a time translation, so that it begins when the

other ends:

$$\begin{cases} v_{C_O}(t) = K_3 cos(\omega_m(t-t_1)) + K_4 sin(\omega_m(t-t_1)) + V_i \\ i_{L_O}(t) = C_r\omega_m(-K_3 sin(\omega_m(t-t_1)) + K_4 cos(\omega_m(t-t_1))) \\ v_{M_O}(t) = \frac{L_m}{L_m+L_r}(-K_3 cos(\omega_m(t-t_1)) - K_4 sin(\omega_m(t-t_1)) \\ i_{M_O}(t) = i_{L_O}(t) \\ i_{O_O}(t) = i_{M_O}(t) - i_{L_O}(t) = 0 \end{cases} \tag{3.14}$$

For this problem the unknowns are 6: $K_1, K_2, K_3, K_4, i_{M_P}(0), t_1$. The article [20] derives direct formulas for all these value except for t_1:

$$\begin{cases} K_1 = \frac{2NC_rR_LV_oV_if_{sw} - C_rR_LV_i^2f_{sw} - V_o^2}{2C_rR_LV_if_{sw}} \\ K_2 = \frac{NV_ot_1\omega_r}{K(cos(t_1\omega_r))-1} + sin(t_1\omega_r)\frac{2C_rR_LNV_oV_ff_{sw} - V_o^2}{2R_Lf_{sw}C_rV_i(cos(t_1\omega_r)-1)} \\ K_3 = K_1 cos(t_1\omega_r) + K_2 sin(t_1\omega_r) - NV_o \\ K_4 = \sqrt{(\frac{L_m}{L_r}+1)}(-K_1 sin(t_1\omega_r) + K_2 cos(t_1\omega_r)) \\ i_{M_P}(0) = K_2C_r\omega_r \end{cases} \tag{3.15}$$

Then [20] proposes a numerical solution to find t_1; it consist in finding the zero of the following equation, in which the only unknown is θ knowing that $t_1\omega_r = \theta$:

$$\begin{aligned} &C_r(8N^2R_LV_iV_of_{sw} - 4NR_LV_i^2f_{sw} + NR_LV_i^2f_{sw}\theta^2 + 4NR_LV_i^2f_{sw}cos(\theta) \\ &+ 2N^2R_LV_iV_of_{sw}\theta^2 - 8N^2R_LV_iV_ocos(\theta) + NR_LV_i^2f_{sw}\theta^2cos(\theta) + \\ &+ 2N^2R_LV_iV_of_{sw}\theta^2cos(\theta) - 8N^2R_LV_iV_of_{sw}\theta sin(\theta)) - (4NV_o^2 - 2V_iV_o + NV_o^2\theta^2 + \\ &- 4NV_o^2cos(\theta) + 2V_iV_ocos(\theta) + NV_o^2\theta^2cos(\theta) - 4NV_o^2\theta sin(\theta)) = 0 \end{aligned} \tag{3.16}$$

All these information are enough to find the waveforms of this mode.

3.3.2 Boundaries with other modes

Looking at figure 2.17 is possible to see that we have to distinguish PO-NP, PO-PN, PO-OPO, and PO-PON boundaries. It is also needed to study the boundary between PO and an hypothetical NPO mode.

PO-NP boundary

This boundary is the easiest to study, because it is the unitary normalized frequency, so to be in PO mode:

$$f_{sw} < f_r = \frac{1}{2\pi\sqrt{L_rC_r}} \tag{3.17}$$

PO-PN boundary

This boundary is the same already studied in section 3.1 for the PN mode, so it is only needed to change the sign of equation 3.5:

$$(V_i - v_C(t_1))\frac{L_m}{L_m+L_r} > -NV_o \tag{3.18}$$

PO-OPO boundary

To find this boundary it is needed to study the passage from the O-state in the first half period (with positive V_i) and the P-state in the second half (with negative V_i). With a similar reasoning of the ones done in previous sections, it's possible to characterize this boundary checking if the voltage across the magnetizing inductance after the transition from $+V_i$ to $-V_i$ in the hypothetical O-state is such that the system goes into P-state. The studied transition is present in figure 3.8.

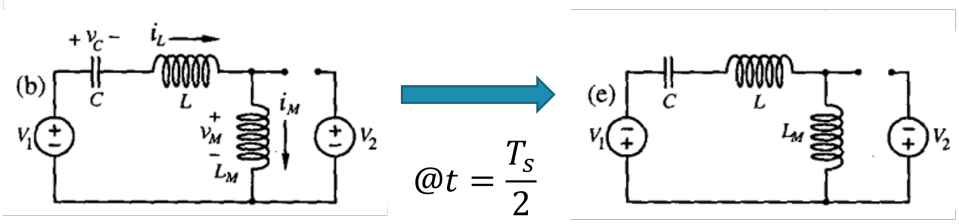

Figure 3.8: Passage from two O state with different input voltage. Source [12].

$$v_M(\frac{T_s}{2}^+) > NV_o$$
$$(-V_i - v_C(t_1))\frac{L_m}{L_m + L_r} > NV_o \tag{3.19}$$

Equation 3.19 is useful to check this boundary.

PO-PON boundary

In this case it's needed to check that in all the O-state, the voltage across the magnetizing ($v_{M_O}(t)$, presented in equation 3.14) never goes below $-V_oN$:

$$v_M(t) > -NV_o, \qquad \forall t \in [t_1; T_s/2] \tag{3.20}$$

That is equal to:

$$v_{M,min}(t) > -NV_o, \qquad t \in [t_1; T_s/2] \tag{3.21}$$

The algorithm in appendix B.5 is useful to find $v_{M,min}$, using the values present in table 3.1.

PO-NPO boundary

To be in PO mode, the resonant current needs to be higher than the magnetizing current from the beginning, and since at the start of the interval they are the same, is sufficient to impose:

$$\left.\frac{di_{L_P}(t)}{dt}\right|_{t=0} > \left.\frac{di_{M_P}(t)}{dt}\right|_{t=0} \tag{3.22}$$

Coefficient	Value for $v_{M,min}$
C_1	$-K_4 L_m/(L_m + L_r)$
C_2	$-K_3 L_m/(L_m + L_r)$
C_3	0
t_{begin}	t_1
t_{end}	$T_s/2 - t_1$
ω	ω_m

TABLE 3.1: Coefficient for minimum voltage on magnetizing inductance in PO mode.

$$\frac{d}{dt}(C_r\omega_r(-K_1 sin(\omega_r t) + K_2 cos(\omega_r t)))\Big|_{t=0} > \frac{d}{dt}(\frac{NV_o}{L_m}t + i_{M_P}(0))\Big|_{t=0} \tag{3.23}$$

So:

$$C_r\omega_r(-\omega_r K_1 cos(\omega_r t) - \omega_r K_2 cos(\omega_r t))\Big|_{t=0} > \frac{NV_o}{L_m}\Big|_{t=0} \tag{3.24}$$

Then equation 3.25 is then useful to find this boundary:

$$-C_r\omega_r^2 K_1 > \frac{NV_o}{L_m} \tag{3.25}$$

3.3.3 Interesting values

In appendix A.3 there is the analytical calculation of the interesting values needed for the loss model.

3.4 PON MODE

This section studies the PON mode.

3.4.1 Waveforms calculation

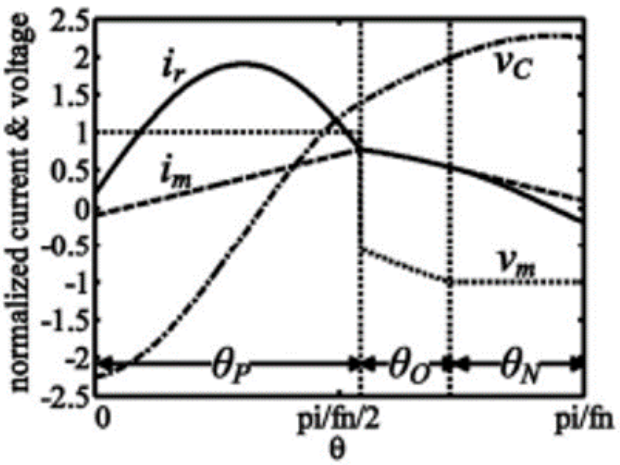

Figure 3.9: General waveforms of PON mode. Source [6].

In the first interval the system is in P-state (equations 2.27):

$$\begin{cases} v_{C_P}(t) = K_1 cos(\omega_r t) + K_2 sin(\omega_r t) + V_i - NV_o \\ i_{L_P}(t) = C_r \omega_r (-K_1 sin(\omega_r t) + K_2 cos(\omega_r t)) \\ v_{M_P}(t) = NV_o \\ i_{M_P}(t) = \frac{NV_o}{L_m} t + i_{M_P}(0) \\ i_{O_P}(t) = i_{L_P}(t) - i_{M_P}(t) \end{cases} \tag{3.26}$$

In the second it is in O-state (equations 2.31 with time translation):

$$\begin{cases} v_{C_O}(t) = K_3 cos(\omega_m (t - t_1)) + K_4 sin(\omega_m (t - t_1)) + V_i \\ i_{L_O}(t) = C_r \omega_m (-K_3 sin(\omega_m (t - t_1)) + K_4 cos(\omega_m (t - t_1))) \\ v_{M_O}(t) = \frac{L_m}{L_m + L_r} (-K_3 cos(\omega_m (t - t_1)) - K_4 sin(\omega_m (t - t_1)) \\ i_{M_O}(t) = i_{L_O}(t) \\ i_{O_O}(t) = i_{M_O}(t) - i_{L_O}(t) = 0 \end{cases} \tag{3.27}$$

While in the last part, the system is in P-state (equations 2.29 with time transla-

tion):

$$\begin{cases} v_{C_N}(t) = K_5 cos(\omega_r(t - T_s/2)) + K_6 sin(\omega_r(t - T_s/2)) + V_i + NV_o \\ i_{L_N}(t) = C_r\omega_r(-K_5 sin(\omega_r(t - T_s/2)) + K_6 cos(\omega_r(t - T_s/2))) \\ v_{M_N}(t) = -NV_o \\ i_{M_N}(t) = -\frac{NV_o}{L_m}(t - t_2) + i_{M_N}(t_2) \\ i_{O_N}(t) = i_{M_N}(t) - i_{L_N}(t) \end{cases} \tag{3.28}$$

Looking at the describing equations, is possible to see that there are 10 unknowns: $K_1, K_2, K_3, K_4, K_5, K_6, i_{M_P}(0), i_{M_N}(t_2), t_1, t_2$. To have easier understanding of the mathematical expressions, the time duration of each state (t_N, t_O and t_P) are used instead of t_1 and t_2, so the number of unknowns increased up to 11. To solve the system, the following are the boundary conditions are imposed:

- Continuity of the current in the resonant inductance
  ($i_{L_P}(t_1) = i_{L_O}(t_1)$, $i_{L_O}(t_2) = i_{L_N}(t_2)$);
- Conditions that state the boundaries of the O-interval
  ($i_{L_P}(t_1) = i_{M_P}(t_1)$, $i_{L_N}(t_2) = i_{M_N}(t_2)$);
- Continuity of the voltage across the resonant capacitor
  ($v_{C_P}(t_1) = v_{C_O}(t_1)$, $v_{C_O}(t_2) = v_{C_N}(t_2)$);
- Symmetry for i_L, i_M and v_C
  ($i_{L_P}(0) = -i_{L_N}(T_s/2)$, $i_{M_P}(0) = -i_{M_N}(T_s/2)$, $v_{C_P}(0) = -v_{C_N}(T_s/2) + V_i$);
- Beginning of the N-interval ($v_{M_O}(t_2) = -NV_o$);
- Total duration of the half period ($t_P + t_O + t_N = T_s/2$).

The relative non-linear equation's system in expressed in 3.29:

$$\begin{cases} C_r\omega_r(-K_1 sin(\omega_r t_P) + K_2 cos(\omega_r t_P)) = C_r\omega_m K_4 \\ C_r\omega_m(-K_3 sin(\omega_m t_O) + K_4 cos(\omega_m t_O)) = C_r\omega_r(-K_5 sin(-\omega_r t_N) + K_6 cos(-\omega_r t_N)) \\ C_r\omega_r(-K_1 sin(\omega_r t_P) + K_2 cos(\omega_r t_P)) = \frac{V_o N}{L_m} t_P + i_{M_P}(0) \\ C_r\omega_r(-K_5 sin(-\omega_r t_N) + K_6 cos(-\omega_r t_N)) = i_{M_N}(t_2) \\ K_1 cos(\omega_r t_P) + K_2 sin(\omega_r t_P) + V_i - NV_o = K_3 + V_i \\ K_3 cos(\omega_m t_O) + K_4 sin(\omega_m t_O) + V_i = K_5 cos(-\omega_r t_N) + K_6 sin(-\omega_r t_N) + V_i + NV_o \\ C_r\omega_r K_2 = -C_r\omega_r K_6 \\ i_{M_P}(0) = -i_{M_N}(t_2) + \frac{V_o N}{L_m} t_N \\ K_1 + V_i - NV_o = -(K_5 + V_i + NV_o) + V_i \\ \frac{L_m}{L_m + L_r}(-K_3 cos(\omega_m t_O) - K_4 sin(\omega_m t_O)) = -V_o N \\ t_P + t_O + t_N = \frac{T_s}{2} \end{cases} \tag{3.29}$$

This system is then solved using numerical methods to have waveform on which apply the formulas to find the values of interest.

3.4.2 Boundaries with other modes

Looking at figure 2.17 is possible to see this mode is confined by NP, PN and PO mode.

PON-NP boundary

The threshold between the two is the unitary normalized frequency:

$$f_{sw} < f_r = \frac{1}{2\pi\sqrt{L_r C_r}} \tag{3.30}$$

PON-PN and PON-PO boundary

Since it's a numerical solution method, even if the system is in PN or PO mode the solver can converge, having a O-state or N-state duration very small, to detect so two thresholds are implemented and equations 3.31 and 3.32 can be used to check if the solution is in PON:

$$t_O > \frac{1}{100} T_s \tag{3.31}$$

$$t_N > \frac{1}{100} T_s \tag{3.32}$$

O-duration check

Once the solution of the solver is computed, a check of the duration of the O-interval is necessary, in order to see that during the O-interval the voltage across the magnetizing inductance doesn't exit its limits $[-NV_o; NV_o]$ as it's sketched in figure 3.10.

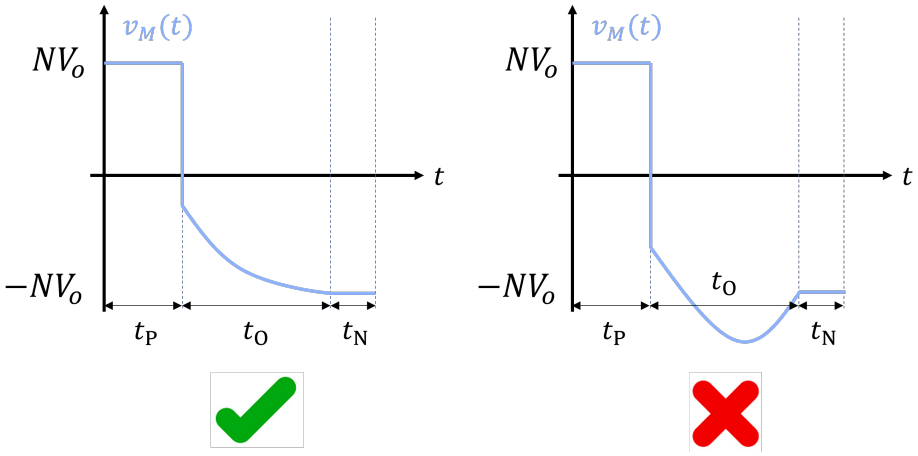

Figure 3.10: Sketch of O-interval duration problem.

As derived in appendix B.5 the timing of the minimum in the O-interval is:

$$t_{zero} = \frac{1}{\omega} tan^{-1}(\frac{C_1}{C_2}) = \frac{1}{\omega_m} tan^{-1}(\frac{K_4}{K_3}) \tag{3.33}$$

So it's needed to check if:

$$t_O < t_{zero} = \frac{1}{\omega_m} tan^{-1}(\frac{K_4}{K_3}) \tag{3.34}$$

3.4.3 Interesting values

In appendix A.4 there is the analytical calculation of the interesting values needed for the loss model.

3.5 NOP MODE

This section studies NOP mode.

3.5.1 Waveforms calculation

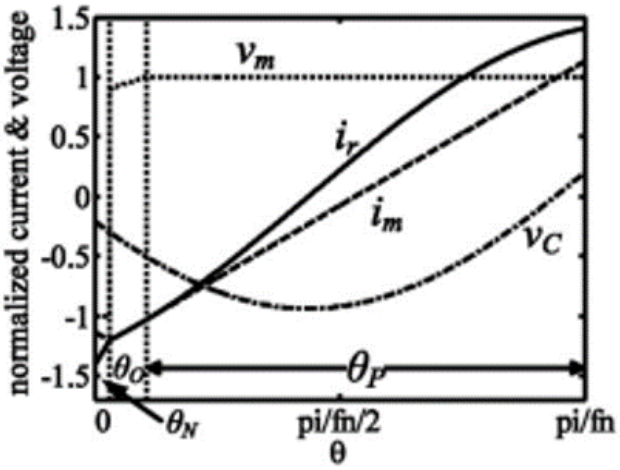

Figure 3.11: General waveforms of NOP mode. Source [6].

In the first interval the system is in N-state (equations 2.29):

$$\begin{cases} v_{C_N}(t) = K_1 cos(\omega_r t) + K_2 sin(\omega_r t) + V_i + NV_o \\ i_{L_N}(t) = C_r \omega_r (-K_1 sin(\omega_r t) + K_2 cos(\omega_r t)) \\ v_{M_N}(t) = -NV_o \\ i_{M_N}(t) = -\frac{NV_o}{L_m} t + i_{M_N}(0) \\ i_{O_N}(t) = i_{M_N}(t) - i_{L_N}(t) \end{cases} \tag{3.35}$$

In the second it is in O-state (equations 2.31 with time translation):

$$\begin{cases} v_{C_O}(t) = K_3 cos(\omega_m (t - t_1)) + K_4 sin(\omega_m (t - t_1)) + V_i \\ i_{L_O}(t) = C_r \omega_m (-K_3 sin(\omega_m (t - t_1)) + K_4 cos(\omega_m (t - t_1))) \\ v_{M_O}(t) = \frac{L_m}{L_m + L_r} (-K_3 cos(\omega_m (t - t_1)) - K_4 sin(\omega_m (t - t_1)) \\ i_{M_O}(t) = i_{L_O}(t) \\ i_{O_O}(t) = i_{M_O}(t) - i_{L_O}(t) = 0 \end{cases} \tag{3.36}$$

While in the last part the system is in P-state (equations 2.27 with time transla-

tion):

$$\begin{cases} v_{C_P}(t) = K_5 cos(\omega_r(t - T_s/2)) + K_6 sin(\omega_r(t - T_s/2)) + V_i - NV_o \\ i_{L_P}(t) = C_r\omega_r(-K_5 sin(\omega_r(t - T_s/2)) + K_6 cos(\omega_r(t - T_s/2))) \\ v_{M_P}(t) = NV_o \\ i_{M_P}(t) = \frac{NV_o}{L_m}(t - t_2) + i_{M_P}(t_2) \\ i_{O_P}(t) = i_{L_P}(t) - i_{M_P}(t) \end{cases} \tag{3.37}$$

Looking at the describing equations, it is possible to see that there are 10 unknowns: $K_1, K_2, K_3, K_4, K_5, K_6, i_{M_N}(0), i_{M_P}(t_2), t_1, t_2$. To have easier understanding of the mathematical expressions, the time durations of each state (t_N, t_O and t_P) are used instead of t_1 and t_2, so the number of unknowns increased up to 11. To solve the system, the following boundary conditions are imposed:

- Continuity of the current in the resonant inductance ($i_{L_N}(t_1) = i_{L_O}(t_1)$, $i_{L_O}(t_2) = i_{L_P}(t_2)$);
- Conditions that state the boundaries of the O-interval ($i_{L_N}(t_1) = i_{M_N}(t_1)$, $i_{L_P}(t_2) = i_{M_P}(t_2)$);
- Continuity of the voltage across the resonant capacitor ($v_{C_N}(t_1) = v_{C_O}(t_1)$, $v_{C_O}(t_2) = v_{C_P}(t_2)$);
- Symmetry for i_L, i_M and v_C ($i_{L_N}(0) = -i_{L_P}(T_s/2)$, $i_{M_N}(0) = -i_{M_P}(T_s/2)$, $v_{C_N}(0) = -v_{C_P}(T_s/2) + V_i$);
- Beginning of the P-interval ($v_{M_O}(t_2) = NV_o$);
- Total duration of the half period ($t_N + t_O + t_P = T_s/2$).

The resulting non-linear equation's system is 3.38:

$$\begin{cases} C_r\omega_r(-K_1 sin(\omega_r t_N) + K_2 cos(\omega_r t_N)) = C_r\omega_m K_4 \\ C_r\omega_m(-K_3 sin(\omega_m t_O) + K_4 cos(\omega_m t_O)) = C_r\omega_r(-K_5 sin(-\omega_r t_P) + K_6 cos(-\omega_r t_P)) \\ C_r\omega_r(-K_1 sin(\omega_r t_N) + K_2 cos(\omega_r t_N)) = -\frac{V_o N}{L_m} t_N + i_{M_N}(0) \\ C_r\omega_r(-K_5 sin(-\omega_r t_P) + K_6 cos(-\omega_r t_P)) = i_{M_P}(t_2) \\ K_1 cos(\omega_r t_N) + K_2 sin(\omega_r t_N) + V_i + NV_o = K_3 + V_i \\ K_3 cos(\omega_m t_O) + K_4 sin(\omega_m t_O) + V_i = K_5 cos(-\omega_r t_P) + K_6 sin(-\omega_r t_P) + V_i - NV_o \\ C_r\omega_r K_2 = -C_r\omega_r K_6 \\ i_{M_N}(0) = -i_{M_P}(t_2) - \frac{V_o N}{L_m} t_P \\ K_1 + V_i + NV_o = -(K_5 + V_i - NV_o) + V_i \\ \frac{L_m}{L_m + L_r}(-K_3 cos(\omega_m t_O) - K_4 sin(\omega_m t_O)) = +V_o N \\ t_N + t_O + t_P = \frac{T_s}{2} \end{cases} \tag{3.38}$$

This system is then solved using numerical methods to have waveform on which apply the formulas to find the values of interest.

3.5.2 Boundaries with other modes

Looking at figure 2.17 it is possible to see that this mode is confined by NP and OP mode.

NOP-NP and NOP-OP boundary

Since it's a numerical solution method, even if the system is in NP or OP mode the solver can converge, having a O-state or N-state duration very small, to detect so two thresholds are implemented and equations 3.39 and 3.40 can be used to check if the solution is in NOP:

$$t_O > \frac{1}{100} T_s \tag{3.39}$$

$$t_N > \frac{1}{100} T_s \tag{3.40}$$

O-duration check

Once the solution of the solver is computed, a check of the duration of the O-interval is necessary, in order to see that during the O-interval the voltage across the magnetizing inductance doesn't exit its limits $[-NV_o; NV_o]$ as it's sketched in figure 3.12.

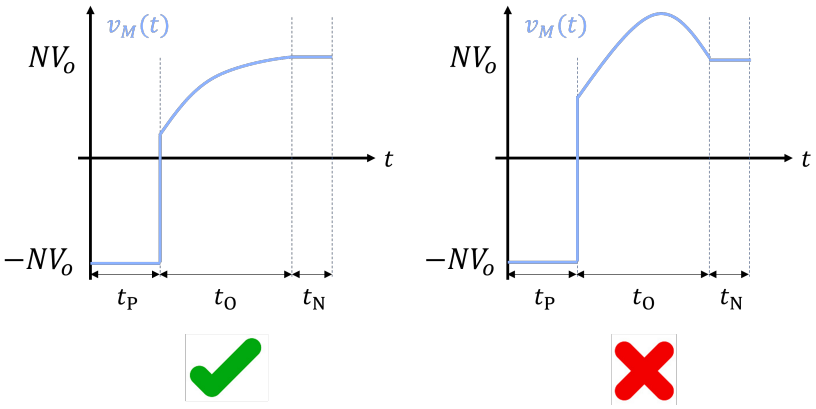

Figure 3.12: Sketch of O-interval duration problem.

As derived in appendix B.5 the timing of the minimum in the O-interval is:

$$t_{zero} = \frac{1}{\omega} tan^{-1}\left(\frac{C_1}{C_2}\right) = \frac{1}{\omega_m} tan^{-1}\left(\frac{K_4}{K_3}\right) \tag{3.41}$$

So it's needed to check if:

$$t_O < t_{zero} = \frac{1}{\omega_m} tan^{-1}\left(\frac{K_4}{K_3}\right) \tag{3.42}$$

3.5.3 Interesting values

The analytical calculation of the interesting values needed for the loss model is shown in appendix A.5.

3.6 Conclusion

This chapter explains all the mathematical treatment that will be applied in chapter 4 to implement the single solvers and the main solver.

Chapter 4

Main solver and simulation environment

This chapter explains the idea behind the main program that has been realized and its implementation.
In each section a part of that is analyzed and in the last part the used simulation environment is shown.
Here there is a short introduction about how this main solver works:
initially, during the execution of the main solver, a big number of set of input values is generated.
Each set can be interpreted as a vector of four values that represent the passives of the converter, in fact, it contains:

- L_r: value of the resonant inductance;
- L_m: value of the magnetizing inductance;
- C_r: value of the resonant capacitance;
- N: value of the transformer turn ratio.

Each of this set, together with the values of the parasitic and non-ideal elements (that are fixed), is given to the different solvers to understand what is the operating mode with that set of passives values, and then to compute the waveforms of that mode. In the case studied in this thesis, the efficiency is the figure of merit that is wanted to investigate, so a loss calculation is performed.
To do so, with the formulas derived in appendix A and the loss model described in section 2.4 the losses are calculated.
Then all results that match with the wanted requirements, are collected in a database so that are easily accessible after the run of the program.
It's also needed to take into account that solvers for modes that have a close form are computationally fast, but the one that need to numerically solve systems of equation aren't, so to speed-up the calculation is needed to add some sub-scipts that can exclude, with low computational effort, some set of passives.

4.1 Elements needed for the general algorithm of the solver

Before explaining the algorithm of the main solver something else should be described:

- How the set of the passives are generated;
- What fixed values are needed;
- How does a solver for a single mode work;
- What are the considered elements in the loss model;
- How the database is generated;
- What are the methods used to exclude part of the set of parameter.

These are explained one by one in the next sections.

4.1.1 Input value generation

This section explains the proposed value generation method. The possible values are described here as vectors $(L_r[i], L_m[j], C_r[k], N[h])$.
Each solver tests all possible combinations with a code similar to the one present in listing 4.1.

Listing 4.1: MATLAB code for passive sets generation.

```
for i = 1:N_L
    for j = 1:N_Lm
        for k = 1:N_C
            for h = 1:N_n

                L=Lr_v(i);
                Lm=Lm_v(j);
                C=Cr_v(k);
                N=N_v(h);

                %Code for the solver
                ...
            end
        end
    end
end
```

Resonant inductance

For the resonant inductance the possible values are generated subdividing equally a certain number of values between a minimum and a maximum that is given as input of the solver, the input value needed are then:

- N_{L_r}, the number of tested values for the resonant inductance;
- $L_{r,min}$, the minimum value of the resonant inductance that is wanted to test, this value should not be too low, since in the real implementation, part of this inductance will be the leakage inductance of the transformer.
- $L_{r,max}$, this should not be too high since it could be difficult to make resonant inductor with too high inductance without having enormous cores or big core losses.

$$L_r[i] = \sum_{i=0}^{N_{L_r}-1} L_{r,min} + i(\frac{L_{r,min} - L_{r,min}}{N_{L_r}}) \tag{4.1}$$

Magnetizing inductance

Also for the magnetizing inductance the possible values are generated subdividing equally a certain number of values between a minimum and a maximum then:

- N_{L_m}, the number of tested values for the magnetizing inductance;
- $L_{m,min}$, the minimum value of the magnetizing inductance that is wanted to test, this limit can be given by possible realization problems of the transformer.
- $L_{m,max}$, this should not be too high since could be difficult to make resonant transformer with too high inductance without having enormous cores or big core losses.

$$L_m[j] = \sum_{i=0}^{N_{L_m}-1} L_{m,min} + i(\frac{L_{m,min} - L_{m,min}}{N_{L_m}}) \tag{4.2}$$

Resonant capacitance

Since the possible range for the resonant capacitance is bigger and due to the fact that it's a component that has fixed value imposed by the market, the tested values are divided according to the E12 series between a maximum and a minimum value:

- N_{C_r}, the number of tested values for the resonant capacitor;
- $C_{r,min}$, the minimum value of the resonant capacitor, that it should be bigger than parasitic capacitance that can be present in the circuit.
- $C_{r,max}$, the maximum value, limited by the available component on the market and their volume.

Transformer turn ratio

For the transformer values the formulas are slightly different in case the output voltage is higher or lower than the input voltage. The needed values are:

- N_N, the number of tested values for the turn ratio;
- N_{max}, a value that set the maximum, limited by construction problems that can occur.

If the output voltage is lower than the input voltage the following is used:

$$N[h] = \sum_{i=0}^{N_N-1} 1 + i(\frac{N_{max}}{N_N}) \tag{4.3}$$

While if output voltage is higher than the input voltage:

$$N[h] = \sum_{i=0}^{N_N-1} \frac{1}{1 + i(\frac{N_{max}}{N_N})} \tag{4.4}$$

4.1.2 Other values needed

The other values that describes the LLC converter and its non-idealities are fixed and have to be inserted at the beginning. This means that the choice of the parameters and components like the wanted input-output voltage relationship, the MOSFETs, the diodes and output capacitance should be done in advance. In table 4.1 these parameters are fully listed.

Input-output relationship	
V_i	DC input voltage
V_o	DC output voltage
R_L	Load resistance
f_{sw}	Switching frequency
MOSFETs non-idealities	
C_{ds}	Channel capacitance
R_{ch}	Channel resistance
t_{rise}	Rise time
t_{fall}	Fall time
$V_{\gamma,body}$	Forward voltage drop of body diode
Rectifying diodes non-idealities	
V_γ	Forward voltage drop
R_{diode}	ON resistance
Resonant inductor non-idealities	
R_{L_r}	AC resistance
Transformer non-idealities	
R_p	Primary side AC resistance
R_s	Secondary side AC resistance
Capacitors non-idealities	
$tan(\delta)_{C_r}$	Dissipation Factor of resonant capacitor
$ESR_{C_{out}}$	ESR of output capacitor

TABLE 4.1: Value needed as input for the solver.

4.1.3 Solvers algorithm

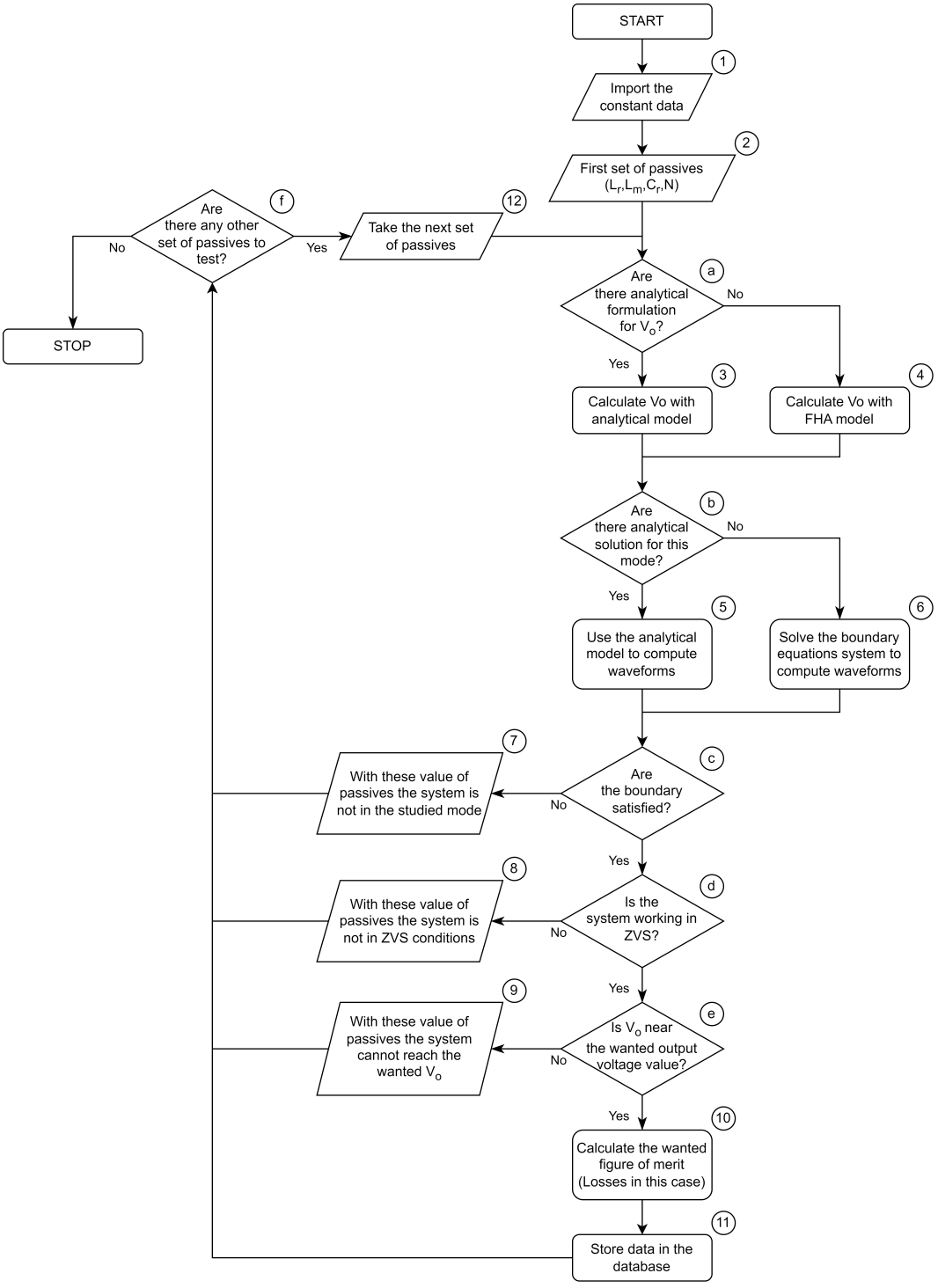

Figure 4.1: Flowchart of a generic solver.

For each mode a different, separate solver has been implemented in MATLAB, in this section the general algorithm that is applied for each solver separately is briefly explained. In figure 4.1 there is the flowchart and here some parts of it are explained more in details.

Processing blocks:

- **Block 1**: These are the data of table 4.1;
- **Blocks 2 and 12**: These are the values generated with the processes explained in section 4.1.1;
- **Block 3**: These modes are PN and NP;
- **Block 4**: Using the model derived in section 2.1;
- **Blocks 5 and 6**: The ones described in chapter 3;
- **Block 10**: Losses are calculated using the loss model described in section 2.4.

Decision blocks:

- **Block b**: The ones described in chapter 3 while checking the boundaries between the various modes;
- **Block d**: It is checked looking if formula 2.35 is satisfied and if the resulting dead time computed with 2.36 is not too long;
- **Block e**: Checks if the computed output voltage is near the wanted one, not the exact value, because it can be adjusted changing the switching frequency of the real implementation.

4.1.4 Loss model application

In the described implemented code the following losses have been implemented from section 2.4:

- MOSFETs turn-on losses;
- MOSFETs turn-off losses;
- MOSFETs conduction losses;
- Resonant inductor conduction losses;
- Resonant capacitor conduction losses;
- Transformer conduction losses;
- Rectifying diodes conduction losses;
- Output capacitor conduction losses.

4.1.5 Database

As shown from the flowchart, the suitable results are stored in a database, it is a CSV file that can be easily read using a spreadsheet software like EXCEL, the idea behind this is that after the run of the main program it is possible to compare in a fast way the obtained results to choose the most suitable for the wanted application.

4.1.6 Method to exclude some set of passives

This method is based on the FHA approximation and it consist in excluding the sets of passives that according to FHA analysis have output voltage that is far away the wanted one.
The sets for which the following is not valid are excluded:

$$K_{FHA,min}V_{o,wanted} < V_{o,FHA} < K_{FHA,max}V_{o,wanted} \tag{4.5}$$

4.2 Time consumption

In this section there are the results about time consumption and mode distribution of a run made in the condition of table 4.2.
In table 4.3 there are the results, from them it is possible to see the big time difference between analytical and numerical modes.
If the only run solvers are the simpler ones (PN,NP,PO) the number of results is still high and the time consumed is drastically reduced, so it could be used only these modes if time consumption needs to be low.

Nominal input voltage	$V_i = 380V$
Output voltage	$V_o = 24V$
Nominal load	$R_L = 1.92\Omega$
Nominal output current	$I_o = 12.5A$
Nominal output power	$P_{out} = 300W$
Minimum resonant inductance value	$L_{r,min} = 10\mu$
Maximum resonant inductance value	$L_{r,max} = 100\mu$
Minimum magnetizing inductance value	$L_{m,min} = 100\mu$
Maximum magnetizing inductance value	$L_{m,max} = 400\mu$
Minimum resonant capacitance value	$C_{r,min} = 1n$
Maximum resonant capacitance value	$C_{r,max} = 2.2\mu$
Number of tested values for resonant inductance	$N_{L_r} = 20$
Number of tested values for magnetizing inductance	$N_{L_m} = 30$
Number of tested values for resonant capacitance	$N_{C_r} = 41$
Number of tested values for transformer turn ratio	$N_N = 20$

Table 4.2: Specification used for the test of the solver.

Mode	Found sets of passives	Time used (s)
PN	62474	0.39
NP	209419	1.65
PO	28794	20.16
PON	4052	15879
NOP	651	330104
TOTAL	305390	346005.2

TABLE 4.3: Results of number of evaluated sets and time consumed.

4.3 General algorithm of the solver

In this section there is the explanation of the algorithm of the main solver.
Figure 4.2 shows the algorithm, it simply consist in running all the single solvers one by one, storing the useful data in the database.
After each single solver, the sets of passives for which the converter works in that mode are excluded for all the next solvers in order to reduce execution time.

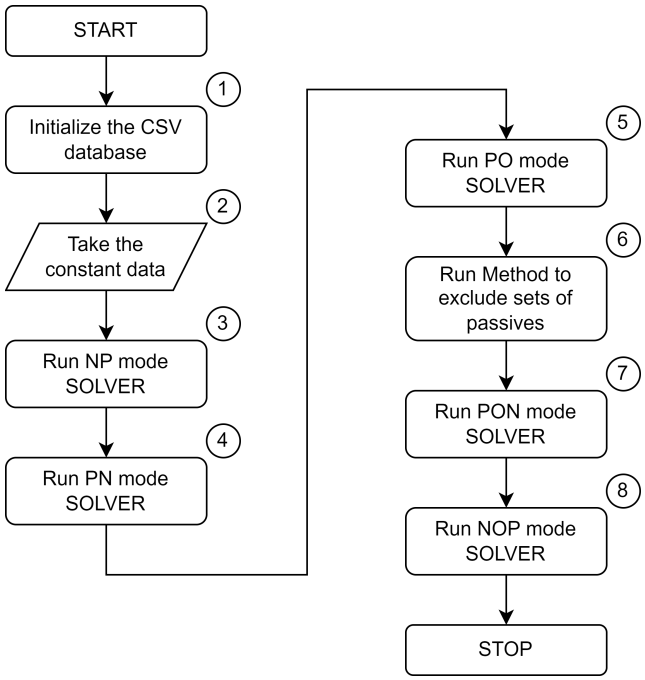

FIGURE 4.2: Flowchart of the main solver.

4.4 Simulation environment

In this section the two simulation environment used are briefly described. The choice was to use both Simulink and LTSPICE. Simulink because is directly linked with MATLAB, where the main program is developed and LTSPICE because it is faster and more intuitive.

4.4.1 SIMULINK MODEL

This model is shown in figure 4.3, it is made using the elements of the Simscape library [15] and is divided in parts:

- Red box: FHA model output voltage simulation in which the model in figure 2.12 is implemented;
- Yellow box: Large signal model of the converter is implemented (in black the elements of the converter);
- Blue boxes: here the measurements are performed and the waveforms are generated to be shown.

Calculated quantities

All the input parameter are shared between FHA and TDA models and can arrive directly from MATLAB workspace.

The computed quantities are the following, and they are obtained averaging over one period the instantaneous dissipated power of the element:

- Dissipated power by the high-side and the low-side MOSFETs;
- Dissipated power by the high-side and the low-side body diode;
- Dissipated power by the two rectifying diodes;
- Dissipated power by the resonant capacitor;
- Dissipated power by the resonant inductor (only resistive);
- Dissipated power by the primary and secondary side (only resistive since this losses are only simulated using a resistor on each side);
- Dissipated power in the output capacitor;
- Efficiency.

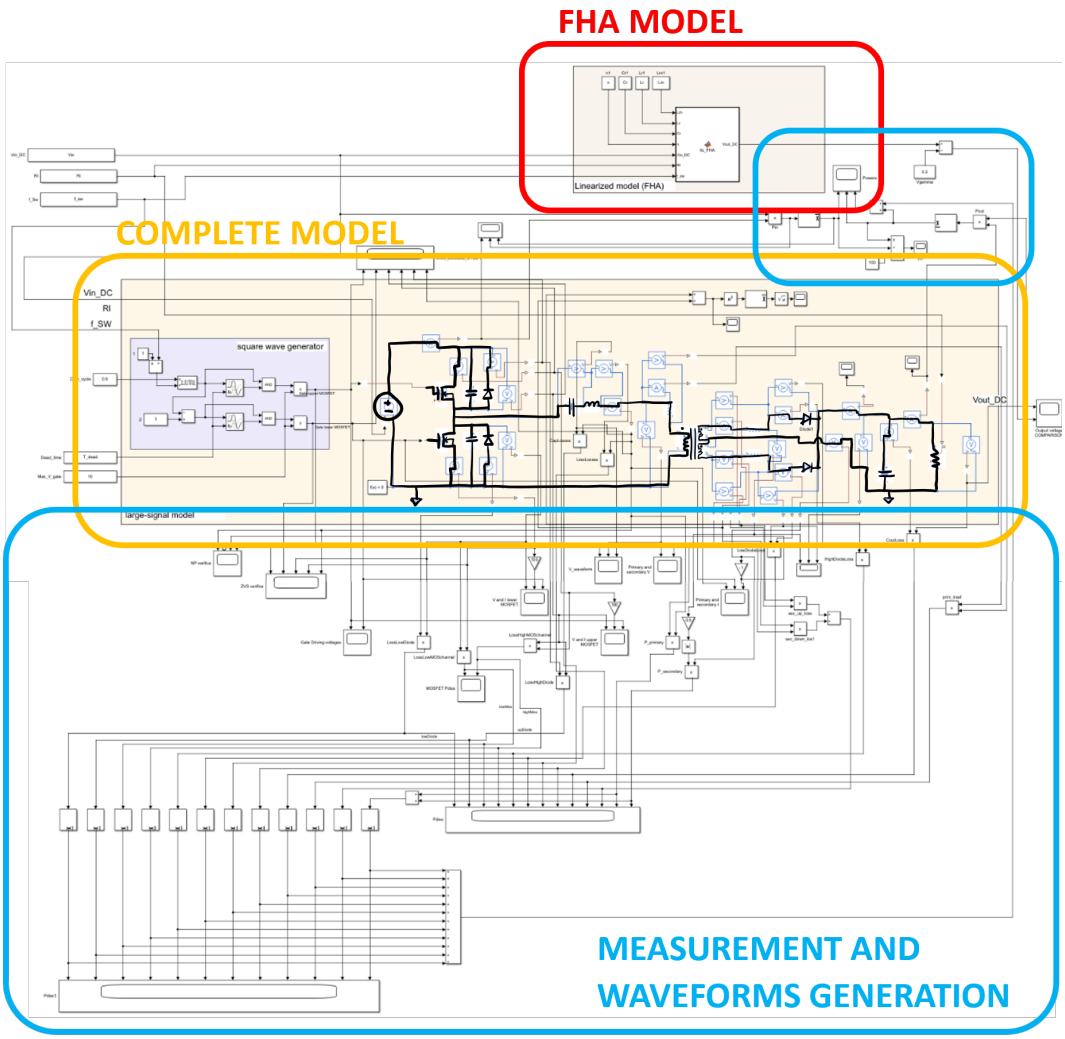

FIGURE 4.3: Complete model implemented in Simulink.

4.4.2 LTSPICE MODEL

The circuit has been implemented also in LTSPICE, in order to have a faster, easier and stand-alone simulation tool, it is shown in figure 4.4.

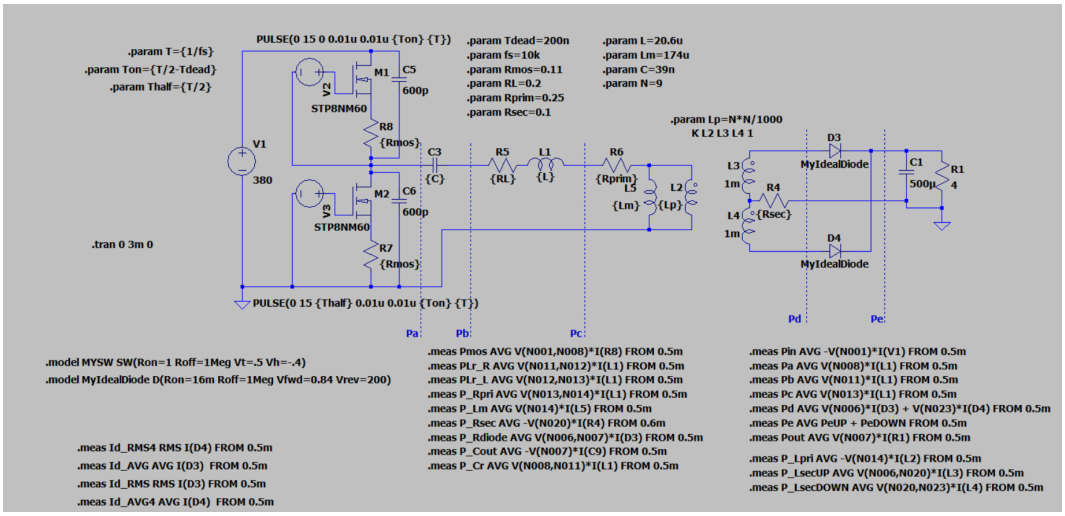

Figure 4.4: Complete model implemented in LTSPICE.

In this model all parasitic elements are explicit, to have a better control and understanding. Also in this case the losses are calculated integrating the instantaneous power of each element as explained in the previous section.

4.5 Conclusion

Thanks to this chapter, the mechanism of the main solver is explained, it can be then implemented in MATLAB using also the expressions in appendix and it can be used as a tool in the next chapter for the proposed design algorithm.

Chapter 5

Proposed algorithm and example of use

5.1 Proposed algorithm

The proposed algorithm is based on the solver described in the previous chapters and this are its steps:

1. Choose the input-output relationship that the converter needs to have (V_i, V_o, R_L);
2. Choose the frequency around which the converter would work in nominal conditions (f_{sw});
3. Choose MOSFETs according to the input voltage and current, then find from their datasheet the needed values to insert in the solver ($C_{ds}, R_{ch}, t_{rise}, t_{fall}, V_{\gamma,body}$);
4. Choose diodes according to the output current and reverse voltage that they have to resist, then find from the datasheet the needed values to insert in the solver (V_γ, R_{diode});
5. Choose output capacitor and from its datasheet take the ESR value to insert in the solver ($ESR_{C_{out}}$);
6. Make assumption about the ESR of the resonant capacitor, since the value of the capacitor is not decided yet (ESR_{C_r});
7. Make assumption on the resistance of the windings of the transformer and of the inductor that you think you are able to get (R_p, R_s, R_{L_r});
8. Choose the range of the passives according to the reasoning in section 4.1.1;
9. Run the main solver with all the parameters found in the previous steps;
10. Choose from the database of the possible outputs the most suitable design, basing the decision on the problems that can occur designing the magnetics (dimension of the cores, core losses).

5.2 Example

The algorithm was tested one time.
The idea was to realize a second stage of an hypothetical medium power LED power supply, that is connected to a first PFC stage connected to the European grid.
The chosen topology is the one studied for all this work, so there is an half bridge at primary, a center-tapped secondary and diode rectification. In table 5.1 the specifications.

Nominal input voltage	$380V$
Input voltage range	$350 - 410V$
Output voltage	$24V$
Nominal load	1.92Ω
Nominal output current	$12.5A$
Nominal output power	$300W$

Table 5.1: Specification of the converter.

In the following section there is the explanation of the algorithm step-by-step.

STEP 1

The chosen input-output relationship is the following:

- Nominal input voltage: $V_i = 380V$;
- Output voltage: $V_o = 24V$;
- Nominal load: $R_L = 1.92\Omega$.

STEP 2

The chosen frequency is $f_{sw} = 100kHz$ so the nominal frequency for which the converter stays in nominal condition is expected to stay near this value.

STEP 3

The MOSFET chosen for the bridge is the IPx65R110CFDA [9], it is a superjunction device that can withstand up to 650V, it has a fast body diode and low on-resistance, from the datasheet:

- Drain-source capacitance: $C_{ds} = 553pF$;
- Channel resistance: $R_{ch} = 0.11\Omega$;
- Rise time: $t_{rise} = 11ns$;
- Fall time: $t_{fall} = 6ns$;
- Forward voltage drop of body diode: $V_{\gamma,body} = 0.9V$.

STEP 4

The diode chosen for the rectification is the DPG30C400HB [11] that has a maximum reverse blocking voltage of $400V$, that is high enough for this application since the theoretical maximum voltage that a single diode has to block is the double of V_o. The maximum (average) current that can support is 15A, that is okay since each diode takes half of the output current.
From the datasheet ("*Values for power loss calculation only*"):

- Forward voltage drop: $V_\gamma = 1V$.
- ON resistance: $R_{diode} = 25m\Omega$.

STEP 5

The output capacitance is made by two electrolytic capacitors of $230\mu F$ that can withstand up to $400V$, from Nippon CHEMI-CON [2], this was an obliged choice since they were already mounted on the board used in the lab. Their Dissipation Factor is $tan(\delta) = 0.15$, so for a single capacitor:

$$ESR_C = \frac{tan(\delta)}{2\pi fC} = \frac{0.15}{2\pi \cdot 100kHz \cdot 230\mu F} = 1m\Omega \tag{5.1}$$

And finally since there are two in parallel:

$$ESR_{C_{out}} = 0.5m\Omega \tag{5.2}$$

STEP 6

Looking at some datasheet of film capacitor suitable to be resonant capacitors, the taken value is the following:

$$tan(\delta)_{C_r} = 0.0015 \tag{5.3}$$

STEP 7

The values chosen for the resistance of the winding of the transformer and of the resonant inductor are:

- Primary winding resistance: $R_p = 100m\Omega$;
- Secondary winding resistance: $R_s = 5m\Omega$;
- Resonant inductor resistance: $R_{L_r} = 100m\Omega$.

STEP 8

Here there are the chosen values for the generation of the input sets:

- Number of tested values for the resonant inductance: $N_{L_r} = 35$;

- Minimum value of the resonant inductance: $L_{r,min} = 10\mu H$;
- Maximum value of the resonant inductance: $L_{r,max} = 100\mu H$;
- Number of tested values for the magnetizing inductance: $N_{L_m} = 45$;
- Minimum value of the magnetizing inductance: $L_{m,min} = 100\mu H$;
- Maximum value of the magnetizing inductance: $L_{m,max} = 400\mu H$;
- Number of tested values for the resonant capacitor: $N_{C_r} = 41$;
- Minimum value of the resonant inductance: $C_{r,min} = 1nF$;
- Maximum value of the resonant inductance: $C_{r,max} = 2.2\mu F$;
- Number of tested values for the turn ratio: $N_n = 10$;
- Maximum value for turn ratio: $N_{max} = 10$.

STEP 9

This step consist in running the main solver with all the parameter chosen in the previous steps. In table 5.2 there is a report of the solver.

Total configuration studied	645750
Elaboration time for NP solver	1.94s
Elaboration time for PN solver	1.33s
Elaboration time for PO solver	212s
Elaboration time for PON solver	734s
Elaboration time for NOP solver	1510s
Sets stored in the database	21564

Table 5.2: Report of the run of the main solver.

STEP 10

From the database, the final design to implement in laboratory has been chosen looking at the results that has higher efficiency according to the solver, taking the one that has lower peak resonant current so that losses in the magnetic elements (that are only calculated in the lab and not in the solver) are lower, according to 2.41.
The peak value on the resonant capacitor have to be checked to see if it is manageable by standard component, and for this set it was not too high. Detailed description of the chosen design in the next section.

Resonant inductance	$L_r = 20.6\mu H$
Magnetizing inductance	$L_m = 168\mu H$
Resonant capacitor	$C_r = 39nF$
Transformer turn ratio	$N = 10$

TABLE 5.3: Passives of the implemented converter.

5.3 Chosen design

In table 5.3 there is the chosen set of passives.

In table 5.4 the outputs of the solvers that represent the *"Interesting values"* from the analysis of the waveforms.

RMS resonant current	$i_{L,RMS} = 2.53A$
Peak resonant current	$i_{L,peak} = 3.42A$
RMS secondary current	$i_{O,RMS} = 16.2A$
Average secondary current	$i_{O,AVG} = 12.2A$
RMS current in output capacitor	$i_{C_{out},RMS} = 11.8A$
Peak voltage on resonant capacitor	$v_{C_p,peak} = 329V$

TABLE 5.4: Interesting values from the waveforms.

In table 5.5 there are the results of the loss model applied on data from table 5.4.

MOSFETs conduction losses	$P_{MOS,cond} = 0.71W$
MOSFETs turn-on losses	$P_{MOS,turn-ON} = 0.003W$
MOSFETs turn-off losses	$P_{MOS,turn-OFF} = 0.60W$
Resonant inductor conduction losses	$P_{L_r,cond} = 0.61W$
Resonant capacitor conduction losses	$P_{C_r,cond} = 0.35W$
Primary side conduction losses	$P_{primary,cond} = 0.59W$
Secondary side conduction losses	$P_{secondary,cond} = 0.13W$
Diodes conduction losses	$P_{diode} = 19.1W$
Output capacitor conduction losses	$P_{C_o,cond} = 0.1W$
Total losses	$P_{tot} = 22.1W$
Theoretical efficiency	$Eff = 93\%$

TABLE 5.5: Loss model applied on the chosen design.

5.4 Simulation of the chosen design

In this section there are the simulations of this design: in figure 5.1 and 5.2 the comparison between the analytical solution of chapter 3 and the SIMULINK simulation, while in figure 5.3 and 5.4 the waveforms from the SPICE simulation.

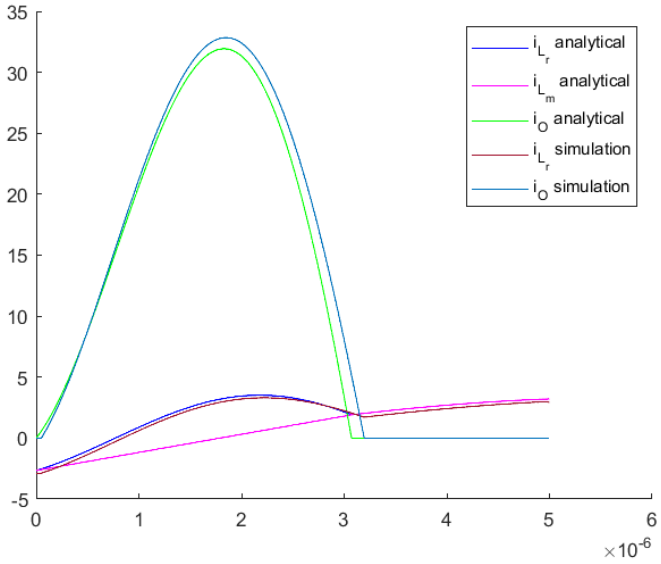

Figure 5.1: Half period of: 1) Resonant current from the analytical model, 2) Magnetizing current from the analytical model, 3) Secondary current from the analytical model, 4) Resonant current from the SIMULINK simulation, 5) Secondary current from the SIMULINK simulation.

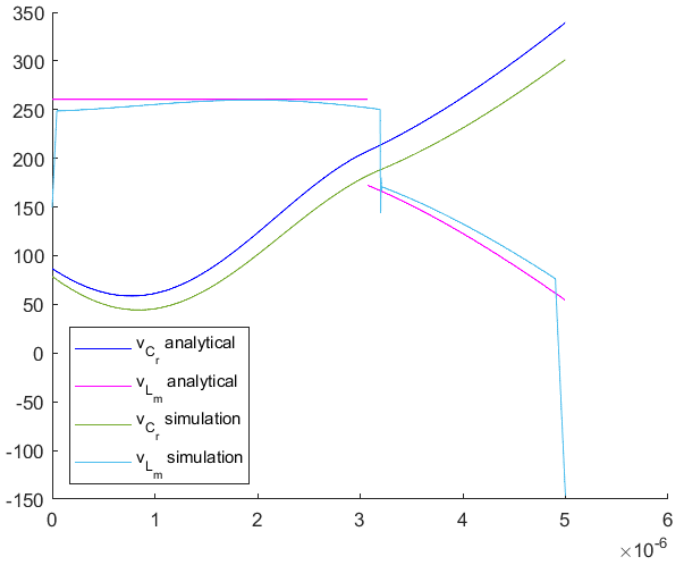

Figure 5.2: Half period of: 1) Voltage on resonant capacitor from the analytical model, 2) Voltage on primary side from the analytical model, 3) Voltage on resonant capacitor from the SIMULINK simulation, 4) Voltage on primary side from the SIMULINK simulation.

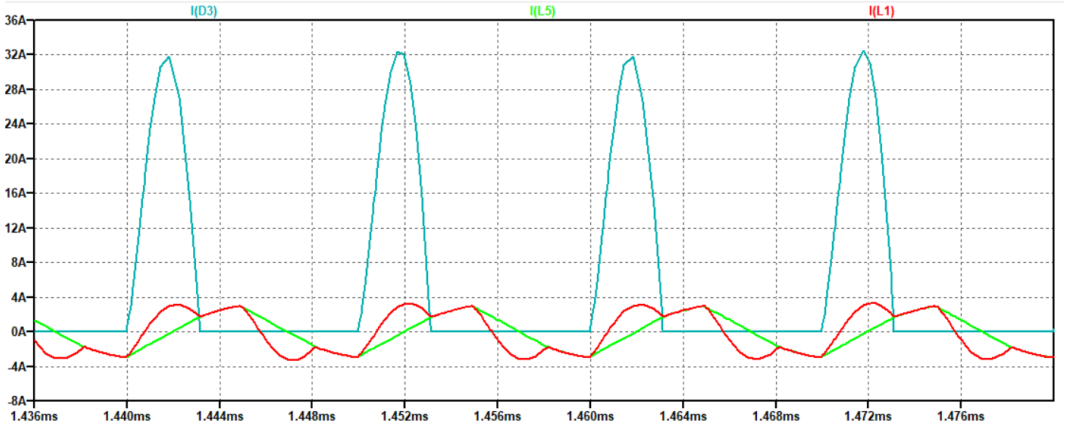

FIGURE 5.3: Some periods of: RED) Resonant current from the SPICE simulation, GREEN) Magnetizing current from the SPICE simulation, LIGHT BLUE) Secondary current from the SPICE simulation.

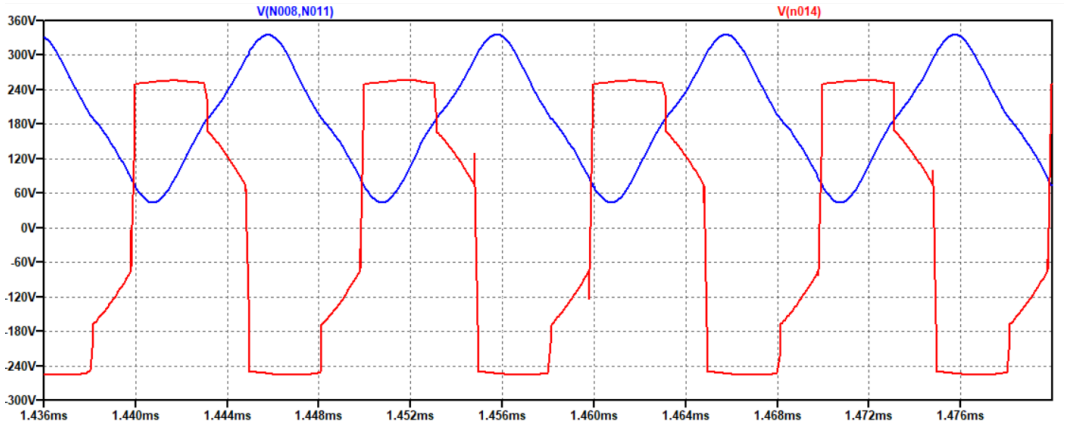

FIGURE 5.4: Some periods of: BLUE) Voltage on resonant capacitor from the SPICE simulation, RED) Voltage on primary side from the SPICE simulation.

5.5 Conclusion

This chapter explained and show the algorithm, from the results and the waveforms, the design seems to be good, so it will be implemented in laboratory, with the process explained in the next chapter.
It is good to notice that the output values for L_r, L_m and C_r are in the middle of the chosen range, so they can be seen as "optimized" while the value for the turn-ratio is the maximum possible, so probably using higher value for that will further improve efficiency.

Chapter 6

Laboratory implementation

This chapter shows the laboratory experience done for this thesis, the goal is to replicate in laboratory the configuration that the solver gave as output to see if simulation and reality are similar and consistent. The laboratory activity basically consisted in:

1. Design magnetics (with analytical formulas);
2. Implement magnetics in laboratory;
3. Measure them;
4. Test the complete circuit.

The process that can be roughly described with the flowchart in figure 6.1. The process was done in an iterative way and several designs of magnetics has been done to match the wanted one.
First there is an introduction on how the magnetic elements has been designed then there is the actual laboratory experience.

6.1 Magnetic design

6.1.1 Transformer design

Since it was the first time that I was going to make a transformer, I decided to use the ETD54 [18] for two reason: it was already available in the lab so I didn't have to wait for a new one to arrive since I had not a lot of time, and because being big it would be easier to wound it (Interesting data from the datasheet in table 6.1).
The used core material is N87 [19] that is suitable for the used frequency.
The windings were made with Litz wires since they were available in the laboratory and the following were used:

- RUPALIT Safety V155 90x0.10mm for the primary side;
- RUPALIT V155 80x0.20mm for the secondary side.

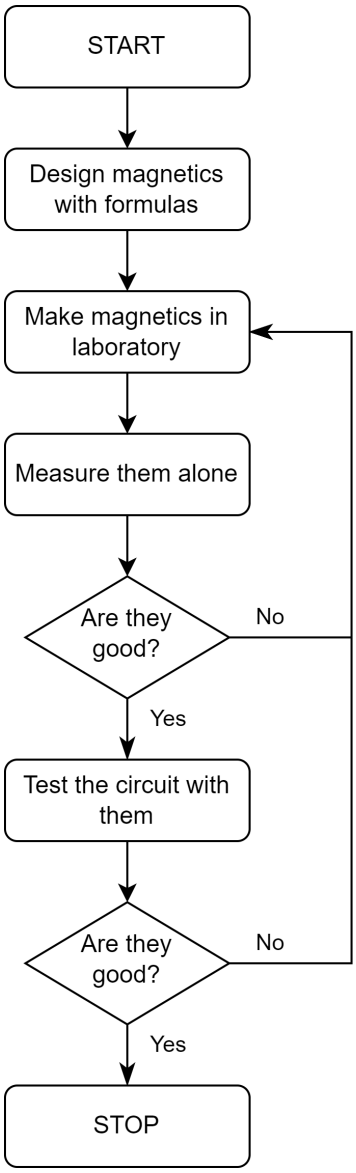

Figure 6.1: Indicative iterative flowchart of the work done in laboratory.

Effective magnetic cross section	$A_e = 280mm^2$
Effective magnetic volume	$V_e = 35600mm^3$
Width of the available space for the windings	$W_w = 36.8mm$
Height of the available space for the windings	$H_w = 8.55mm$
Average length of a turn	$l_N = 70mm$

Table 6.1: Interesting values from ETD54 datasheet.

	90x0.10mm	80x0.2mm
Copper cross section	$A_{Cu} = 0.7mm^2$	$A_{Cu} = 2.5mm^2$
Outer diameter	$D_w = 1.5mm$	$D_w = 2.7mm$

TABLE 6.2: Interesting values from Litz wires datasheets.

The used design method was the one from [5] that is based on Unitrode/TI Magnetics Design Handbook [4], using the data present on the datasheets of the core and core material; it is presented step by step in the following part.

STEP 1 - Core losses

This step consists in the definition of the wanted core losses and in the search of the maximum magnetic flux density that it is allowed for the wanted losses, from the datasheet of the ferrite [19].
The chosen losses are:

$$P_{Core,transformer} = 2W \tag{6.1}$$

The corresponding power loss density in the core is:

$$P_v = P_{Core,transformer}/V_e = 56.2kW/m^3 \tag{6.2}$$

The corresponding maximum flux density is (from [19]):

$$B_{max,P} = 70mT \tag{6.3}$$

STEP 2 - Maximum flux density

The maximum flux density that it is available in the core is then the minimum between the maximum due to power loss found in the previous step and the saturation value (read from [18]):

$$B_{max} = min(B_{max,P}, B_{sat}) = min(70mT, 320mT) = 70mT \tag{6.4}$$

STEP 3 - Number of turns

The minimum number of turns of the primary side should be designed so that the maximum flux density in the core is B_{max} and also that it is an integer number of the wanted turn ratio.

$$N_{P,min} = \frac{LI_{peak}}{B_{max}A_e} = \frac{168\mu H \cdot 3.42A}{70mT \cdot 280mm^2} = 29.3 \tag{6.5}$$

So the chosen number of turns at primary is $N_p = 30$ while at secondary N_s=3.

STEP 4 - Airgap

In this step a starting point for the airgap that will be put in the transformer is computed, then it will be adjusted during the actual construction of the transformer. First the needed inductance factor is calculated:

$$A_L = \frac{L_m}{N_p^2} = \frac{168\mu H}{30^2} = 186.7nH/T^2 \tag{6.6}$$

Then with the coefficients (K_1, K_2) present in the datasheet of the transformer [18], plugged in the general formula present in [17], a first approximation of the needed airgap can be found:

$$s = (\frac{A_L}{K_1})^{(\frac{1}{K_2})} = (\frac{186.7}{393})^{(\frac{1}{-0.779})} = 2.6mm \tag{6.7}$$

STEP 5 - Check of the dimensions and choice of the topology

This step is needed to check if all the turns that are needed can physically fit into the coil former. Maximum number of turns on single layer for the primary (made with Litz wire 90x0.10mm):

$$N_{P,single-layer} = \frac{W_w}{D_w} = \frac{36.8mm}{1.5mm} = 24.1 \tag{6.8}$$

Maximum number of turns on single layer for the secondary (made with Litz wire 80x0.20mm):

$$N_{S,single-layer} = \frac{W_w}{D_w} = \frac{36.8mm}{2.7mm} = 13.6 \tag{6.9}$$

So it is possible to state that the primary will fit in two layers while the secondary only in one, so the total height will be:

$$2 \cdot D_{w_{primary}} + D_{w_{secondary}} = 2 \cdot 1.5 + 2.5 = 5.5mm < H_w \tag{6.10}$$

It's less that the maximum available height, so it's possible to say that all will fit in the chosen coil former.

6.1.2 Inductor design

For the inductor the choice was to use a distributed airgap toroidal core, the chosen core was the 0077076A7 from MAGNETICS [13], in table 6.3 ther are some useful data from the datasheet.
The used conductor was an enamelled wire with copper cross section of $A_{cu} = 0.28mm^2$, that has an external diameter of about $D_w = 0.7mm$. In the following part there are the steps used for the design of a $10\mu H$ inductor used during the experiments.

Inductance factor	$A_L = 56nH/T^2$
$80\%A \cdot T$	$AT_{max} = 260AT$
Internal diameter	$D_{int} = 21.54mm$
Average turn length	$l_N = 37.9mm$
Effective magnetic volume	$V_e = 6090mm^3$
Effective magnetic cross section	$A_e = 68mm^2$

TABLE 6.3: Interesting values from 0077076A7 datasheet.

Coefficient a	$a = 44.3$
Coefficient b	$b = 1.988$
Coefficient c	$c = 1.541$

TABLE 6.4: Coefficients for core losses calculation for the chosen core of the inductor.

STEP 1 - Number of turns

Apply the usual formula to compute the needed number of turns:

$$N_t = \sqrt{\frac{L_r}{A_L}} = \sqrt{\frac{10\mu}{56n}} = 13.36 \tag{6.11}$$

And the chosen number of turn is $N = 13$.

STEP 2 - Check constrains

The second step firstly consists in checking if the peak current is not too big:

$$I_{peak}N < 80\%AT \tag{6.12}$$

That means:

$$N_t < \frac{80\%AT}{I_{peak}} = \frac{260}{3.42} = 76\ Turns \tag{6.13}$$

Then it is needed to check if the number of turn found at the previous point can be fit in the core, it means checking if:

$$N_t < N_{max} = \frac{3}{4} \cdot \frac{\pi D_{int}}{D_w} = 72\ Turns \tag{6.14}$$

In this specific case all constraints are largely satisfied.

STEP 3 - Check core losses

The formulas provided by the manufacturer [14] are useful to estimate the core losses, using the coefficients in table 6.4:

$$P_{core} = V_e a B_{peak}^b f^c = 0.49W \tag{6.15}$$

Where:

$$B_{max} = \frac{LI_{peak}}{N_t A_e} = \frac{10\mu \cdot 3.42}{13 \cdot 68mm^2} = 38mT \tag{6.16}$$

6.2 Measuring the transformer

In this section, there is the description of the procedure used to measure the transformer, according to the one in [7]. It is made using an LCR meter and it is based on the three measurements sketched in figure 6.2.

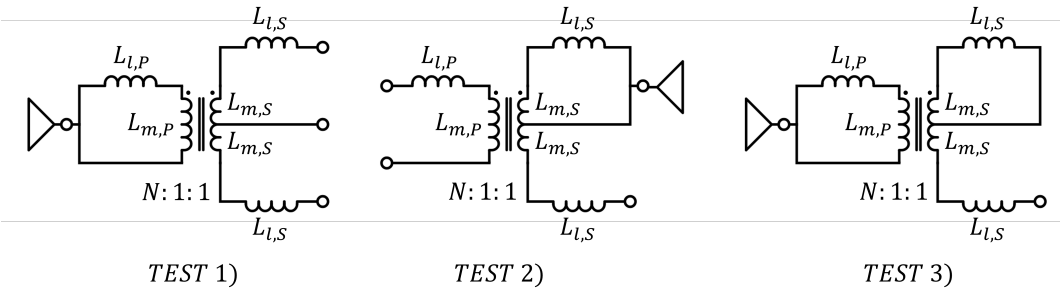

Figure 6.2: Three tests performed to characterize the transformer.

Here there is what is measured each test:

$$\begin{cases} L_{TEST,1} = L_{l,P} + L_{m_P} \\ L_{TEST,2} = L_{l,S} + L_{m_S} \\ L_{TEST,3} = L_{l,P} + L_{l_S} N^2 // L_{m_P} \\ N \approx \frac{L_{TEST,1}}{L_{TEST,2}} \end{cases} \tag{6.17}$$

And here there is the solution of the system:

$$\begin{cases} M = \sqrt{(L_{TEST,1} - L_{TEST,3}) L_{TEST,2}} \\ N \approx \frac{L_{TEST,1}}{L_{TEST,2}} L_{m,P} = MN \\ L_{m,S} = M/N \\ L_{l,P} = L_{TEST,1} - L_{m,P} \\ L_{l,S} = L_{TEST,2} - L_{m,S} \end{cases} \tag{6.18}$$

This procedure should be done for both secondaries to test if there are not negligible asymmetries.

6.3 Measuring the inductor

Measuring the inductor is simple, it's just needed to measure it with the LCR meter, and in the case of the inductor designed the result was:

- Inductance: $L_r = 9.37 \mu H$;
- Resistance: $R_r = 200 m\Omega$;

6.4 Test setup

In this section there is the explanation of the test setup used in laboratory.
In figure 6.3:

- RED: DSP that generate the PWMs to drive the gates at the wanted frequency with the wanted deadtime;
- ORANGE: Gate driver and half-bridge (MOSFETs and capacitors are in the back of the board;
- YELLOW: Resonant capacitor;
- GREEN: Resonant inductor;
- BLUE: Transformer;
- PINK: Rectifier, output capacitors are on the back of the board.

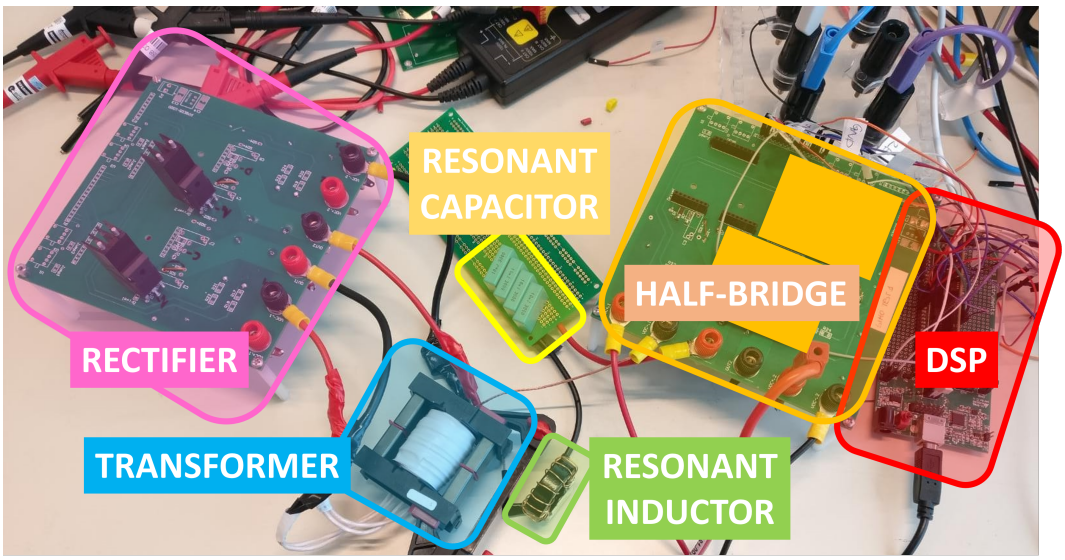

FIGURE 6.3: Test setup used in the laboratory.

The used instruments were:

- 4-channel oscilloscope to get the waveforms;
- Isolated power supply to supply the circuits;
- Active load to load the converter.

6.5 Implementation A

6.5.1 Transformer A

The first transformer was made with the values found in the theoretical analysis, inserting 30 turns for the primary side, 3 turns for each secondary put all in the same direction and an airgap of 2.6 mm, in figure 6.4 there is the sketch of the winding cross-section.

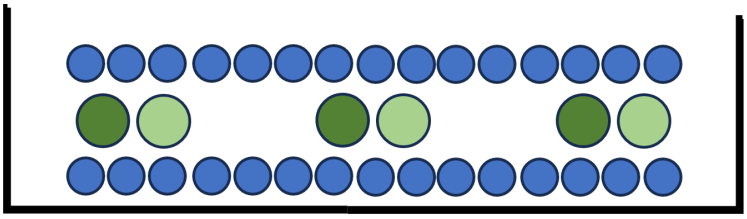

Figure 6.4: In BLUE the primary side and in the two different GREENs the secondary sides of transformer A.

With this design there were two problems:

- The measured turn ratio was lower than expected because was about 9.1;
- Was very difficult to construct the third layer since in the second one there was a lot of free space.

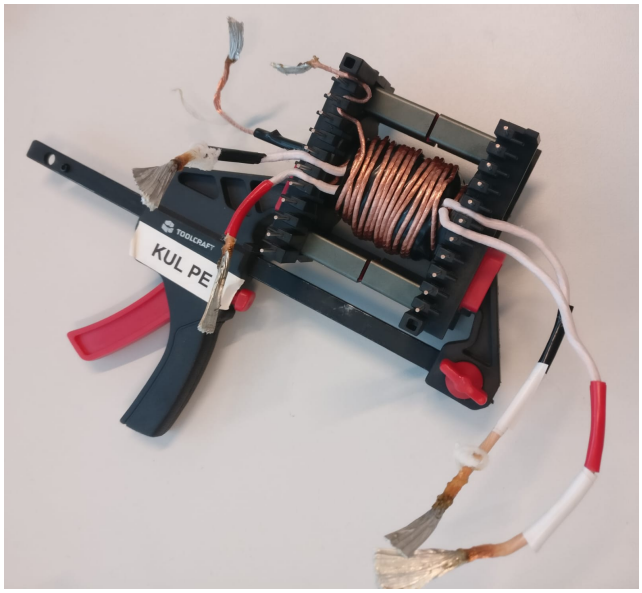

Figure 6.5: Photo of transformer A.

6.6 Implementation B

6.6.1 Transformer B

A second transformer was then made with the characteristics shown in table 6.5 increasing the number of turns at primary to adjust for the turn ratio and inserting two parallel cables for each secondary to fill the second layer. In figure 6.6 there is its sketch.

Primary turns	$N_P = 32$, divided equally into two layers
Secondary turns	$N_S = 3$, two parallel cables for each winding
Airgap	$s = 3.3mm$ (made with tape)

TABLE 6.5: Characteristics of transformer B.

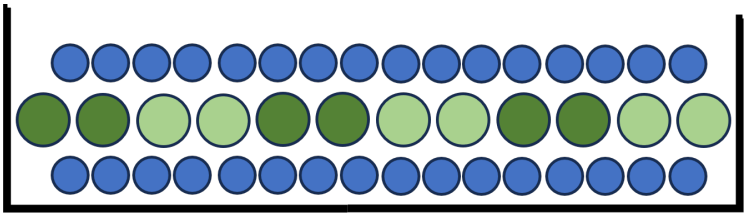

FIGURE 6.6: In BLUE the primary side and in the two different GREENs the secondary sides of transformer B.

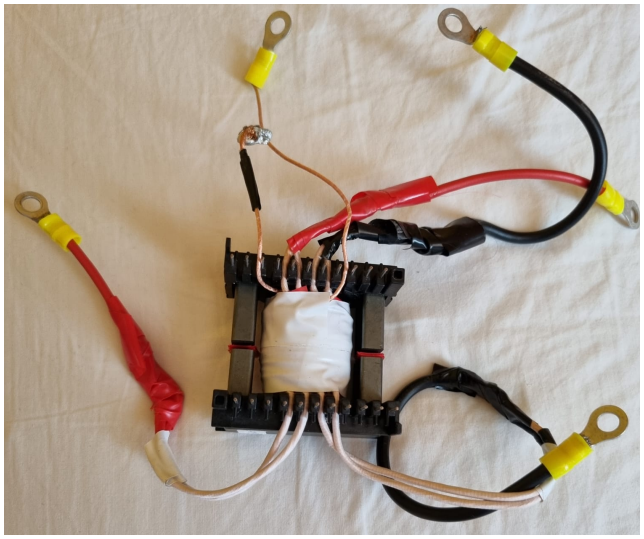

FIGURE 6.7: Photo of transformer B.

The results of the characterization are present in table 6.6.

Turn ratio	$N = 9.54$
Magnetizing inductance of primary side	$L_{m,P} = 167.5\mu H$
Leakage inductance of primary side	$L_{l,P} = 23.5\mu H$
Magnetizing inductance of secondary side 1	$L_{m,S} = 1.84\mu H$
Leakage inductance of secondary side 1	$L_{l,S} = 0.26\mu H$
Magnetizing inductance of secondary side 2	$L_{m,S} = 2.09\mu H$
Leakage inductance of secondary side 2	$L_{l,S} = 0.21\mu H$

Table 6.6: Characterization of transformer B.

6.6.2 Experiment B

In this experiment the converter was tested with the transformer B both with and without the inductor, in the conditions stated in table 6.7.

Input Voltage	$V_i = 380V$
Switching frequency	$f_{sw} = 100kHz$
Dead time	$t_{dead} = 200ns$
Output Power	$P_{out} = 300W$

Table 6.7: Test condition of the circuit with transformer B.

In figures 6.8, 6.9 and 6.10 there are the resulting waveform for the circuit with the inductor and in figures 6.11, 6.12 and 6.13 there are the ones for the circuit without the inductor.

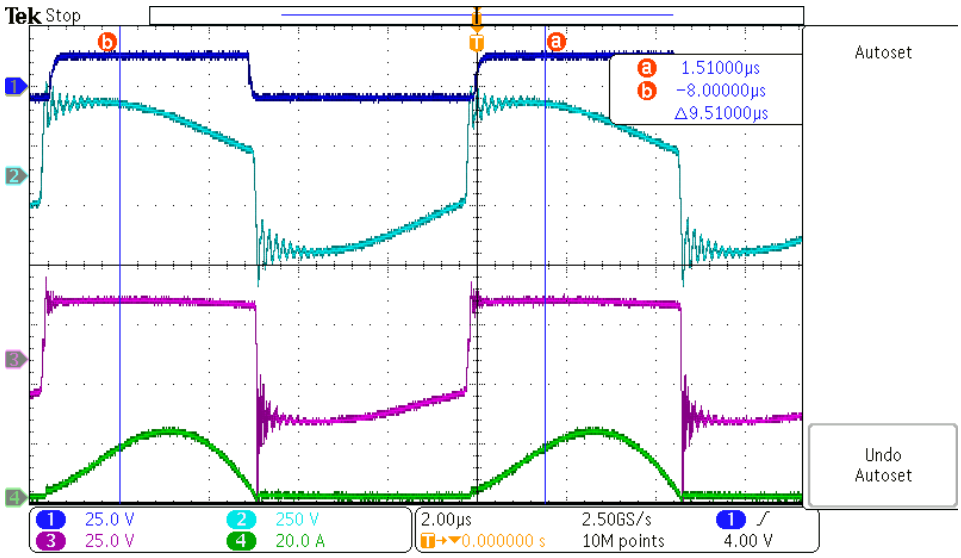

Figure 6.9: WITH INDUCTOR: 1) Gate of high-side MOSFET, 2) Voltage on the primary side of the trasformer, 3) Voltage on upper secondary side, 4) Current of the upper diode.

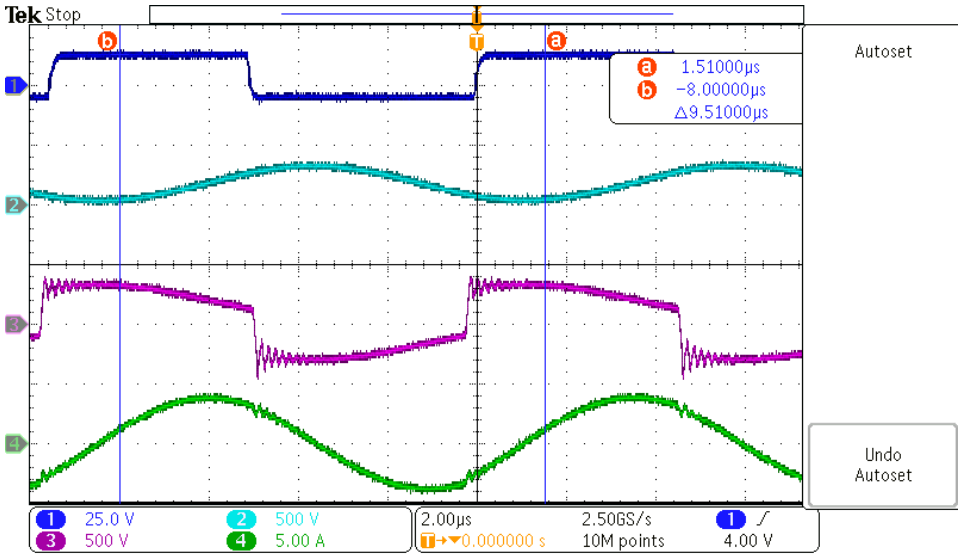

FIGURE 6.8: WITH INDUCTOR: 1) Gate of high-side MOSFET, 2) Voltage on the resonant capacitor, 3) Voltage on the primary side of the trasformer, 4) Resonant current.

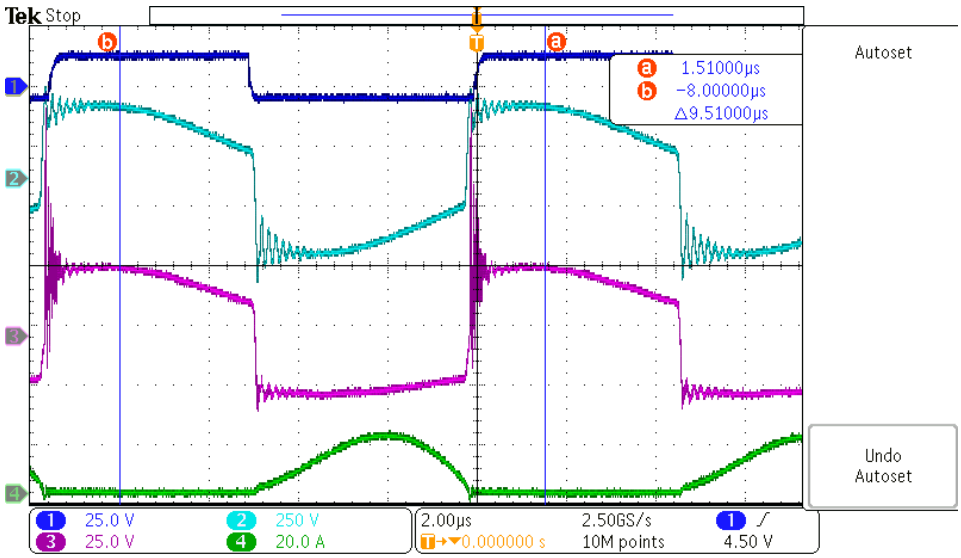

FIGURE 6.10: WITH INDUCTOR: 1) Gate of high-side MOSFET, 2) Voltage on the primary side of the trasformer, 3) Voltage on lower secondary side, 4) Current of the lower diode.

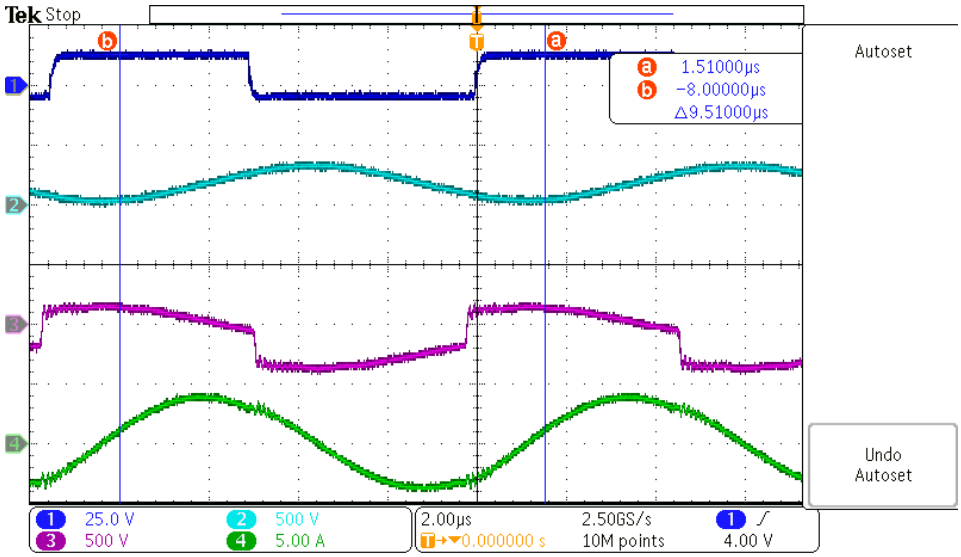

Figure 6.11: NO INDUCTOR: 1) Gate of high-side MOSFET, 2) Voltage on the resonant capacitor, 3) Voltage on the primary side of the trasformer, 4) Resonant current.

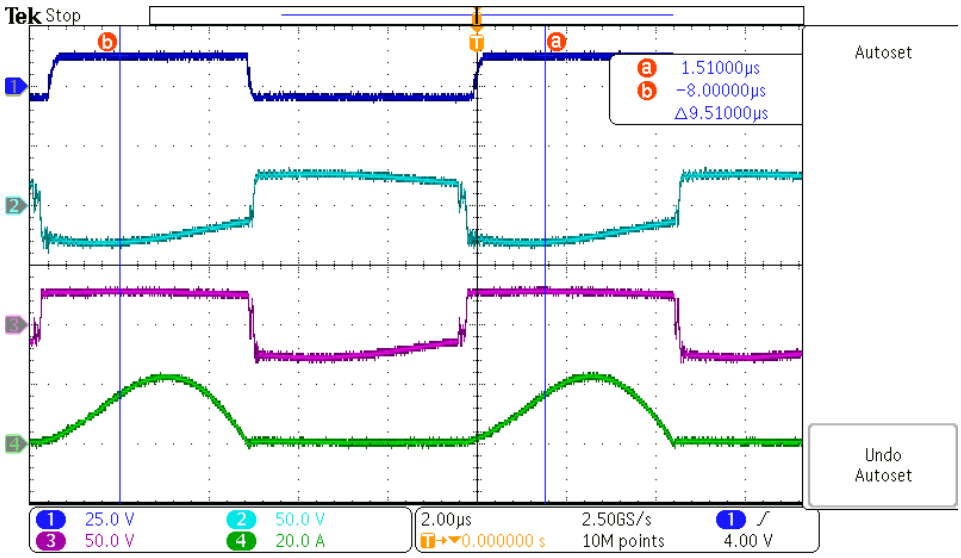

Figure 6.12: NO INDUCTOR: 1) Gate of high-side MOSFET, 2) Voltage on the primary side of the trasformer, 3) Voltage on upper secondary side, 4) Current of the upper diode.

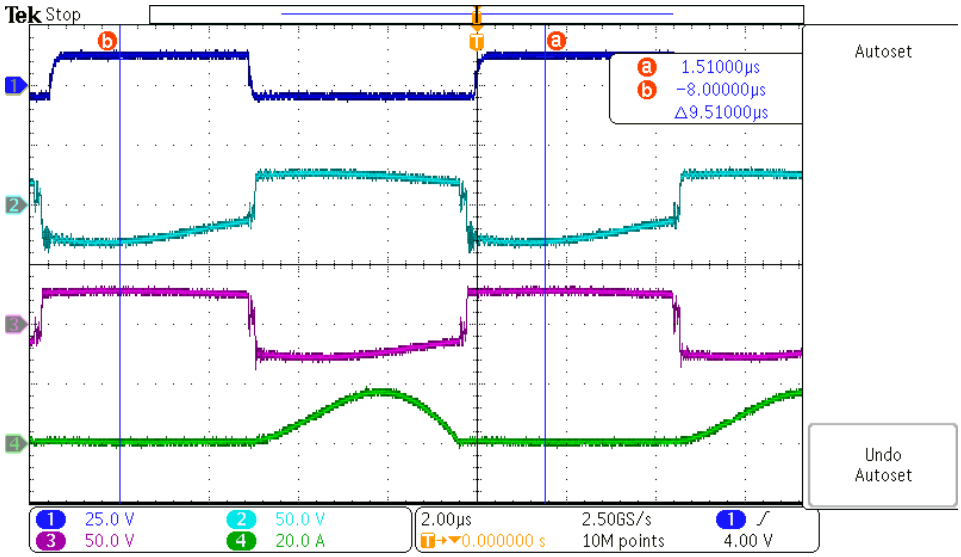

FIGURE 6.13: NO INDUCTOR: 1) Gate of high-side MOSFET, 2) Voltage on the primary side of the trasformer, 3) Voltage on lower secondary side, 4) Current of the lower diode.

Looking at the waveforms it was possible to see that the converter works but the series resonant frequency was lower than expected. It is possible to see this making a comparison between the conduction time of these graphs with the one for example in figure 5.1. There was also asymmetry in the transformer since the conduction times were not the same for the two diodes.

Comparing the conduction time ($t_{conduction}$) of the two diodes with the results of simulations from LTSPICE (L_{SPICE} is the inductance that in the simulation gives the same conduction time), assuming that the difference in resonant frequency is given only by the difference in total resonant inductance the results in table 6.8 can be found. In the third column of the table there is also an approximation of the total leakage inductance seen from the primary side, the formula that give rise number is the following (using the experimental data from table 6.6):

$$L_{l,seen} = L_{l,P} + N^2 L_{l,S} + L_{inductor} \tag{6.19}$$

	$t_{conduction}$ $[\mu s]$	L_{SPICE} $[\mu H]$	$L_{l,seen}$ $[\mu H]$
WITH inductor, UP diode	4.6	60	44.7
WITH inductor, LOW diode	4.8	65	56.5
NO inductor, UP diode	4.3	45	35.3
NO inductor, LOW diode	4.4	50	47.1

TABLE 6.8: Analysis of the seen inductance in experiment B.

The asymmetry of the transformer and the big impact that secondary leakage inductance and secondary stray inductance has on the system are visible from the experimental results.

The fact that the connection cables on the secondary side had different length can explain partially the the asymmetry; the following two factors could instead explain the leakage:

- Stray inductance due to connection cables on secondary side;
- Leakage inductance due to the fact that making the two secondary winding in the same direction, the connection of the center tap is made by a "long" cable that pass from a side to the other of the transformer.

These problems were the one addressed in the next transformer's realization.

6.7 Implementation C

6.7.1 Transformer C

A third transformer was then made with the same characteristics of the previous shown in table 6.9 but with the following differences:

- Use of gapped cores and yokes to have a more stable and cleaner design;
- The two secondary were wound in opposite direction to have the center tap on the same side of the transformer so that could easily connected without inserting leakage;
- Shorter connection cables to connect to the rest of the circuit.

Primary turns	$N_P = 32$, divided equally into two layers
Secondary turns	$N_S = 3$, two parallel cables for each winding
Airgap	$s = 3mm$ (made with already gapped cores)

Table 6.9: Characteristics of transformer C.

Comparing the characterization (table 6.10), with the previous one is noticeable that this transformer was more symmetric and had less leakage at secondary.

6.7.2 Experiment C

In this experiment the converter was tested with the transformer C both with and without the inductor, in the conditions stated in table 6.11.

In figures 6.15 and 6.16 there are the resulting waveforms for the circuit with the inductor and in figures 6.17, and 6.18 there are the ones for the circuit without the inductor.

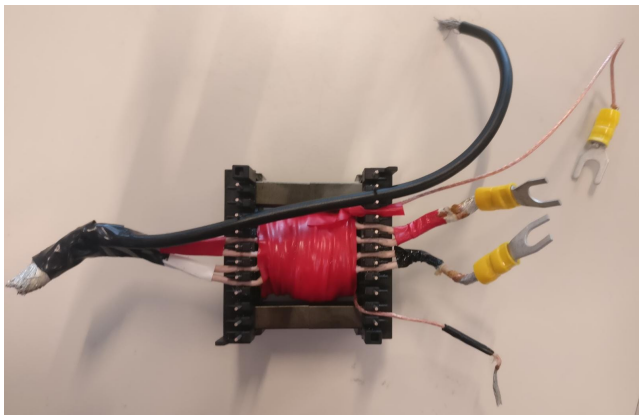

FIGURE 6.14: Photo of transformer C.

Turn ratio	$N = 10$
Magnetizing inductance of primary side	$L_{m,P} = 167.9\mu H$
Leakage inductance of primary side	$L_{l,P} = 13.5\mu H$
Magnetizing inductance of secondary side 1	$L_{m,S} = 1.68\mu H$
Leakage inductance of secondary side 1	$L_{l,S} = 0.14\mu H$
Magnetizing inductance of secondary side 2	$L_{m,S} = 1.67\mu H$
Leakage inductance of secondary side 2	$L_{l,S} = 0.13\mu H$

TABLE 6.10: Characterization of transformer C.

Input Voltage	$V_i = 380V$
Switching frequency	$f_{sw} = 100kHz$
Dead time	$t_{dead} = 200ns$
Output Power	$P_{out} = 300W$

TABLE 6.11: Testing condition of transformer C.

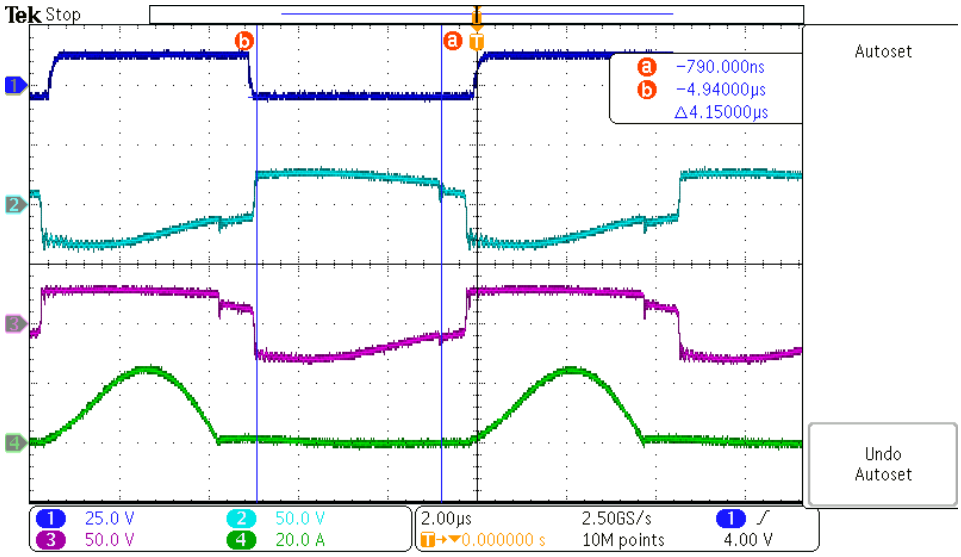

FIGURE 6.17: NO INDUCTOR: 1) Gate of high-side MOSFET, 2) Lower secondary side, 3) Upper secondary side, 4) Current of the upper diode.

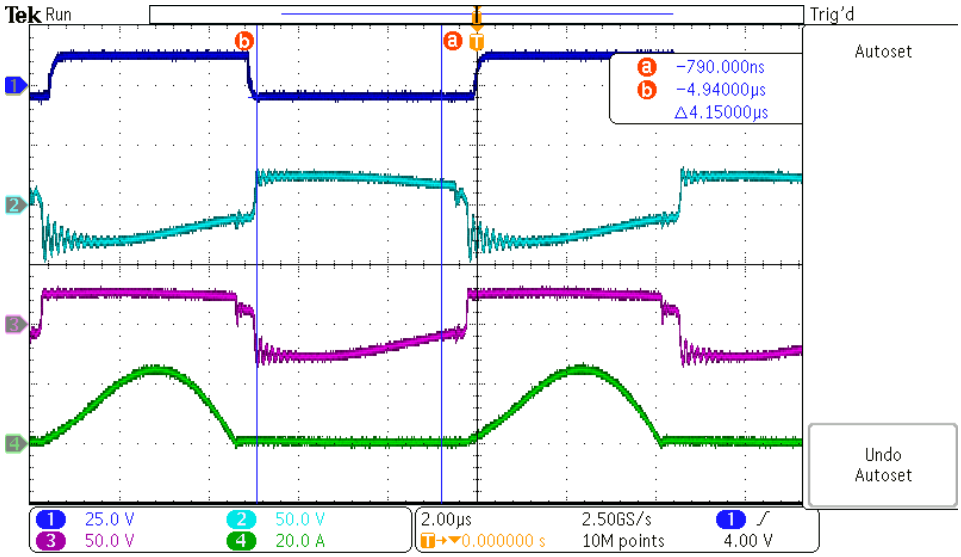

Figure 6.15: WITH INDUCTOR: 1) Gate of high-side MOSFET, 2) Lower secondary side, 3) Upper secondary side, 4) Current of the upper diode.

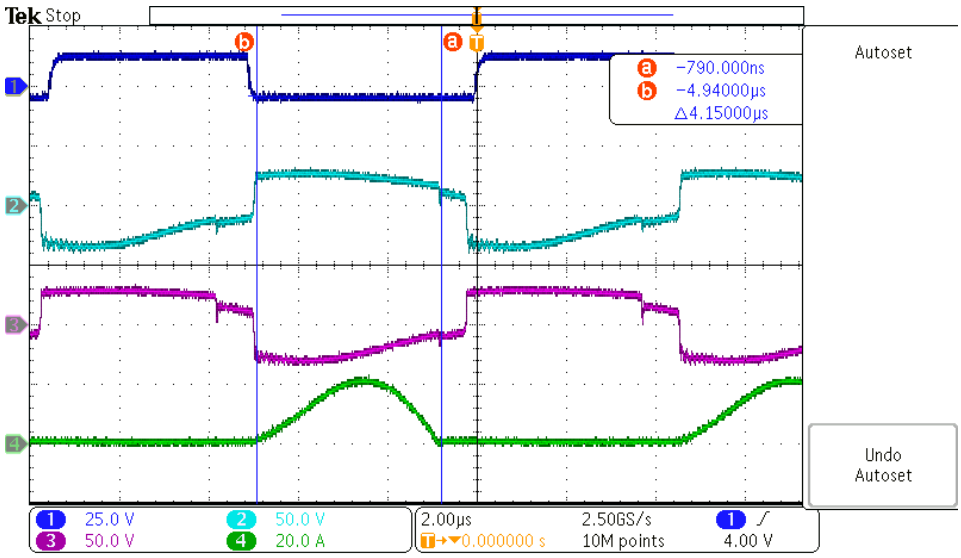

Figure 6.18: 1) Gate of high-side MOSFET, 2) Lower secondary side, 3) Upper secondary side, 4) Current of the lower diode.

Looking at the waveforms is possible to see that as expected the series resonant frequency was increased respect to the previous experiment but still lower than the wanted one.

In table 6.12 there is the comparison between the conduction time ($t_{conduction}$) of

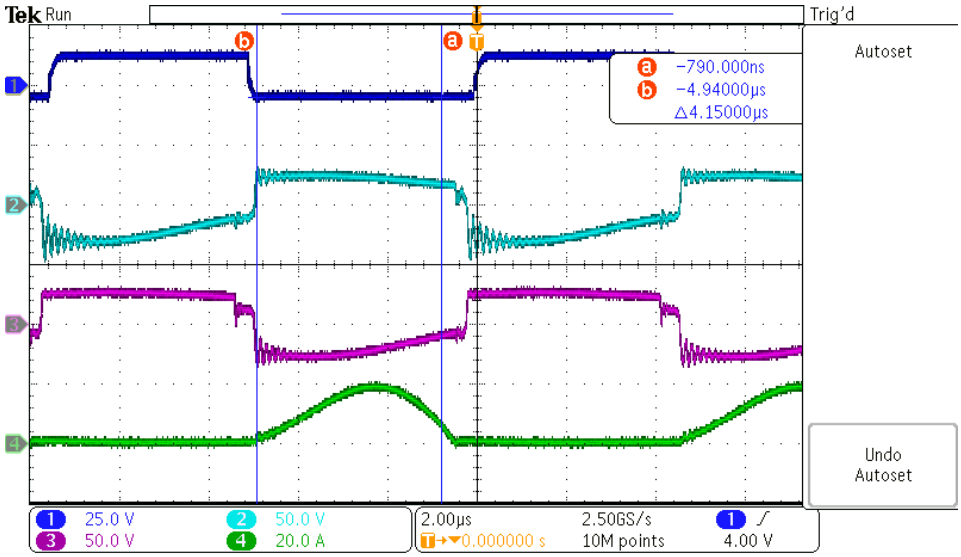

FIGURE 6.16: WITH INDUCTOR: 1) Gate of high-side MOSFET, 2) Lower secondary side, 3) Upper secondary side, 4) Current of the lower diode.

the two diodes with results of simulations from LTSPICE (L_{SPICE} is the inductance that in the simulation gives the same conduction time) and an approximation of the total leakage inductance seen from the primary side, given using 6.19 is presented.

	$t_{conduction}$ $[\mu s]$	L_{SPICE} $[\mu H]$	$L_{l,seen}$ $[\mu H]$
WITH inductor, UP diode	4.2	43	36.0
WITH inductor, LOW diode	4.4	50	36.6
NO inductor, UP diode	3.8	33	26.7
NO inductor, LOW diode	4.0	39	27.4

TABLE 6.12: Analysis of the seen inductance in experiment C.

Looking at the datas, it was possible to see that there was still some asymmetry even if it is hardly noticeable, and that there was still too much stray inductance to achieve the wanted resonant frequency.

The only plausible answer was that there was some little inductive asymmetry in the board where the rectifier was mounted and it creates a problem since every stray inductance is multiplied by N^2.

6.8 Implementation D

For this last experiment, the idea was to:

- Make connection cable of secondary side as short as possible, removing the black cable visible in figure 6.14 that were there to connect the center tap of

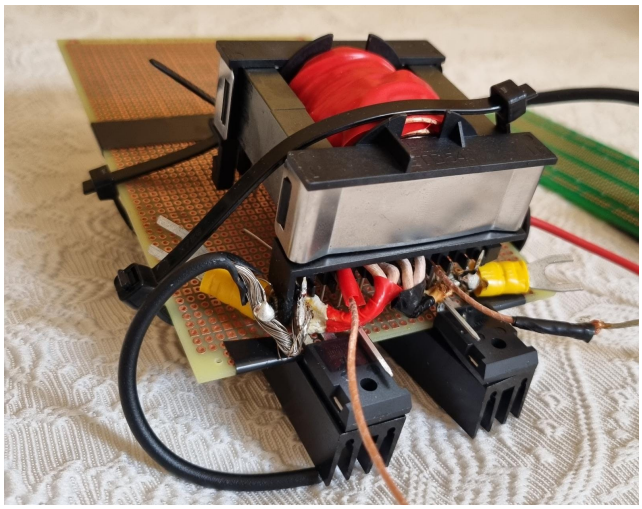

Figure 6.19: Photo of the front of the improved secondary side.

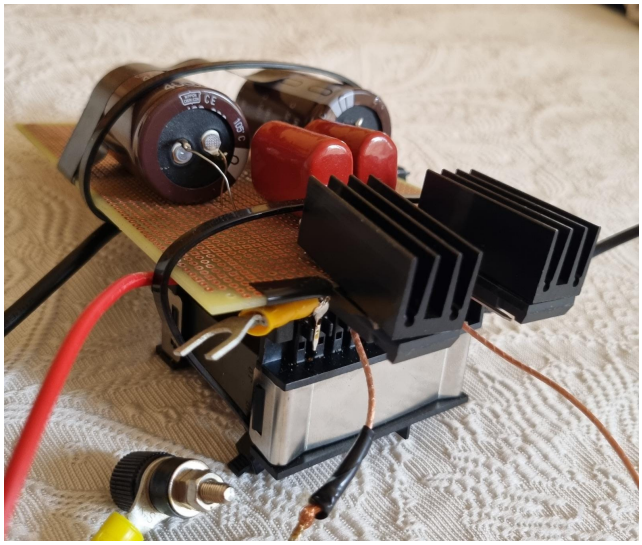

Figure 6.20: Photo of the back side of the improved secondary side.

the transformer to the output capacitors;

- Reduce the possible asymmetry of the board at secondary putting the diodes and the output capacitors as close as possible to the transformer.

This was done by:

- Shortening as much as possible the not wound wires from the "transformer C";
- Mounting the transformer on one side of a proto-board;

- Mounting diodes and capacitors on the other side of the proto-board, putting diodes directly soldered on the secondary side exit cables.

In figure 6.19 and 6.20 there are the photos of the improved secondary side, to make the reader better understand what was done.

6.8.1 Experiment D

The converter was tested with the improved secondary both with and without the inductor in the nominal conditions, the ones in table 6.13.

Input Voltage	$V_i = 380V$
Switching frequency	$f_{sw} = 100kHz$
Dead time	$t_{dead} = 200ns$
Output Power	$P_{out} = 300W$

TABLE 6.13: Testing condition of transformer C.

In figures 6.21 and 6.22 there are the resulting waveform that characterize the conduction time for the configuration with and without inductor, this time it was characterized using the voltage on the diode because there was no space to insert the current probes.

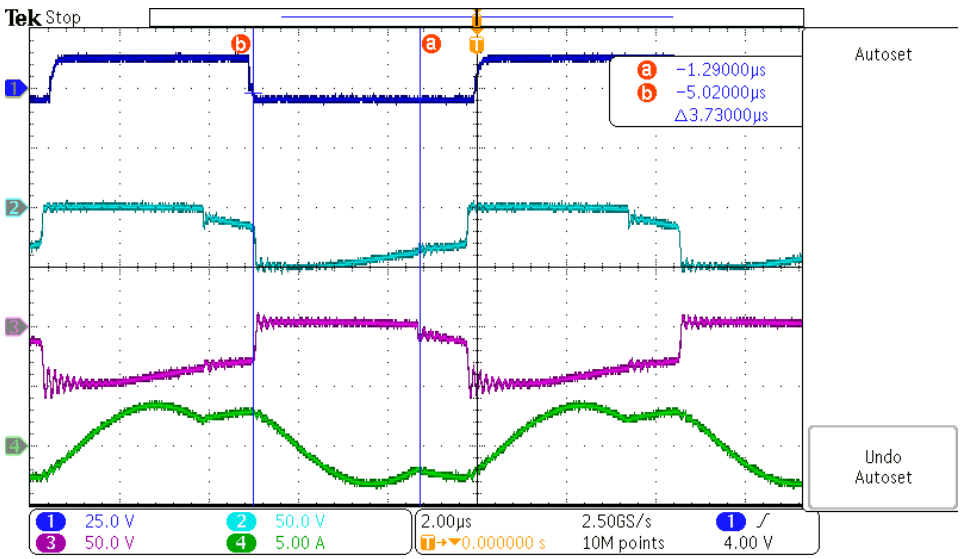

FIGURE 6.21: WITH INDUCTOR: 1) Gate of high-side MOSFET, 2) Upper diode voltage, 3) Lower diode voltage, 4) Resonant current.

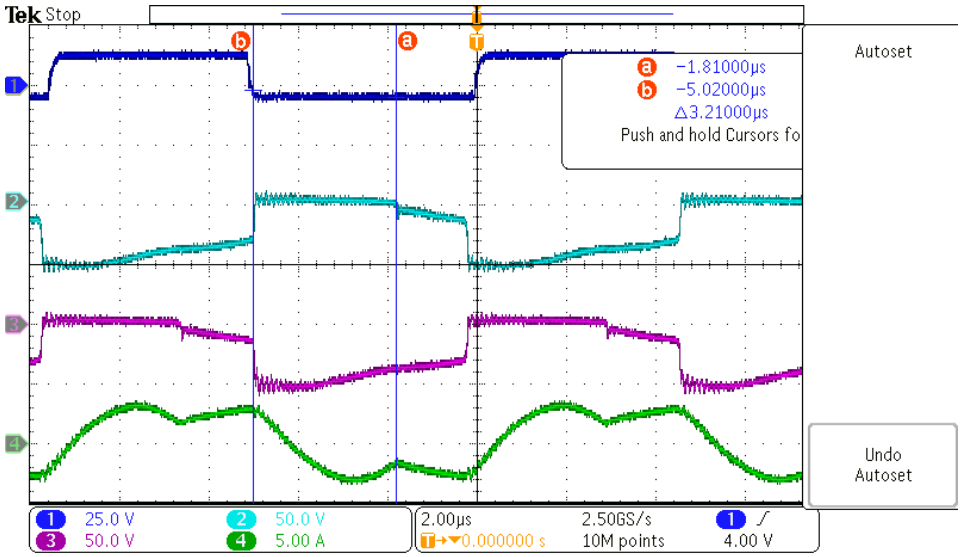

Figure 6.22: NO INDUCTOR: 1) Gate of high-side MOSFET, 2) Upper diode voltage, 3) Lower diode voltage, 4) Resonant current.

	$t_{conduction}$ $[\mu s]$	L_{SPICE}
WITH inductor	3.73	30
NO inductor	3.21	20

Table 6.14: Analysis of the seen inductance in experiment D.

From the experiment with the usual procedure the conduction time and relative "seen inductance" were computed, using the values of conduction time present in figure 6.21 and 6.22, and shown in table 6.14.

The experiment worked because the asymmetry was solved and the "seen inductance" from the primary side was again lowered, arriving to the target value.

6.9 Testing of the final configuration

At this point the converter was implemented with the wanted values of passives, the frequency was changed to have the wanted voltage at output with nominal output power. This point was found to be when the frequency is around $f_{sw} = 102kHz$. In this working point the converter is characterized.

6.9.1 Efficiency calculations

Efficiency calculation started from the data displayed (in figure 6.23) from the power supply and the active load; these data are shown in table 6.15.

FIGURE 6.23: Display of the power supply and active load in the nominal conditions.

Input voltage	$V_i = 380V$
Input current	$I_i = 0.88A$
Input power	$P_i = 337W$
Output voltage	$V_o = 24.5V$
Output current	$I_o = 12.4A$
Output power	$P_o = 300W$

TABLE 6.15: Values to calculate efficiencies.

Connection cables

The connection cables between the converter and the active load has been characterized, as visible in figure 6.24 and 6.25, to have a total DC resistance of:

$$R_{cable} = R_{positive} + R_{negative} = 24.56 + 24.77 = 49.3m\Omega \tag{6.20}$$

That means a power dissipation of about:

$$P_{cable} = R_{cable} I_o^2 = 49.3m \cdot 12.4^2 = 7.6W \tag{6.21}$$

Efficiency estimation

With all these data, the efficiency can be estimated as:

$$Eff = \frac{V_o I_o + P_{cable}}{V_i I_i} = \frac{24.5 \cdot 12.4 + 7.6}{380 \cdot 0.88} \approx 93\% \tag{6.22}$$

And this is a similar value to the theoretical one 5.5.

Figure 6.24: Impedance of the positive cable for the connection to the active load.

Figure 6.25: Impedance of the negative cable for the connection to the active load.

Chapter 7

Conclusion

In this chapter there are the conclusions of the work.

7.1 Evaluation of research question

The research question was:
Is it possible to generate a straightforward design method for an LLC converter using TDA theory and loss calculation?

Looking at what has been done in the last chapters, the answer is affirmative, it is possible to design an LLC converter at least in this specific case with straightforward algorithm, but further researches are needed to expand this sentence.
The efficiency results are also similar to the one from the solver, so it possible to assume that the loss model is enough accurate.

7.2 Further research

Here there are some paragraphs that explains further possible research topics that can expand this work.

Verification of the effectiveness of the algorithm

To have a more complete work, it is needed to verify if the proposed algorithm works also with other input-output relationships and not only in the considered one. To do that other runs and laboratory implementation needs to be done.

Improve performances of the solvers

The solvers for numerical method are very slow, since no optimization have been done on them, a deep mathematical analysis is needed in order to see if this is the performance limit or if there is some room for improvements.

Expand the capabilities of the solver

This work makes the basis of the solver, but it can be still improved in order to study different topologies like full-bridge at primary, not center-tapped transformer and active rectification. It can be also expanded in order to study different figures of merit like power density, volume, total height, weight, and others.

Improve the loss model

The study of other losses is possible, to improve the loss model, like:

- Recovery losses of body and rectifying diodes;
- Magnetic losses of inductor and transformer;
- Improve the calculation of joule losses in magnetic element, using Dowell's equations.

Improve the implemented design

Even if an efficiency of around 93% is not bad with a diode rectification, it can be further improved for example using Schottky diodes on the secondary side that can increase the efficiency of one or two percentage points. The design is now done with an ETD54, it could be good to use a smaller and less expensive one since the power is not that big.

Platform development

As it is clear from the results of the last experiment, if a transformer with high turn ratio is used, stray inductances on the secondary have a very big role. They should be minimized and possibly known in order to have an efficient realization procedure. This cannot be done using protoboards and not dedicated hardware since each time the construction is slightly different and the value of the stray inductance can change. The solution could be to make a PCB on which they can be mounted both the transformer and the rectification stage, putting the diodes as close as possible to the output of the transformer. An idea could be, for example, mounting transformer and diodes on the opposite sides of the board as in the last experiment.
While doing that it is possible to prepare a PCB on which different size of transformers can be mounted on, so that transformer comparisons become easier.

Appendices

Appendix A

Interesting values

This appendix shows the calculations needed to find the so called "interesting values", for all the considered modes.

A.1 Interesting values for PN mode

This section shows how to find the needed values for the loss model and for the converter design, in the case of the PN mode.

RMS resonant current

Resonant current in PN mode is:

$$\begin{cases} i_{L_P}(t) = C_r\omega_r(-K_1 sin(\omega_r t) + K_2 cos(\omega_r t)), & 0 < t < t_1 \\ i_{L_N}(t) = C_r\omega_r(-K_3 sin(\omega_r (t-t_1)) + K_4 cos(\omega_r (t-t_1))), & t_1 < t < T_s/2 \end{cases} \tag{A.1}$$

And the integral to solve to get RMS value of resonant current is:

$$i_{L,RMS} = \sqrt{\frac{2}{T_s}\int_0^{\frac{T_s}{2}} i_L(t)^2 dt} = \sqrt{\frac{2}{T_s}(\int_0^{t_1} i_{L_P}(t)^2 dt + \int_{t_1}^{\frac{T_s}{2}} i_{L_N}(t)^2 dt)} \tag{A.2}$$

In appendix B.1 there is the general solution of the integral and in table A.1 there are the coefficients to find K (see appendix B.1).

Finally, the following helps to find the RMS resonant current:

$$i_{L,RMS} = \sqrt{\frac{1}{D}K} \tag{A.3}$$

Peak resonant current

The maximum between $i_{L_P,peak}$ (the peak of i_{L_P} in $0 < t < t_1$) and $i_{L_N,peak}$ (the peak of i_{L_N} in $t_1 < t < T_s/2$), is the peak resonant current.
The algorithm present in appendix B.5 shows how to find $i_{L_P,peak}$ and $i_{L_N,peak}$, with the parameters present in table A.2.

Coefficient	Value
A	t_1
B	$-C_r\omega_r K_1$
C	$C_r\omega_r K_2$
D	$\frac{T_s}{2}$
E	$-C_r\omega_r K_3$;
F	$C_r\omega_r K_4$
V	ω_r
W	ω_r

Table A.1: Coefficient for RMS resonant current in PN mode.

Coefficient	Value for $i_{L_P,peak}$	Value for $i_{L_N,peak}$
C_1	$-C_r\omega_r K_1$	$-C_r\omega_r K_3$
C_2	$C_r\omega_r K_2$	$C_r\omega_r K_4$
C_3	0	0
t_{begin}	0	0
t_{end}	t_1	$T_s/2 - t_1$
ω	ω_r	ω_r

Table A.2: Coefficient for peak resonant current in PN mode.

RMS current on secondary

Output current in PN mode is:

$$\begin{cases} i_{O_P}(t) = N[C_r\omega_r(-K_1 sin(\omega_r t) + K_2 cos(\omega_r t)) - \frac{NV_o}{L_m}t - i_{M_P}(0)], & 0 < t < t_1 \\ i_{O_N}(t) = N[-\frac{NV_o}{L_m}(t - t_1) + i_{M_N}(t_1) - \\ \qquad +C_r\omega_r(-K_3 sin(\omega_r(t - t_1)) + K_4 cos(\omega_r(t - t_1)))], & t_1 < t < T_s/2 \end{cases} \tag{A.4}$$

The following integral needs to be solved to find RMS output current:

$$i_{O,RMS} = \sqrt{\frac{2}{T_s}\int_0^{\frac{T_s}{2}} i_O(t)^2 dt} = \sqrt{\frac{2}{T_s}(\int_0^{t_1} i_{O_P}(t)^2 dt + \int_{t_1}^{\frac{T_s}{2}} i_{O_N}(t)^2 dt)} \tag{A.5}$$

The expression present in appendix B.3 with the values of coefficients in table A.3 shows how to find K. Then:

$$i_{O,RMS} = \sqrt{\frac{1}{F}K} \tag{A.6}$$

Average current on diodes

The output current (equations A.4) needs to be integrated to find the average current on diodes:

Coefficient	Value
A	t_1
B	$-NC_r\omega_r K_1$
C	$NC_r\omega_r K_2$
D	$-N^2V_o/L_m$
E	$-Ni_{M_P}(0);$
F	$T_s/2$
G	$-NC_r\omega_r K_3$
H	$NC_r\omega_r K_4$
L	$-N^2V_o/L_m$
M	$i_{M_N}(t_1)$
T	t_1
U	t_1
W	ω_r

TABLE A.3: Coefficient for RMS and average output current in PN mode.

$$i_{O,AVG} = \frac{2}{T_s}\int_0^{\frac{T_s}{2}} i_O(t)dt = \frac{2}{T_s}[\int_0^{t_1} i_{O_P}(t)dt + \int_{t_1}^{\frac{T_s}{2}} i_{O_N}(t)dt] \tag{A.7}$$

Using the solution present in appendix B.2 using the coefficients in table A.3, is possible to find the value K, from which:

$$i_{O,AVG} = \frac{2}{T_s}K \tag{A.8}$$

RMS current in the output capacitor

Assuming that the output capacitor acts as an ideal capacitor and it make all AC components of the current that exits from the diodes to pass, output current has only DC component and it can be shown that:

$$i_{C_{out},RMS} = \sqrt{i^2_{O,RMS} - i^2_{O,AVG}} \tag{A.9}$$

Peak voltage on the resonant capacitor

From equations at the beginning of this section, it is possible to rewrite the equations for the resonant capacitor voltage:

$$\begin{cases} v_{C_P}(t) = K_1 cos(\omega_r t) + K_2 sin(\omega_r t) + V_i - NV_o, & 0 < t < t_1 \\ v_{C_N}(t) = K_3 cos(\omega_r (t - t_1)) + K_4 sin(\omega_r (t - t_1)) + V_i + NV_o, & t_1 < t < T_s/2 \end{cases} \tag{A.10}$$

To find $v_{C_P,peak}$ and $v_{C_N,peak}$, the algorithm present in appendix B.5 can be used with the parameters present in table A.4, that describes this situation. The total peak voltage is the maximum between $v_{C_P,peak}$ and $v_{C_N,peak}$.

Coefficient	Value for $v_{C_P,peak}$	Value for $v_{C_N,peak}$
C_1	K_2	K_4
C_2	K_1	K_3
C_3	$V_i - NV_o$	$V_i + NV_o$
t_{begin}	0	0
t_{end}	t_1	$T_s/2 - t_1$
ω	ω_r	ω_r

Table A.4: Coefficient for peak resonant voltage in PN mode.

A.2 Interesting values for NP mode

This section shows how to find the needed values for the loss model and for the converter design, in the case of the NP mode.

RMS resonant current

Resonant current in NP mode is:

$$\begin{cases} i_{L_N}(t) = C_r\omega_r(-K_1 sin(\omega_r t) + K_2 cos(\omega_r t)), & 0 < t < t_1 \\ i_{L_P}(t) = C_r\omega_r(-K_3 sin(\omega_r(t-t_1)) + K_4 cos(\omega_r(t-t_1))), & t_1 < t < T_s/2 \end{cases} \tag{A.11}$$

The integral to solve to get RMS value of resonant current is:

$$i_{L,RMS} = \sqrt{\frac{2}{T_s}\int_0^{\frac{T_s}{2}} i_L(t)^2 dt} = \sqrt{\frac{2}{T_s}(\int_0^{t_1} i_{L_N}(t)^2 dt + \int_{t_1}^{\frac{T_s}{2}} i_{L_P}(t)^2 dt)} \tag{A.12}$$

In appendix B.1 there is the general solution of the integral and in table A.5 there are the coefficients to find K (see appendix B.1).

Coefficient	Value
A	t_1
B	$-C_r\omega_r K_1$
C	$C_r\omega_r K_2$
D	$\frac{T_s}{2}$
E	$-C_r\omega_r K_3$;
F	$C_r\omega_r K_4$
V	ω_r
W	ω_r

Table A.5: Coefficient for RMS resonant current in NP mode.

Finally, the following helps to find the RMS resonant current:

$$i_{L,RMS} = \sqrt{\frac{1}{D}K} \tag{A.13}$$

Peak resonant current

The maximum between $i_{L_N,peak}$ (the peak of i_{L_N} in $0 < t < t_1$) and $i_{L_P,peak}$ (the peak of i_{L_P} in $t_1 < t < T_s/2$), is the peak resonant current.
The algorithm present in appendix B.5 shows how to to find $i_{L_N,peak}$ and $i_{L_P,peak}$, with the parameters present in table A.6.

Coefficient	Value for $i_{L_N,peak}$	Value for $i_{L_P,peak}$
C_1	$-C_r\omega_r K_1$	$-C_r\omega_r K_3$
C_2	$C_r\omega_r K_2$	$C_r\omega_r K_4$
C_3	0	0
t_{begin}	0	0
t_{end}	t_1	$T_s/2 - t_1$
ω	ω_r	ω_r

TABLE A.6: Coefficient for peak resonant current in NP mode.

RMS current on secondary

Output current in NP mode is:

$$\begin{cases} i_{O_N}(t) = N[-\frac{NV_o}{L_m}t + i_{M_N}(0) - C_r\omega_r(-K_1 sin(\omega_r t) + K_2 cos(\omega_r t))], & 0 < t < t_1 \\ i_{O_P}(t) = N[C_r\omega_r(-K_3 sin(\omega_r(t-t_1)) + K_4 cos(\omega_r(t-t_1)))+ \\ \qquad -\frac{NV_o}{L_m}(t-t_1) + i_{M_P}(t_1)], & t_1 < t < \frac{T_s}{2} \end{cases} \tag{A.14}$$

The following integral needs to be solved to find RMS output current:

$$i_{O,RMS} = \sqrt{\frac{2}{T_s}\int_0^{\frac{T_s}{2}} i_O(t)^2 dt} = \sqrt{\frac{2}{T_s}(\int_0^{t_1} i_{O_N}(t)^2 dt + \int_{t_1}^{\frac{T_s}{2}} i_{O_P}(t)^2 dt)} \tag{A.15}$$

The expression present in appendix B.3 with the values of coefficients in table A.7 shows how to find K.

Then:

$$i_{O,RMS} = \sqrt{\frac{1}{F}K} \tag{A.16}$$

Average current on diodes

The output current (equations A.14) needs to be integrated to find the average current on diodes:

$$i_{O,AVG} = \frac{2}{T_s}\int_0^{\frac{T_s}{2}} i_O(t) dt = \frac{2}{T_s}[\int_0^{t_1} i_{O_N}(t) dt + \int_{t_1}^{\frac{T_s}{2}} i_{O_P}(t) dt] \tag{A.17}$$

Coefficient	Value
A	t_1
B	$-NC_r\omega_r K_1$
C	$NC_r\omega_r K_2$
D	$-N^2V_o/L_m$
E	$-Ni_{M_N}(0);$
F	$T_s/2$
G	$-NC_r\omega_r K_3$
H	$NC_r\omega_r K_4$
L	$-N^2V_o/L_m$
M	$Ni_{M_N}(t_1)$
T	t_1
U	t_1
W	ω_r

Table A.7: Coefficient for RMS and average output current in NP mode.

Using the solution present in appendix B.2 using the coefficients in table A.3, is possible to find the value K, from which:

$$i_{O,AVG} = \frac{2}{T_s}K \tag{A.18}$$

RMS current in the output capacitor

As in the previous case, assuming that the output capacitor acts as an ideal capacitor and it make all AC components of the current that exits from the diodes to pass, output current has only DC component and it can be shown that:

$$i_{C_{out},RMS} = \sqrt{i^2_{O,RMS} - i^2_{O,AVG}} \tag{A.19}$$

Peak voltage on the resonant capacitor

From equations at the beginning of this section, is possible to rewrite the equations for the resonant capacitor voltage:

$$\begin{cases} v_{C_N}(t) = K_1 cos(\omega_r t) + K_2 sin(\omega_r t) + V_i + NV_o, & 0 < t < t_1 \\ v_{C_P}(t) = K_3 cos(\omega_r (t - t_1)) + K_4 sin(\omega_r (t - t_1)) + V_i - NV_o, & t_1 < t < T_s/2 \end{cases} \tag{A.20}$$

To find $v_{C_N,peak}$ and $v_{C_P,peak}$, the algorithm present in appendix B.5 can be again used with the parameters present in table A.8, that describes this situation. The total peak voltage is the maximum between $v_{C_N,peak}$ and $v_{C_P,peak}$.

Coefficient	Value for $v_{C_P,peak}$	Value for $v_{C_N,peak}$
C_1	K_2	K_4
C_2	K_1	K_3
C_3	$V_i - NV_o$	$V_i + NV_o$
t_{begin}	0	0
t_{end}	t_1	$T_s/2 - t_1$
ω	ω_r	ω_r

TABLE A.8: Coefficient for peak resonant voltage in NP mode.

A.3 Interesting values for PO mode

This section shows how to find the needed values for the loss model and for the converter design, in the case of the PO mode.

RMS resonant current

Resonant current in PO mode is:

$$\begin{cases} i_{L_P}(t) = C_r\omega_r(-K_1 sin(\omega_r t) + K_2 cos(\omega_r t)), & 0 < t < t_1 \\ i_{L_O}(t) = C_r\omega_m(-K_3 sin(\omega_m(t-t_1)) + K_4 cos(\omega_m(t-t_1))), & t_1 < t < T_s/2 \end{cases} \tag{A.21}$$

The integral to solve to get RMS value of resonant current is:

$$i_{L,RMS} = \sqrt{\frac{2}{T_s}\int_0^{\frac{T_s}{2}} i_L(t)^2 dt} = \sqrt{\frac{2}{T_s}(\int_0^{t_1} i_{L_P}(t)^2 dt + \int_{t_1}^{\frac{T_s}{2}} i_{L_O}(t)^2 dt)} \tag{A.22}$$

In appendix B.1 there is the general solution of the integral and in table A.9 there are the coefficients to find K (see appendix B.1).

Coefficient	Value
A	t_1
B	$-C_r\omega_r K_1$
C	$C_r\omega_r K_2$
D	$\frac{T_s}{2}$
E	$-C_r\omega_m K_3$
F	$C_r\omega_m K_4$
V	ω_r
W	ω_m

TABLE A.9: Coefficient for RMS resonant current in PO mode.

Finally, the following helps to find the RMS resonant current:

$$i_{L,RMS} = \sqrt{\frac{1}{D}K} \tag{A.23}$$

Peak resonant current

The maximum between $i_{L_P,peak}$ (the peak of i_{L_P} in $0 < t < t_1$) and $i_{L_O,peak}$ (the peak of i_{L_O} in $t_1 < t < T_s/2$), is the peak resonant current.
The algorithm present in appendix B.5 shows how to find $i_{L_P,peak}$ and $i_{L_O,peak}$, with the parameters present in table A.10.

Coefficient	Value for $i_{L_P,peak}$	Value for $i_{L_O,peak}$
C_1	$-C_r\omega_r K_1$	$-C_r\omega_r K_3$
C_2	$C_r\omega_r K_2$	$C_r\omega_r K_4$
C_3	0	0
t_{begin}	0	0
t_{end}	t_1	$T_s/2 - t_1$
ω	ω_r	ω_m

Table A.10: Coefficient for peak resonant current in PO mode.

RMS current on secondary

Output current in PO mode is:

$$\begin{cases} i_{O_P}(t) = N[C_r\omega_r(-K_1 sin(\omega_r t) + K_2 cos(\omega_r t)) - \frac{NV_o}{L_m}t + i_{M_P}(0)], & 0 < t < t_1 \\ i_{O_O}(t) = 0, & t_1 < t < \frac{T_s}{2} \end{cases} \tag{A.24}$$

The following integral needs to be solved to find RMS output current:

$$i_{O,RMS} = \sqrt{\frac{2}{T_s}\int_0^{\frac{T_s}{2}} i_O(t)^2 dt} = \sqrt{\frac{2}{T_s}\int_0^{t_1} i_{O_P}(t)^2 dt} \tag{A.25}$$

The expression present in appendix B.3 with the values of coefficients in table A.11 shows how to find K.

Then:

$$i_{O,RMS} = \sqrt{\frac{1}{F}K} \tag{A.26}$$

Average current on diodes

The output current (equations A.24) needs to be integrated to find the average current on diodes:

$$i_{O,AVG} = \frac{2}{T_s}\int_0^{\frac{T_s}{2}} i_O(t)dt = \frac{2}{T_s}\int_0^{t_1} i_{O_P}(t)dt] \tag{A.27}$$

Using the solution present in appendix B.2 using the coefficients in table A.11, is possible to find the value K, from which:

$$i_{O,AVG} = \frac{2}{T_s}K \tag{A.28}$$

Coefficient	Value
A	t_1
B	$-NC_r\omega_r K_1$
C	$NC_r\omega_r K_2$
D	$-N^2 V_o/L_m$
E	$-i_{M_P}(0);$
F	$T_s/2$
G	0
H	0
L	0
M	0
T	t_1
U	t_1
W	ω_r

TABLE A.11: Coefficient for RMS and average output current in PO mode.

RMS current in the output capacitor

As in the previous case, assuming that the output capacitor acts as an ideal capacitor and it make all AC components of the current that exits from the diodes to pass, output current has only DC component and it can be shown that:

$$i_{C_{out},RMS} = \sqrt{i^2_{O,RMS} - i^2_{O,AVG}} \tag{A.29}$$

Peak voltage on the resonant capacitor

From equations at the beginning of this section, is possible to rewrite the equations for the resonant capacitor voltage:

$$\begin{cases} v_{C_P}(t) = K_1 cos(\omega_r t) + K_2 sin(\omega_r t) + V_i - NV_o, & 0 < t < t_1 \\ v_{C_O}(t) = K_3 cos(\omega_m (t - t_1)) + K_4 sin(\omega_m (t - t_1)) + V_i, & t_1 < t < T_s/2 \end{cases} \tag{A.30}$$

To find $v_{C_P,peak}$ and $v_{C_O,peak}$, the algorithm present in appendix B.5 can be used with the parameters present in table A.12, that describes this situation. The total peak voltage is the maximum between $v_{C_P,peak}$ and $v_{C_O,peak}$.

A.4 Interesting values for PON mode

This section shows how to find the needed values for the loss model and for the converter design, in the case of the PON mode.

Coefficient	Value for $v_{C_P,peak}$	Value for $v_{C_O,peak}$
C_1	K_2	K_4
C_2	K_1	K_3
C_3	$V_i - NV_o$	V_i
t_{begin}	0	0
t_{end}	t_1	$T_s/2 - t_1$
ω	ω_r	ω_m

Table A.12: Coefficient for peak resonant voltage in PO mode.

RMS resonant current

Resonant current in PON mode is:

$$\begin{cases} i_{L_P}(t) = C_r\omega_r(-K_1 sin(\omega_r t) + K_2 cos(\omega_r t)), & 0 < t < t_1 \\ i_{L_O}(t) = C_r\omega_m(-K_3 sin(\omega_m(t-t_1)) + K_4 cos(\omega_m(t-t_1))), & t_1 < t < t_2 \\ i_{L_N}(t) = C_r\omega_r(-K_5 sin(\omega_r(t-T_s/2)) + K_6 cos(\omega_r(t-T_s/2))), & t_2 < t < T_s/2 \end{cases} \tag{A.31}$$

The integral to solve to get RMS value of resonant current is:

$$i_{L,RMS} = \sqrt{\frac{2}{T_s}\int_0^{\frac{T_s}{2}} i_L(t)^2 dt} = \sqrt{\frac{2}{T_s}(\int_0^{t_1} i_{L_P}(t)^2 dt + \int_{t_1}^{t_2} i_{L_O}(t)^2 dt) + \int_{t_2}^{\frac{T_s}{2}} i_{L_N}(t)^2 dt)} \tag{A.32}$$

In appendix B.4 there is the general solution of the integral and in table A.13 there are the coefficients to find K (see appendix B.4).

Coefficient	Value
A	t_P
B	$-C_r\omega_r K_1$
C	ω_r
D	$C_r\omega_r K_2$
F	$-C_r\omega_m K_3$
G	$C_r\omega_m K_4$
H	$T_s/2$
L	ω_m
M	$C_r\omega_r K_6$
N	$-C_r\omega_r K_5$
P	$t_P + t_O$

Table A.13: Coefficient for RMS resonant current in PON mode.

Finally, the following helps to find the RMS resonant current:

$$i_{L,RMS} = \sqrt{\frac{1}{H}K} \tag{A.33}$$

Peak resonant current

The maximum between $i_{L_P,peak}$ (the peak of i_{L_P} in $0 < t < t_1$), $i_{L_O,peak}$ (the peak of i_{L_O} in $t_1 < t < t_2$) and $i_{L_N,peak}$ (the peak of i_{L_N} in $t_2 < t < T_s/2$) is the peak resonant current.
The algorithm present in appendix B.5 shows how to find $i_{L_P,peak}$, $i_{L_O,peak}$ and $i_{L_N,peak}$, with the parameters present in table A.14.

Coefficient	Value for $i_{L_P,peak}$	Value for $i_{L_O,peak}$	Value for $i_{L_N,peak}$
C_1	$-C_r\omega_r K_1$	$-C_r\omega_r K_3$	$-C_r\omega_r K_5$
C_2	$C_r\omega_r K_2$	$C_r\omega_r K_4$	$C_r\omega_r K_6$
C_3	0	0	0
t_{begin}	0	0	$-t_N$
t_{end}	t_P	t_O	0
ω	ω_r	ω_m	ω_r

TABLE A.14: Coefficient for peak resonant current in PON mode.

RMS current on secondary

Output current in PON mode is:

$$\begin{cases} i_{O_P}(t) = N[C_r\omega_r(-K_1 sin(\omega_r t) + K_2 cos(\omega_r t)) - \frac{NV_o}{L_m}t + i_{M_P}(0)], & 0 < t < t_1 \\ i_{O_O}(t) = 0, & t_1 < t < t_2 \\ i_{O_N}(t) = N[-\frac{NV_o}{L_m}(t - t_2) + i_{M_N}(t_2) + \\ \qquad -C_r\omega_r(-K_5 sin(\omega_r(t - T_s/2)) + K_6 cos(\omega_r(t - T_s/2)))], & t_2 < t < T_s/2 \end{cases} \tag{A.34}$$

The following integral needs to be solved to find RMS output current:

$$i_{O,RMS} = \sqrt{\frac{2}{T_s}\int_0^{\frac{T_s}{2}} i_O(t)^2 dt} = \sqrt{\frac{2}{T_s}(\int_0^{t_1} i_{O_P}(t)^2 dt + \int_{t_2}^{T_s/2} i_{O_N}(t)^2 dt)} \tag{A.35}$$

The expression present in appendix B.3 with the values of coefficients in table A.15 shows how to find K.

Then:

$$i_{O,RMS} = \sqrt{\frac{1}{F}K} \tag{A.36}$$

Average current on diodes

The output current (equations **??**) needs to be integrated to find the average current on diodes:

$$i_{O,AVG} = \frac{2}{T_s}\int_0^{\frac{T_s}{2}} i_O(t) dt = \frac{2}{T_s}[\int_0^{t_1} i_{O_P}(t) dt + \int_{t_2}^{\frac{T_s}{2}} i_{O_N}(t) dt] \tag{A.37}$$

Coefficient	Value
A	t_1
B	$-NC_r\omega_r K_1$
C	$NC_r\omega_r K_2$
D	$-N^2V_o/L_m$
E	$+i_{M_P}(0);$
F	$T_s/2$
G	$NC_r\omega_r K_5$
H	$-NC_r\omega_r K_6$
L	$-N^2V_o/L_m$
M	$i_{M_N}(t_2)$
T	t_2
U	$T_s/2$
W	ω_r

Table A.15: Coefficient for RMS and average output current in PON mode.

Using the solution present in appendix B.2 using the coefficients in table A.15, is possible to find the value K, from which:

$$i_{O,AVG} = \frac{2}{T_s}K \tag{A.38}$$

RMS current in the output capacitor

As in the previous case, assuming that the output capacitor acts as an ideal capacitor and it make all AC components of the current that exits from the diodes to pass, output current has only DC component and it can be shown that:

$$i_{C_{out},RMS} = \sqrt{i^2_{O,RMS} - i^2_{O,AVG}} \tag{A.39}$$

Peak voltage on the resonant capacitor

From equations at the beginning of this section, is possible to rewrite the equations for the resonant capacitor voltage:

$$\begin{cases} v_{C_P}(t) = K_1 cos(\omega_r t) + K_2 sin(\omega_r t) + V_i - NV_o, & 0 < t < t_1 \\ v_{C_O}(t) = K_3 cos(\omega_m (t - t_1)) + K_4 sin(\omega_m (t - t_1)) + V_i, & t_1 < t < t_2 \\ v_{C_N}(t) = K_5 cos(\omega_r (t - T_s/2)) + K_6 sin(\omega_r (t - T_s/2)) + V_i + NV_o, & t_2 < t < T_s/2 \end{cases} \tag{A.40}$$

To find $v_{C_P,peak}$, $v_{C_O,peak}$ and $v_{C_N,peak}$, the algorithm present in appendix B.5 can be used with the parameters present in table A.16, that describes this situation. The total peak is the maximum between the three.

Coefficient	Value for $v_{C_P,peak}$	Value for $v_{C_O,peak}$	Value for $v_{C_N,peak}$
C_1	K_2	K_4	K_6
C_2	K_1	K_3	K_5
C_3	$V_i - NV_o$	V_i	$V_i + NV_o$
t_{begin}	0	0	$-t_N$
t_{end}	t_1	$T_s/2 - t_1$	$T_s/2$
ω	ω_r	ω_m	ω_r

TABLE A.16: Coefficient for peak resonant voltage in PON mode.

A.5 Interesting values for NOP mode

This section shows how to find the needed values for the loss model and for the converter design, in the case of the NOP mode.

RMS resonant current

Resonant current in NOP mode is:

$$\begin{cases} i_{L_N}(t) = C_r\omega_r(-K_1 sin(\omega_r t) + K_2 cos(\omega_r t)), & 0 < t < t_1 \\ i_{L_O}(t) = C_r\omega_m(-K_3 sin(\omega_m(t-t_1)) + K_4 cos(\omega_m(t-t_1))), & t_1 < t < t_2 \\ i_{L_P}(t) = C_r\omega_r(-K_5 sin(\omega_r(t-T_s/2)) + K_6 cos(\omega_r(t-T_s/2))), & t_2 < t < T_s/2 \end{cases} \tag{A.41}$$

The integral that to solve to get RMS value of resonant current is:

$$i_{L,RMS} = \sqrt{\frac{2}{T_s}\int_0^{\frac{T_s}{2}} i_L(t)^2 dt} = \sqrt{\frac{2}{T_s}(\int_0^{t_1} i_{L_N}(t)^2 dt + \int_{t_1}^{t_2} i_{L_O}(t)^2 dt) + \int_{t_2}^{\frac{T_s}{2}} i_{L_P}(t)^2 dt)} \tag{A.42}$$

In appendix B.4 there is the general solution of the integral and in table A.17 there are the coefficients to find K (see appendix B.4).

Finally, the following helps to find the RMS resonant current:

$$i_{L,RMS} = \sqrt{\frac{1}{H}K} \tag{A.43}$$

Peak resonant current

The maximum between $i_{L_N,peak}$ (the peak of i_{L_N} in $0 < t < t_1$), $i_{L_O,peak}$ (the peak of i_{L_O} in $t_1 < t < t_2$) and $i_{L_P,peak}$ (the peak of i_{L_P} in $t_2 < t < T_s/2$) is the peak resonant current.
The algorithm present in appendix B.5 shows how to find $i_{L_N,peak}$, $i_{L_O,peak}$ and $i_{L_P,peak}$, with the parameters present in table A.18.

Coefficient	Value
A	t_1
B	$-C_r\omega_r K_1$
C	ω_r
D	$C_r\omega_r K_2$
F	$-C_r\omega_m K_3$
G	$C_r\omega_m K_4$
H	$T_s/2$
L	ω_m
M	$C_r\omega_r K_6$
N	$-C_r\omega_r K_5$
P	t_2

Table A.17: Coefficient for RMS resonant current in NOP mode.

Coefficient	Value for $i_{L_N,peak}$	Value for $i_{L_O,peak}$	Value for $i_{L_P,peak}$
C_1	$-C_r\omega_r K_1$	$-C_r\omega_r K_3$	$-C_r\omega_r K_5$
C_2	$C_r\omega_r K_2$	$C_r\omega_r K_4$	$C_r\omega_r K_6$
C_3	0	0	0
t_{begin}	0	0	$-t_P$
t_{end}	t_N	t_O	0
ω	ω_r	ω_m	ω_r

Table A.18: Coefficient for peak resonant current in NOP mode.

RMS current on secondary

Output current in NOP mode is:

$$\begin{cases} i_{O_N}(t) = N[-\frac{NV_o}{L_m}t + i_{M_N}(0) - C_r\omega_r(-K_1 sin(\omega_r t) + K_2 cos(\omega_r t))], & 0 < t < t_1 \\ i_{O_O}(t) = 0, & t_1 < t < t_2 \\ i_{O_P}(t) = N[C_r\omega_r(-K_5 sin(\omega_r(t - T_s/2)) + K_6 cos(\omega_r(t - T_s/2))) + \\ \qquad -\frac{NV_o}{L_m}(t - t_2) - i_{M_P}(T_2)], & t_2 < t < T_s/2 \end{cases} \tag{A.44}$$

The following integral needs to be solved to find RMS output current:

$$i_{O,RMS} = \sqrt{\frac{2}{T_s}\int_0^{\frac{T_s}{2}} i_O(t)^2 dt} = \sqrt{\frac{2}{T_s}(\int_0^{t_1} i_{O_N}(t)^2 dt + \int_{t_2}^{T_s/2} i_{O_P}(t)^2 dt)} \tag{A.45}$$

The expression present in appendix B.3 with the values of coefficients in table A.19 shows how to find K.

Then:

$$i_{O,RMS} = \sqrt{\frac{1}{F}K} \tag{A.46}$$

Coefficient	Value
A	t_1
B	$NC_r\omega_r K_1$
C	$-NC_r\omega_r K_2$
D	$-N^2V_o/L_m$
E	$+i_{M_N}(0);$
F	$T_s/2$
G	$-NC_r\omega_r K_5$
H	$NC_r\omega_r K_6$
L	$-N^2V_o/L_m$
M	$-i_{M_P}(t_2)$
T	t_2
U	$T_s/2$
W	ω_r

TABLE A.19: Coefficient for RMS and average output current in NOP mode.

Average current on diodes

The output current (equations A.44) needs to be integrated to find the average current on diodes:

$$i_{O,AVG} = \frac{2}{T_s}\int_0^{\frac{T_s}{2}} i_O(t)dt = \frac{2}{T_s}[\int_0^{t_1} i_{O_N}(t)dt + \int_{t_2}^{\frac{T_s}{2}} i_{O_P}(t)dt] \tag{A.47}$$

Using the solution present in appendix B.2 using the coefficients in table A.19, is possible to find the value K, from which:

$$i_{O,AVG} = \frac{2}{T_s}K \tag{A.48}$$

RMS current in the output capacitor

As in the previous case, assuming that the output capacitor acts as an ideal capacitor and it make all AC components of the current that exits from the diodes to pass, output current has only DC component and it can be shown that:

$$i_{C_{out},RMS} = \sqrt{i_{O,RMS}^2 - i_{O,AVG}^2} \tag{A.49}$$

Peak voltage on the resonant capacitor

From equations at the beginning of this section, is possible to rewrite the equations for the resonant capacitor voltage:

$$\begin{cases} v_{C_N}(t) = K_1 cos(\omega_r t) + K_2 sin(\omega_r t) + V_i + NV_o, & 0 < t < t_1 \\ v_{C_O}(t) = K_3 cos(\omega_m (t - t_1)) + K_4 sin(\omega_m (t - t_1)) + V_i, & t_1 < t < t_2 \\ v_{C_P}(t) = K_5 cos(\omega_r (t - T_s/2)) + K_6 sin(\omega_r (t - T_s/2)) + V_i - NV_o, & t_2 < t < T_s/2 \end{cases} \tag{A.50}$$

To find $v_{C_N,peak}$, $v_{C_O,peak}$ and $v_{C_P,peak}$, the algorithm present in appendix B.5 can be used with the parameters present in table A.20, that describes this situation. The total peak voltage is the maximum between the three.

Coefficient	Value for $v_{C_P,peak}$	Value for $v_{C_O,peak}$	Value for $v_{C_N,peak}$
C_1	K_2	K_4	K_6
C_2	K_1	K_3	K_5
C_3	$V_i + NV_o$	V_i	$V_i - NV_o$
t_{begin}	0	0	$-t_P$
t_{end}	t_1	$T_s/2 - t_1$	$T_s/2$
ω	ω_r	ω_m	ω_r

Table A.20: Coefficient for peak resonant voltage in NOP mode.

Appendix B

Mathematical Analysis

In this appendix are present basic calculations that are needed multiple times in the dissertion.

B.1 Integral of general form, 1

This is a type of integral that is often present in this text, can be shown that it's value is:

$$\begin{aligned} K =& \int_0^A (Bsin(Vx) + Ccos(Vx))^2 dx + \int_A^D (Esin(W(x-A)) + Fcos(W(x-A)))^2 dx = \\ =& \frac{1}{4V}(2AV(B^2+C^2) + (C^2-B^2)sin(2AV) - 2BCcos(2AV) + 2BC) + \\ &+ \frac{1}{4W}(2W(F^2+E^2)(D-A) + (E^2-F^2)sin(2W(A-D)) \\ &- 2EFcos(2W(A-D)) + 2EF) \end{aligned} \tag{B.1}$$

B.2 Integral of general form, 2

This is a type of integral that is often present in this text, can be shown that it's value is:

$$\begin{aligned} K =& \int_0^A (Bsin(Wx) + Ccos(Wx) + Dx + E)dx + \\ &+ \int_T^F (Gsin(W(x-U)) + Hcos(W(x-U)) + L(x-T) + M)dx = \\ =& \frac{1}{2W}(A^2DW + 2B(1-cos(AW)) + 2Csin(AW) + 2AEW + F^2LW + \\ &+ 2G(cos(W(U-T)) - cos(W(U-F))) - 2WFLT + \\ &+ 2WFM + LWT^2 - 2WMT) \end{aligned} \tag{B.2}$$

B.3 Integral of general form, 3

This is a type of integral that is often present in this text, can be shown that it's value is:

$$\begin{aligned}
K =& \int_0^A (Bsin(Wx) + Ccos(Wx) + Dx + E)^2 dx + \\
&+ \int_T^F (Gsin(W(x-U)) + Hcos(W(x-U)) + L(x-T) + M)^2 dx = \\
=& \frac{1}{12W^2}(2AW^2(2A^2D^2 + 6ADE + 3B^2 + 3C^2 + 6E^2) + \\
&+ 24sin(AW)(CW(AD+E) + BD) + 24cos(AW)(CD - BW(AD+E)) + \\
&+ 3W(C-B)(B+C)sin(2AW) - 6BCWcos(2AW) + 6BW(C+4E) + \\
&- 24CD - 2W^2(U-F)(2L^2(F^2 - 3T(F+U) + FU + 3T^2 + U^2) + \\
&+ 6LM(F - 2T + U) + 3G^2 + 3H^2 + 6M^2) + 3W(H^2 - G^2)sin(2W(F-U)) + \\
&+ 24sin(W(F-U))(HW(-TL + FL + M) + GL) + \\
&+ 24cos(W(F-U))(HL - GW(-TL + FL + M)) + \\
&- 6GHWcos(2W(F-U)) + 2W^2(U-T)(3G^2 + 3H^2 + 2L^2(T-U)^2 + \\
&+ 6LM(U-T) + 6M^2) + 3W(G^2 - H^2)sin(2W(T-U)) + \\
&- 24sin(W(T-U))(GL + HMW) - 24cos(W(T-U))(HL - GMW) + \\
&+ 6GHWcos(2W(T-U))).
\end{aligned} \tag{B.3}$$

B.4 Integral of general form, 4

This is a type of integral that is sometimes present in this text, can be shown that it's value is:

$$\begin{aligned}
K =& \int_0^A (Bsin(Cx) + Dcos(Cx))^2 dx + \int_A^P (Fsin(L(x-A)) + Gcos(L(x-A)))^2 dx + \\
&+ \int_P^H (Nsin(C(x-H)) + Mcos(C(x-H)))^2 dx = \\
=& \frac{1}{4C}(2AC(B^2 + D^2) + (D^2 - B^2)sin(2AC) - 2BDcos(2AC) + 2BD) + \\
&+ \frac{1}{4L}(2L(P-A)(F^2 + G^2) + (G^2 - F^2)sin(2L(P-A)) + \\
&- 2FGcos(2L(P-A)) + 2FG) + \\
&+ \frac{1}{4C}(2C(H-P)(M^2 + N^2) + (N^2 - M^2)sin(2C(P-H)) + \\
&+ MNcos(2C(P-H)) - 2MN)
\end{aligned} \tag{B.4}$$

B.5 Peak of general form, 1

In this section, the maximum, the minimum and the peak over the definition period of this type of function is derived:

$$f(t) = C_1 sin(\omega t) + C_2 cos(\omega t) + C_3, \qquad t_{begin} < t < t_{end} \tag{B.5}$$

Is firstly needed to compute the position of the first derivative null:

$$f'(t) = \frac{d}{dt}(C_1 sin(\omega t_{zero}) + C_2 cos(\omega t_{zero})) = 0$$

$$\omega C_1 cos(\omega t_{zero}) - \omega C_2 sin(\omega t_{zero}) = 0$$

$$tan(\omega t_{zero}) = \frac{C_1}{C_2}$$

So the interesting point is:

$$t_{zero} = \frac{1}{\omega} tan^{-1}(\frac{C_1}{C_2}) \tag{B.6}$$

Using the algorithm shown in the flowchart in figure B.1 is then possible to calculate the value of the maximum, of the minimum and of the peak of the initial function.

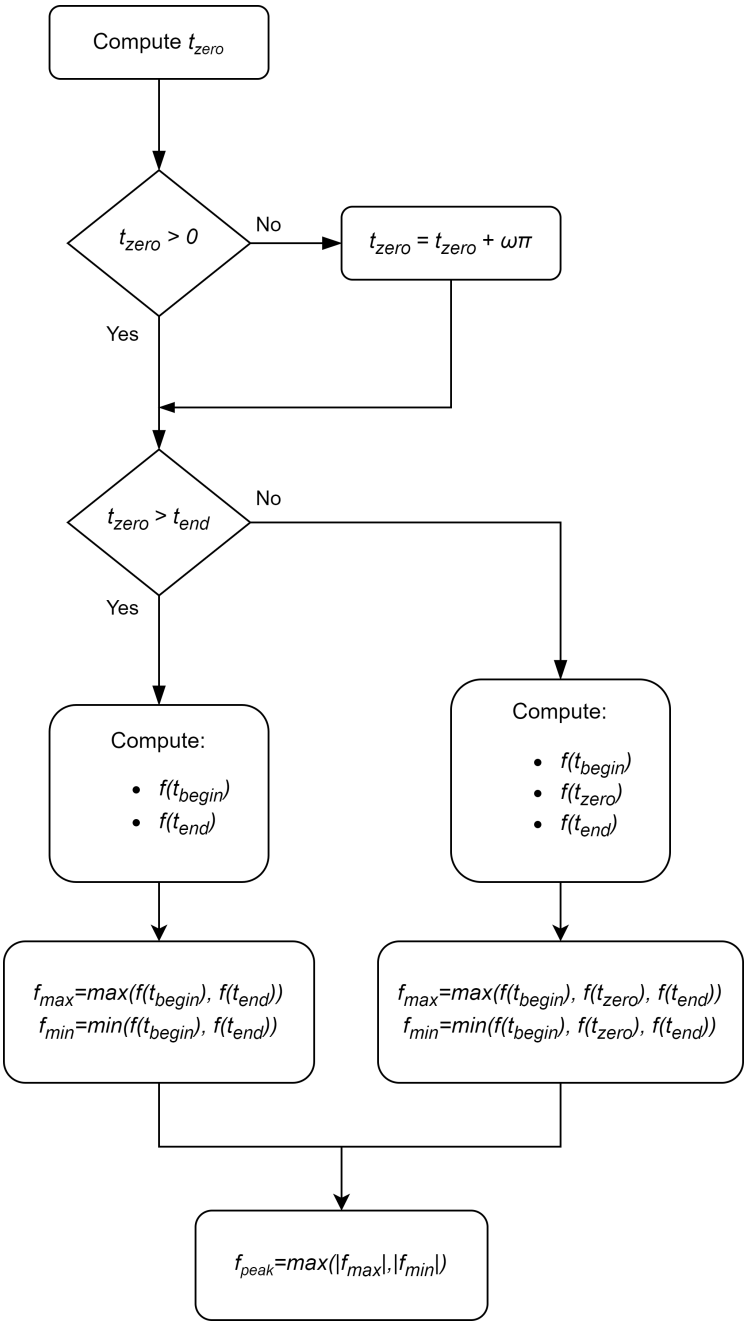

Figure B.1: Flowchart of the algorithm to compute the minimum, the maximum and the peak

Bibliography

[1] B. C. and R. S. R. Babu. A review on llc resonant converter. In *2016 International Conference on Computation of Power, Energy Information and Commuincation (ICCPEIC)*, pages 620–623, 2016.

[2] N. CHEMI-CON. Lrbseries datasheet. URL: https://www.chemi-con.co.jp/products/relatedfiles/capacitor/catalog/LRBN-e.PDF, last checked on 2023-07-14.

[3] H. Choi and P. C. Team. Design considerations for an llc resonant converter. In *Fairchild Power Seminar*, volume 2007. Citeseer, 2007.

[4] L. Dixon. *Magnetics Design Handbook*. Unitrode Products from Texas Instruments, 2001.

[5] L. H. Dixon. Transformer and inductor design for optimum circuit performance. 2003.

[6] X. Fang, H. Hu, Z. J. Shen, and I. Batarseh. Operation mode analysis and peak gain approximation of the llc resonant converter. *IEEE Transactions on Power Electronics*, 27(4):1985–1995, 2012.

[7] J. Hayes, N. O'Donovan, M. Egan, and T. O'Donnell. Inductance characterization of high-leakage transformers. In *Eighteenth Annual IEEE Applied Power Electronics Conference and Exposition, 2003. APEC '03.*, volume 2, pages 1150–1156 vol.2, 2003.

[8] Z. Hu, L. Wang, Y. Qiu, Y.-F. Liu, and P. C. Sen. An accurate design algorithm for llc resonant converters-part ii. *IEEE Transactions on Power Electronics*, 31(8):5448–5460, 2015.

[9] Infineon. Ipx65r110cfda datasheet. URL: https://www.infineon.com/dgdl/Infineon-IPX65R110CFDA-DS-v02_00-en.pdf?fileId=db3a304336797ff90136ba7c820925a5, last checked on 2023-07-14.

[10] T. Instrument. Slup376, survey of resonant converter topologies. *Texas Instrument Power Supply Design Seminar SEM2300*, (1), 2018.

[11] IXYS. Dpg30c400hb datasheet. URL: https://ixapps.ixys.com/datasheet/dpg30c400hb.pdf, last checked on 2023-07-14.

[12] J. Lazar and R. Martinelli. Steady-state analysis of the llc series resonant converter. In *APEC 2001. Sixteenth Annual IEEE Applied Power Electronics Conference and Exposition (Cat. No.01CH37181)*, volume 2, pages 728–735 vol.2, 2001.

[13] MAGNETICS. 0077076a7 datasheet. URL: https://www.mag-inc.com/Media/Magnetics/Datasheets/0077076A7.pdf, last checked on 2023-07-17.

[14] MAGNETICS. Core losses. URL: https://www.mag-inc.com/design/design-guides/powder-core-loss-calculation, last checked on 2023-07-17.

[15] MathWorks. Simscape reference. URL: https://it.mathworks.com/help/pdf_doc/simscape/simscape_ref.pdf, last checked on 2023-07-12.

[16] M. H. Rashid. *Power Electronics Handbook devices, circuits, and applications, 3rd edition*. Butterworth-Heinemann, 2011. ISBN-13: 978-0-12-382036-5.

[17] TDK-Electronics. E-cores. general information. URL: https://www.tdk-electronics.tdk.com/download/540150/f119bbe0ab3d6dd73ae31c6fa9dcf6b9/pdf-ecoresgeneralinformation.pdf, last checked on 2023-07-16.

[18] TDK-Electronics. Etd54 datasheet. URL: https://www.tdk-electronics.tdk.com/inf/80/db/fer/etd_54_28_19.pdf, last checked on 2023-07-16.

[19] TDK-Electronics. N87 datasheet. URL: https://www.tdk-electronics.tdk.com/download/528882/990c299b916e9f3eb7e44ad563b7f0b9/pdf-n87.pdf, last checked on 2023-07-16.

[20] Y. Wei, Q. Luo, X. Du, N. Altin, J. M. Alonso, and H. A. Mantooth. Analysis and design of the llc resonant converter with variable inductor control based on time-domain analysis. *IEEE Transactions on Industrial Electronics*, 67(7):5432–5443, 2020.

[21] Wikipedia. Steinmetz's equation. URL: http://https://en.wikipedia.org/wiki/Steinmetz%27s_equation, last checked on 2023-07-06.

[22] J. Zeng, G. Zhang, S. S. Yu, B. Zhang, and Y. Zhang. Llc resonant converter topologies and industrial applications - a review. *Chinese Journal of Electrical Engineering*, 6(3):73–84, 2020.

[23] Y. Zuo, H. Niu, R. Zhang, and X. Pan. The modified fha and simplified time-doamin analysis methodologies for llc resonant converter. In *2021 IEEE 12th Energy Conversion Congress & Exposition - Asia (ECCE-Asia)*, pages 56–61, 2021.